Addis Ababa University

Addis Ababa Institute of Technology

School of Mechanical and Industrial Engineering

Rolling Contact Fatigue Life Analysis on Rail Track in Ethio-Djibouti Railway Line, Awash Area

A Thesis Submitted to the School of Graduate Studies of Addis Ababa University in Partial Fulfillment of the Requirement of the Degree of Masters of Science in Mechanical Engineering (Mechanical Design Stream)

By

Sisay Petros Michael

Advisor: Dr. Daniel Tilahun (Ph.D.)

Co-advisor: Mr. Natinel Abebaw (Ph.D. Candidate)

Addis Ababa University

Addis Ababa, Ethiopia

June 2020

Addis Ababa University

Addis Ababa Institute of Technology

School of Mechanical and Industrial Engineering

This is to certify that the thesis prepared by Sisay Petros, entitled by "Rolling Contact Fatigue Life Analysis on Rail Track in Ethio-Djibouti Railway Line, Awash Area" and submitted in partial fulfillment of the required for the degree of Masters of Sciences (Mechanical and Industrial Engineering) complies with the regulation of the university and meets the accepted standards with to originality and quality.

Sisay Petros Michael _____ _____

Name Signature Date

This thesis has been submitted for examination with approval as a university advisor.

Dr. Daniel Tilahun (Ph.D.) _____ _____

Advisor Signature Date

Natinel Abebaw (PhD Candidate) _____ _____

Co-Advisor Signature Date

Addis Ababa University

Addis Ababa Institute of Technology

School of Mechanical and Industrial Engineering

Rolling Contact Fatigue Life Analysis on Rail Track in Ethio-Djibouti Railway Line, Awash Area

By

Sisay Petros Michael

Approved by Board of Examiners

Daniel Tilahun (Ph.D.)	_____	_____
Advisor	Signature	Date
Natinel Abebaw (Ph.D. Candidate)	_____	_____
Co-Advisor	Signature	Date
_____	_____	_____
Internal Examiner	Signature	Date
_____	_____	_____
External Examiner	Signature	Date
Yilma Tadess (PD)	_____	_____
Dean of the School	Signature	Date
Ermias Tesfaye (PhD)	_____	_____
Director of Post Graduate	Signature	Date

Acknowledgements

I would like to express my sincere and heartfelt gratitude to my advisor, Dr. Daniel Tilahun (PHD), for his guidance and constructive comments in all the consultation I had with him in this thesis work.

I would also like to thank my co-advisor, Mr. Natnael and other staff who provide me with valuable material, moral and information in conducting this study. I am grateful to, Ethio-Djibouti railway shear company Manager, for providing me with all information relevant to this research.

Besides, I would like to express my gratitude for the Department of Mechanical and Industrial Engineering school, particularly for the design chair for facilitating my work. My deepest gratitude also goes to my friends who constantly provide me with support, encouragement and constructive ideas in the course this thesis work.

Finally, I would like to thank my loving family for their endless encouragement and support during the entire period.

Abstract

Now a day the railway transport is becoming the most important transportation sector in Ethiopia. This research paper presents the analysis of rolling contact fatigue damage of rail due to cyclic axle load between the wheel-rail contact using FEM for the existing and newly selected rail steel, for wheel utilizing the material structural steel with grade of R7T and the wheel profile of S1002. The Ethio-Djibouti Railway existing material is structural steel UCI54Kg/m profile grade of 9000A and newly selected material AS60Kg/m grade of AS1085.1, which is selected by using digital logic method. The three types of boundary conditions are: (1) straight, (2) transition, and (3) curved path in terms of track conditions. A three-dimensional geometry and FEA executed by using in SOLIDWORK 2019 and ANSYS 2019R3 Workbench respectively. In the newly constructed Ethio-Djibouti Railway, the RCF has been analyzed the commencing, if not it may cost more incidents, accidents, fatality and excess maintenance cost now and in the future. This research predicates the effect of axel load and train speed on the wheel-rail track for existing and newly selected material by using fatigue life, equivalent alternative stress, equivalent alternative strain, and total deformation. Finally, the fatigue life result showed that there is an increasing rail track crack initiation life cycle by 16.5%, 22.03% and 27.95% for the newly selected material AS60Kg/m grade of AS1085.1 at the straight, transition curve and circular curve respectively which is the most vital area in the rail track which would assist Ethio-Djibouti Railway heavy duty rail line to predicate the fatigue life resistance and pre-inspections ahead failure.

Key-words: Rolling Contact Fatigue (RCF), Fatigue Life, Finite Element Analysis (FEA), Rail Track, and Digital Logic Method.

Table of Contents

List of Figures

List of Tables

List of Abbreviation

FEM	Finite Element Method
RCF	Rolling Contact Fatigue
AALRT	Addis Ababa Light Rail Transit
ADI	Austempered Ductile Iron
RRD	Rolling Radius Difference
CAL	Constant Amplitude Loading
VAL	Variable Amplitude Loading
PD	Positive Decisions
FOM	Figure of Merit
FEA	Finite Element Analysis
ORR	Office of Rail Regulation
EDR	Ethio-Djibouti Railway
FCG	Fatigue Crack Growth
EDR S.C	Ethio-Djibouti Railway Shear Company

Nomenclature

γ_e	Effective or Equivalent Conicity
y	Lateral Displacement
γ	Wheel Conicity
R	Curve Radius
m	Mass of Axle (25(1+3%)) t = 25750 kg
a_c	Centrifugal Acceleration
V	Operating Speed of Vehicle
S	Maximum Superelevation
r_p	Radius of Curve at Any Point of Transition Curve Length
l_p	Length at Any Point of Transition Curve
L	Total Transition Curve Length
N_{Lw}	Normal Contact Force on The Left Wheel
N_{Rw}	Normal Contact Force on the Right Wheel
F^t_{Lw}	Lateral Contact Force on the Left Wheel Tread
F^t_{Rw}	Lateral Contact Force on the Right Wheel Tread
F^f_{Rw}	Lateral Flange Force on the Right Wheel
F_g	Gravitational Force Acting on the Wheelset
F_C	Centrifugal Force Acting on the Wheelset
Q_{RW}	Vertical Force on the Right Wheel
M_{LR}	Moment at Right Wheel
M_{LR}	Moment at Left Wheel
M_{CA}	Moment at the center of axle
W	Axle Weight
θ	Angle of attack on the left wheel
α	Angle of attack on the right wheel
φ	Superelevation angle or track cant angle
β	Rail inclination angle
μ	Coefficient of Friction
K	Constant

g	Gravitational Acceleration Constant
σ_a	Stress Amplitude
σ_f	The Fatigue Strength Coefficient.
N_f	Number of Cycles to Failure
Se	Stress Amplitude at Zero Mean Stress
σ_m	Mean Stress
Su	Ultimate Tensile Strength
γ_{pi}	Performance index,
C_t	Total cost of material/unit weight,
α_w	Weighting Factor
N	Total Number of Discussion

Chapter One

Introduction

1.1. Background

The history of rail transport begins almost around 600 B.C. With human or horse power and rails or guides made of stone or wood in ancient Rome and Greece. Railway wagon is believed that roads (or "trams") developed in Germany in the 1550s to facilitate the transportation of ore tubs to and from mines, utilizing primitive wooden rails. The first railway was completed in 1604 in British. Mechanized rail transport systems first appeared in England in the 1820s. These systems, using the steam locomotive, were vital to the industrial revolution and the development of export economies around the world [1].

The construction of railway lines in Ethiopia was first started in October 1897 under the regime of Emperor Menelek II of Ethiopia to the port of Djibouti. The first commercial service began in July 1901 from Djibouti to Dire Dawa. In 1915 the line reached Akaki, just 14 miles from the capital, and two years later it reached Addis Ababa. For a decade the railway transportation infrastructure in Ethiopia has been neglected, but is now a priority of the government of Ethiopia and the new network rail transport is under construction [1].

Considering the following parameters, like capacity, speed and environment, railway is a superior means of transportation in the world. Specifically, it has gained a crucial role in limiting traffic activities in heavily crowded regions. From this perspective, rolling contact fatigue (RCF) of railway components is an extremely important issue. Accidents caused by RCF can lead not only to personal injury and economic costs, but also to people commuting by car, which further increases traffic congestion, creates environmental problems and, ultimately, can lead to an increase in personal injury as car traffic is significantly more unsafe than Rail transport [2].

The wheel/rail interface is one of the most extremely important points that must be checked to determine the performance of a train and consider its safety. However, the calculation of the stress at the wheel / rail interface depends on the static and dynamic loading. The damage in this area is due to the train speed, the type of rolling stock, the cyclic axle loads, the track layout and track geometry parameters, the rail material

properties, the temperature or the humidity. Damage affecting fatigue mechanisms is one of the main factors influencing the prediction of railway track life. Fatigue causes unexpected fractures in the railhead and wheel tread. These defects can damage the rails due to the stress caused by the contact force. This research paper introduces the analysis of damage from rolling contact fatigue due to cyclic axle load on the curved rail and its fatigue life of Ethio Addis Ababa - Djibouti line in Awash district [3].

Fatigue cracks in rails can be initiated at the rail head, at the web and at the foot. Their growth can lead to the flaking off of material fragments, which impairs ride comfort and noise as well as the dynamic load increase for both tracks and vehicles. If not detected in time, the fatigue cracks can also cause the rail to break, which in some cases can lead to derailment. The possible failure scenarios including the nucleation and growth of potential fatigue cracks must be known as a necessary basis for assessing the damage tolerance. The structure of a conventional railway tracks as shown in figure below contains elements such as the rails, the sleepers including rail pad sand fastening elements, like clips, the ballast bed and the subgrade [4].

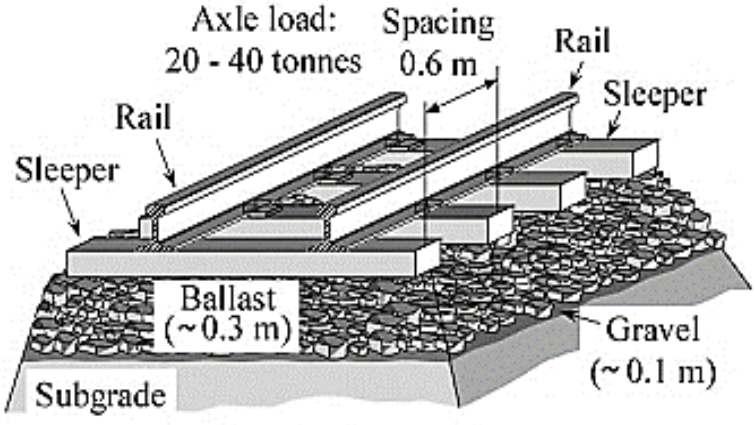

Figure 1.1 Basic elements of a railway track [4]

The rail is always subjected to higher loads, and thus wears and fatigue defects appear faster and more frequently. These degradations limit infrastructure productivity: wear might provoke speed restrictions or even load restrictions, more frequent checkups, increasing maintenance costs etc. In this way, the signs of wear and tear can lead to an improved design of rail vehicles and tracks, but also to improved inspection, maintenance and renewal guidelines for existing and future infrastructures of the rail way projects. Always the rail subject to different types wear exists, such as shelling, squats, head checks and corrugation [4].

The initiation wear and fatigue defects analyzing give detail information about the rail track. Afterward, we take various ways of preventives maintenances to prevent and control such type of degradation. As a result, we are reducing the occurrence of such type of failure. [4]

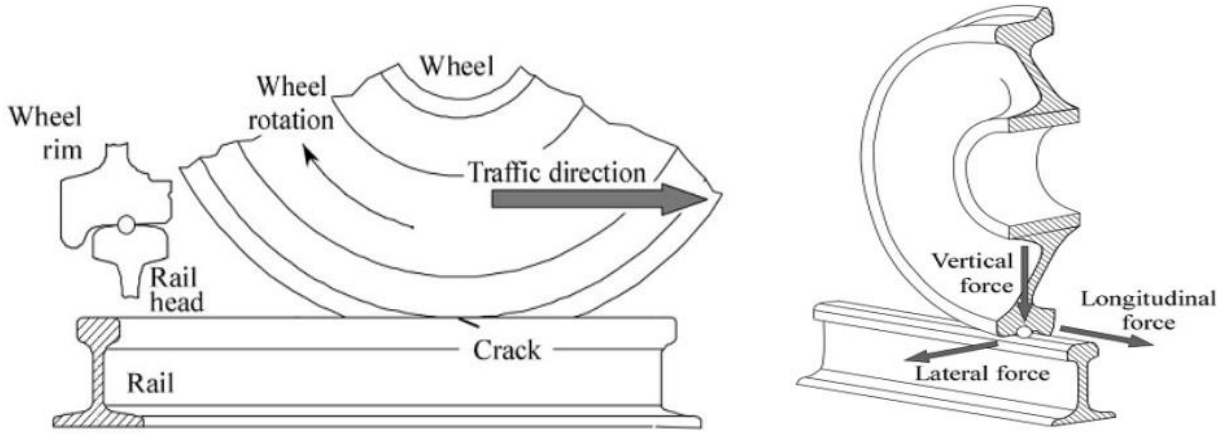

Figure 1.2 Force acting on rolling wheel.

Fatigue began to be recognized as a specific failure mode when the early railways began to suffer failures of axles, wheels, rails, boilers and other components. The railway accident causes due to axle of a locomotive broke. Different engineer demonstrated that cyclic stress ranges determined fatigue lives and that for steels at least, a fatigue limiting stress existed, below which fatigue lives were infinite. The so-called S/N curve, relating stress range to cycles to failure and the fatigue limit, still remain the basis of design against fatigue.

The fatigue is caused by the commencement and growth of cracks. The quantification of crack growth has become possible through the use of fracture mechanics, although the quantification of the initiation stage remains rather provisional. It is well recognized that fatigue initiation usually arises at a free surface, aided by some kind of stress concentration feature. The crack initiated at a predominantly severe stress concentrating feature, which then stops as it grows out of the zone of high local stresses into a bulk stress field which is insufficient to carry.

There are processes govern rolling contact fatigue crack initiation and crack propagation. The processes are determined by a number of factors including environmental conditions, rail and wheel profiles, track curvatures, qualities, lubrication practices, rail metallurgy, vehicle properties, track geometry errors, and rail grinding practices [5].

1.2. Statement of the Problem

When two solid bodies contact each other are mostly victim to the rolling contact fatigue, especially metal to metal contact like a wheel and rail. So, in the wheel-rail contact interface wear or crack initiation happen and also complete failure may happen through gradual operation service of the line due to rolling contact fatigue. And the effect of the cyclical axle load distribution causes the fatigue failure depending on the position of the rolling contact fatigue. Therefore, analyzing of the fatigue life of rail helps to prevent the sudden failure of the line and used to take measurements action at the crack initiation stage.

In this thesis paper the Ethio Djibouti Railway (EDR) in awash area is considered, and choosing this area mainly because of there is traffic loads which come from Hara -Woldia - Djibouti line and Addis Ababa-Djibouti line, the area weather condition (the higher temperature through year), there is a critical location such as curves (circular curve) and other different affecting factors makes the area unique. Also, from site investigation works there is a problem with some crack initiation shows on currently installed material due to cause of cyclic stress intensity as shown the area photo pictures in the figure 1.3 and this may further go through new material improvements. Due to the reasons this paper aim is analyzing the rolling contact fatigue analysis and upgrading/ improving new rail material based on the area real local conditions especially Awash area conditions.

This line is a heavy-duty line that means it is the backbone line for our economy of export-import goods and it must be kept from different defects as much as possible from the binging by preparing different studies based on our local real conditions. Depending on the type of cause and the position of the rolling contact fatigue, the type of distribution of the cyclic axle load and its effects differs accordingly. The effects of this cyclical loading are the initiation, propagation and failure of damage (cracks).

Therefore, this paper addresses the Ethio Djibouti Railway (EDR) rolling contact fatigue analysis, taking into account the Awash actual conditions for existing material and newly upgraded rail material to replace during the complete failure on the track. But this newly upgraded material has equal material cost with the existing one and also have higher / better strength. Thus, the rolling contact fatigue analysis intends to predict the service life of rail track at the wheel - rail interface by using finite element method (FEM) ANSYS 2020R1 software. In this case the fatigue results will help to know the minimum crack initiation life cycle of rail, minimize rail maintenance costs, improves safety, and can also provide clues about rail material.

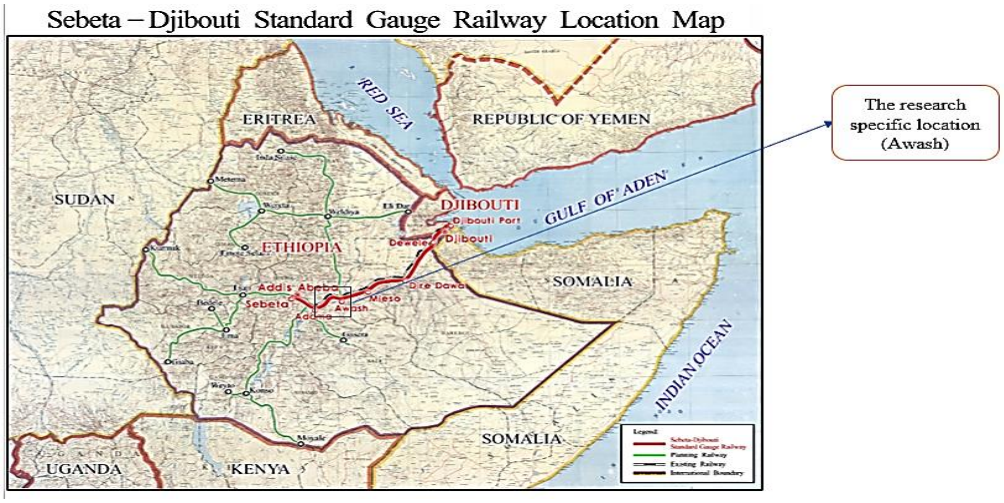

Figure 1.3 Awash standard gauge railway location map.

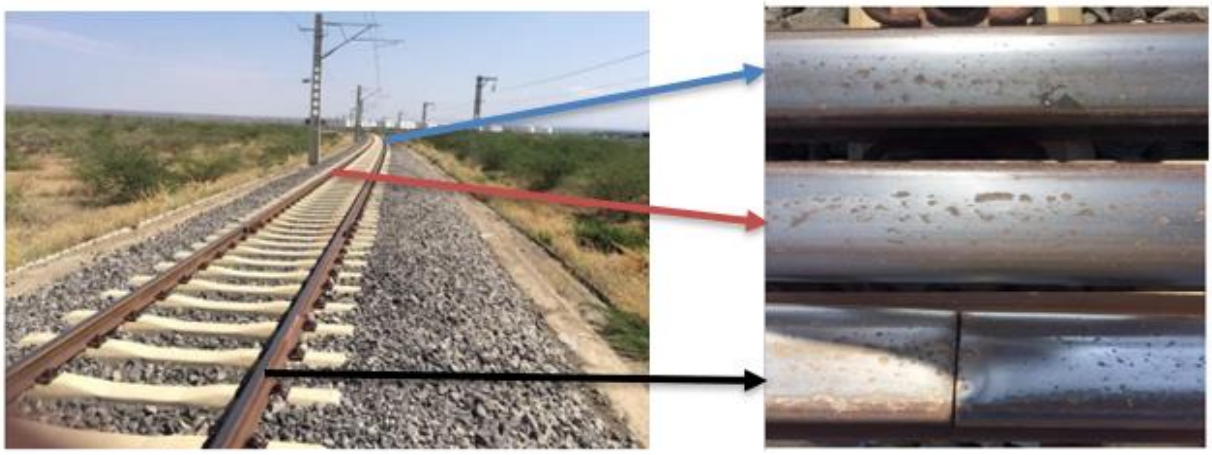

Figure 1.4 Awash area curve of Ethio-Djibouti Railway line and current appearance of rail track.

1.3. Objectives

1.3.1. General Objective

The main objective of this thesis is to analyze the rolling contact fatigue life on a rail in the train of the Ethio-Djibouti Railway of the Awash district using the finite element method.

1.3.2. Specific Objective

The specific objectives are:

- ✓ Prepare the appropriate geometrical model of rail track based on the EDR specifications.
- ✓ Analyze the fatigue life, equivalent alternating stress, equivalent elastic strain, total deformation, and fatigue sensitivity of rail track using ANSYS 2020R1 FEA software for both materials.

- ✓ Select appropriate structure material, which is stiff enough to withstand the loads applied on rail track (axle load, centrifugal force and frictional force) according to the three track conditions (straight, transition curve and circular curve).
- ✓ Compare both materials based on results obtained from ANSYS 2020R1 Workbench.

1.4. Scope of the Study

This thesis paper aims to determine the fatigue life for currently existing and newly selected material in Awash District heavy-duty rail track due to a cyclic axel loading condition in order to periodical inspection to maintenance and control rolling contact fatigue failure.

1.5. Significant of the Study

The work is very valuable for fatigue inspection, control, and regular maintenance planning of the rails for the EDR high-capacity rail line in Awash area.

1.6. Research Methodology

The data collection has been done from Ethio-Djibouti Share Company manuals and modeled by using SOLIDWORK 2019 software from the existing rail and wheel specification. Then the FEA performed on ANSYS 2020R1 to predicate fatigue life of the rail track checking the equivalent alternative stress, equivalent alternative strain, and total deformation. The methods and materials that will be used in order to fulfill the basic objective of this research study are:

1. Data collection (secondary data collection method which is grazing different published papers, and journals).
2. By using SOLIDWORKS 2019 software, a three-dimensional Wheel and Rail track model according to the EDR specification.
3. Model generation from SOLIDWORKS 2019 to ANSYS 2020R1 Workbench:
    - ✓ Define materials/material properties.
    - ✓ Generate a finite element model (mesh).
4. Solution generation stage:
    - ✓ Specify boundary conditions
    - ✓ Obtain the solution.
5. Review the results:

- ✓ Plot/list results (fatigue life of the rail track by checking the fatigue life, equivalent alternating stress, equivalent elastic strain, total deformation, and fatigue sensitivity).
- ✓ Comparing the results that is generated in straight, transition, and circular curve.

Figure 1.3 shows how the Rolling Contact Fatigue Life Analysis on Rail Track in Ethio-Djibouti Railway Line, Awash area performed by using finite element method steps.

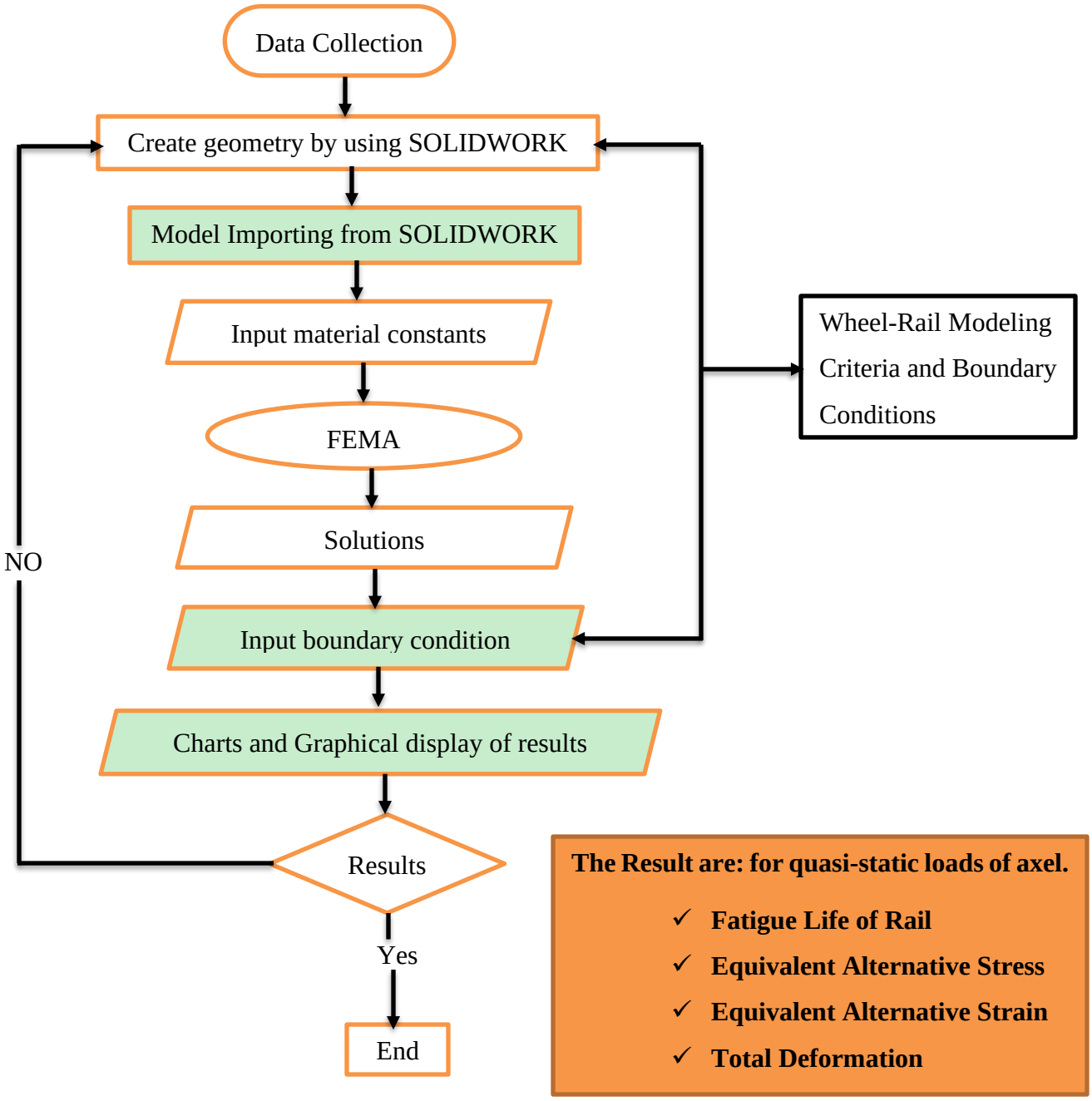

Figure 1.5 Conceptual flow chart of Ethio-Djibouti Railway rail track in Awash area.

1.7. Organization of the Thesis

The thesis is organized in to six chapters. In the first chapter, introduction and background of the thesis, objectives to be achieved, scope of the study and organization of the paper discussed; in the second chapter, related literatures are reviewed, how different researchers have carried out depending up on material, method and experiment they used; the third chapter discusses about materials, conditions and methods based on analytical analysis of the rail and wheel contact in related to fatigue life analysis in accordance with the three track conditions by using ANSYS 2020R1; in the fourth chapter, the analysis results are summarized and discussions are made based on the ANSYS 2020R1 analysis results. Finally, comparison made based on the solution; and the fifth chapter provides the conclusion based on the analysis results and suggests future work.

Chapter Two

Literature Review

2.1. Introduction

Review of literatures reveals that different previous work which helps for the guidance of work. These previous related works may be journals, conference papers, design works and books related to this paper. Selection of appropriate conditions, approaches and methodologies with these journals and other materials will strengthen for the successful accomplishment of the paper.

2.2. Rolling Contact Fatigue of Rail

Rolling contact fatigue (RCF) unescapable mode of failure observed in two surfaces which are rolling with virtual to each other. Rolling contact fatigue is the name given to crack growth and material damage produced as a result of high loads spread between two surfaces. The problem of rolling contact fatigue in rails became evident to a considerable extent in the 1990s. However, Railway Industry was obligated to treat RCF defects extremely after the 2000 Hatfield derailment in United Kingdom in which about 30 rail length crushed completely on the outer rail of 1500 m radius curve. According to Federal Railroad Administration's figures, in the eight years from 1995 to 2002, rolling contact fatigue was the core cause in 122 derailments, and it was suspected that RCF might have underwrote to 160 more derailments [6].

Rolling contact fatigue (RCF) is an assemblage of rail damages which manifest themselves on the surface or close to surface inside the rails due to overstretching of the rail material. The defects can first appear on the rail surface in the form of shells, knee bends and corner cracks or in the subsurface in the form of deep-seated shells. All these defects appear as a consequence of repeated overstretching of the surface or subsurface rail material by the millions of repetitive wheel-rail contact cycles. Two main physical processes that control the development of RCF defects are crack initiation and crack propagation in the rails. These in turn are determined by factors such as rail and wheel profiles, track curvatures, grades, lubrication practices, rail metallurgy, vehicle properties, track geometry errors, environmental conditions and many other factors. All these factors play an important part in the formation and development of RCF and, therefore, could be optimized to switch and diminish RCF defects [6].

2.3. Related Research Works

The relevant fracture mechanics questions for railway components. The topics covered include safety-relevant railway components such as axles, wheels and rails. This article introduces the prediction of the fatigue life and crack propagation in the railroad wheel due to the stress field caused by mechanical loads and the press assembly process of a railroad wheel. The influence of various parameters such as vertical loads, initial crack length and coefficient of friction between rim and hub / wheel on the service life of railway wheels is investigated using the proposed three-dimensional finite element model [7].

One of the most practical points about railways is damage to the wheel caused by different track conditions and thermal loads. The paper provides a method for calculating the fatigue crack growth and the thermal stress induced in the railway wheel. This thermal and fatigue loading is modeled and analyzed using ANSYS 2019R3 14.5 Parametric software and modeled with CATIA. The paper takes into account non-uniform cross-linking in a critical zone, fine cross-linking in a zone with high stress concentration and coarse cross-linking in sensitive areas [4].

Rolling Contact Fatigue (RCF) damage from high-speed wheels is a major factor affecting railway safety. In this article, a finite element model (FEM) of a transient high-speed rolling contact is presented, in which kinetic parameters are considered as initial conditions and the train is driven on a straight line at a speed of 300 km / h. Various geometric contact parameters such as lateral displacement and angle of attack are obtained. Using ABAQUS, a transient elastic-plastic 3D high-speed FEM of the wheel / rail rolling contact is then developed, taking into account the initial geometric parameters of the dynamic contact and the actual geometries of the wheel profile and the rail head as well as the elastic-plastic properties Model. This consideration makes the model very well suited to solving the transient 3D rolling contact behavior. The normal force, the creep force and the contact area in the contact field are solved and used in the fatigue model. And finally, the working conditions of the wheel / rail at 0.2 and 0.5 seconds easily reach the ratchet effect zone, and the fatigue index is large. The fatigue damage to the wheels is generally close to the nominal rolling circle [8].

The analysis of rolling contact fatigue damage due to cyclic axle load between wheel/rail and fatigue life comparison between experimental and ANSYS 12.0 results. It considers the straight rail track conditions only and Addis Ababa light rail transit parameters. The 3D model modeled with CATIA V5 software and analysis with ANSYS 12.0 software considering different loads [1].

According to the document, in United Kingdom a high-speed train causes an accident due to fracture and fragmentation of the outer rail on a curved section. The investigations revealed numerous fatigue cracks on the corner. The damage that penetrated the track and the foot of the rail resulted in adjacent cracks and the breakage of an entire section of rail [9].

The wheel-rail contact surface is on top of the rail, that is, the contact between two convex bodies called the non-conformal contact. Therefore, the contacting part of the wheel near the flange is concave, which means that the wheel and rail radii are close to each other and are called conformal contact. Head tests are groups of fine surface cracks on the running corner (gauge) of the rails with a typical spacing of 0.5 to 10 mm. When the adjacent, pre-damaged rail sections also failed, the damage was so great that it derailed with the tragic consequences mentioned [10].

The head test is preferably carried out on the track width of the outer rail in curved tracks, but is also found on switch rails or crossing rails, since rough plastic deformation occurs when the wheel is driven through due to friction. The cracks grow in the direction of traffic at a shallow angle to the tread, with lubrication playing an essential role. They can cause pieces of material to flake off between the cracks, but also growth and transverse cracks after a deviation of a few millimeters, which can lead to the splint breaking of the rail [11].

The collective effect of contact stresses (rail wheel contact strength) and traction surface and normal strength (due to powered axles or breaking) and shear resistance of the steel, which generates friction, determines the fatigue process in the moment of interaction [11].

Resistance to rolling contact fatigue RCF differs according to steel grade, in particular according to their grade. Indeed, a higher steel grade will reduce the number of contacts higher than the elasto-plastic stable state and thus will decrease RCF damage [12]. There are various manufacturers of wheel and rail materials industries in the world. Wheel and rail materials are quite similar in composition, differing slightly in the amounts of carbon, silica, and manganese in the steels used. It is widely known in tribology that pairs of similar metals can exhibit high adhesion and should generally be avoided in applications where they come into contact with each other, so changing one of these materials might reduce wheel and rail wear [13].

The contact resistance between wheel and rail is influenced by the choice of wheel and rail materials made of the base and inexpensive metals. Steel has one of the highest values of the modulus of elasticity. For

this reason, and because steel is relatively inexpensive and offers a very attractive combination of strength, ductility and wear resistance, almost all wheels and rails worldwide are made from pearlitic carbon-manganese steel, which has a lamellar structure of iron and iron carbide [14].

In general, car wheels tend to be lower in carbon and harder than heavy axle load freight vehicles. Steel with a Brinell hardness of about 300 is typically used for rails in straight track, while rails in the 340 to 390 Brinell hardness range are more likely to be used for curved rails where the stress environment is more severe. In recent times, the constantly growing constructions of high-speed railways and the increased axle loads have led to greater contact forces between the wheel and the rail [14].

Therefore, great efforts have been made to enhance the properties of rail materials to improve the performance and to reduce the cost [15, 16]. Almost all modern rails, due to their high modulus of elasticity and superior strength, ductility and wear resistance, are made from high C-Mn steels that have a fully pearlitic microstructure [21]. The development of pearlitic rail steels has progressed since the invention of the conventional rail and these efforts are mainly focused on either increasing the C content to a uniform hypereutectoid level or further refining the pearlitic lamellar structure either by alloying or heat treatment [16, 17, 18].

A number of material concepts were pursued for passenger traffic up to 160 km / h. Particular attention was paid to the testing of bainitic, barren ductile iron (ADI) for its suitability as a wheel material for rail vehicles [28]. ADI shows a combination of higher wear resistance and high fatigue strength with high ductility compared to other types of cast iron. As a powerless “side effect”, the graphite nodules contained in the cast iron microstructure act as a lubricant on the contact surface between the two friction partners and thus reduce their wear. At the same time, the graphite inclusions cause a dumping effect about three times as strong as steel, which means that ADI wheels promise a reduction in rail traffic noise. Material composition and heat treatment were coordinated in such a way that tensile strengths of approx. 1000N / mm2 were achieved. During the course of the project, wheels were manufactured for test purposes by a foundry and a wheelset manufacturer. In addition to the usual laboratory tests to assess the material and the manufacturing quality of the wheels, special attention was paid to the evaluation of the ADI wheel with regard to its fracture mechanics [20]. In the end, it was found that the critical crack size determined by fracture mechanical calculations can be safely and reliably diagnosed using non-destructive testing methods [20, 21].

According to the study there are parameters that influence the stress state in rails. Some of the parameters are [12]:

- ✓ Axle load: directly influences state stress;
- ✓ Asymmetric loadings: the strain will also be posed asymmetric on the rail head and the rail wheel contact will get irregular and discontinuous;
- ✓ Wheel diameter including mismatched wheel diameters;
- ✓ Track gauge: "tight gauge in tangent track provokes gauge corner contact, hunting of the bogies and thus rolling contact fatigue. In curves, controlling wide gauge is essential for mitigating low rail damage associated with hollow wheels";
- ✓ Wheel transversal profile;
- ✓ Rail transversal profile and profile irregularities;
- ✓ Can't excess/deficiency: wheel sets will tend to shift and to heavily offset to the inner or outer rail respectively;
- ✓ Welds: at too soft/flexible welds a dip will be produced or, in case too hard high spots will be produced this will both leading to geometry irregularities;
- ✓ Hunting of wheel set in tangent tracks;
- ✓ String lining forces on grades tie plate cut in and poor fastening; and
- ✓ Skewed trucks;

Generally, the study reveals basic parameters as: curvature radius, cant deficiency, section type, the section of the rail and the traffic and rolling stock type and traffic structure. If there is a more the rail the support system is stiff, the less it will absorb shocks elastically as a result there is a more subject to the head-checks. According to the parameter particular area of the rail's elements are more exposed to wear phenomena and to rolling contact fatigue due to dynamics effects. But in curves and switches, wheel rail contact area is smaller and flange contact toward the gauge corner can increase tangential forces and slip. [12]

An RCF-related failure cannot be estimated from normal contact pressure alone. It is a mutual dependence of tensile forces and frictional heat. The non-conformity of rail-wheel contact produces creep age which is further aggravated by hunting oscillation of wheels as well as creating temperature rise. As a result, they affect the contact stress to encourage plastic deformation, leads to plastic strain on the material which is

cascaded as layers. Initiates crack formation due to repeated stress at the contact in order to release the plastic deformation energy. Once cracked, its expansion activates the RCF defect and leads to disaster [6].

This article presents the analysis of rolling contact fatigue in wheel-rail contact based on the actual conditions and specifications of Addis Ababa Light Rail Traffic (AALRT). Also take into account different track conditions (straight, transition and circular curves). The elastic-plastic 3D finite element model (FEM) is developed using the CATIA software and the wheel-rail rolling contact fatigue analysis using the ANSYS 2019R3 software. The aim of this thesis is to investigate the effect of rolling contact coefficient friction on the fatigue life of the wheel-rail interface on the straight, transition and circular curve of the Addis Ababa light rail traffic [22].

Chapter Three

Materials, Conditions, and Methods

3.1. Material Selection for Rail Track

3.1.1. The Existing Material of EDR

Currently EDR S.C the wheel and rail track material used based on China National Railways standard which is UIC54 kg/m and S1002 profile respectively. Most of time Wheel and rail materials are quite similar in composition and differ slightly in the amounts of chemical composition in the steels used. The existing rail material specification with the grade of 9000A concerning their chemical compositions rails have great varieties of carbon, manganese, chromium and silicon contents depending on their requirements. Since the rails have to withstand the shock loads, friction and stress of goods, they should have sufficient strength, hardness, toughness and good welding performance. Similarly, the wheel material property is considered with the R7T wheel steel grade and These materials follow the standard EN13262 with a fine-pearlitic microstructure [23]. And the existing rail and wheel material chemical composition and mechanical properties are indicated from Table 3.1 to Table 3.4.

Table 3.1 Chemical compositions of rail steel

Rail materials Compositions (9000A)	C	Si	Cr	Mn	P	S	Al
	0.65-0.76	0.15-0.58	--	0.70-1.20	<0.04	<0.025	<0.010

Table 3.2 Mechanical properties of rail steel

Rail material property (9000A)	Ultimate tensile strength (MPa)	Yield strength (MPa)	Young modulus (GPa)	Poison Ratio	Density (kg/m)	Awash average temperature (c^o)
	900	>580	207	0.3	7800	25.5

Table 3.3 Chemical properties of wheel steel

Wheel materials compositions(R7T)	C	Si	Mn	Mo	Cr	Ni	S	P	V	Fe
	0.52	0.40	0.80	0.08	0.30	0.30	0.015	0.020	0.06	Bal.

Table 3.4 Mechanical properties of wheel steel

Wheel material property (R7T)	Ultimate tensile strength (MPa)	Yield strength (MPa)	Young modulus (GPa)	Poison Ratio	Density (kg/m)	Awash average temperature (c^o)
	940	>520	207	0.3	7800	25.5

In addition, from the different literatures the rail steels of about 300 Brinell hardness is typically used for rail in straight track, while rail in the hardness range 340 to 390 Brinell tends to be used for curved track where the stress environment is more severe. Recently, the ever-growing constructions of highspeed railway and the increased axle loads have led to larger wheel/rail contact forces. [13] Therefore, great efforts have been made to enhance the properties of rail materials to improve the performance and to reduce the cost

Finally, the paper intention is in addition to giving waring of line at the crack initiation stage and to take action in preventive maintenance before the catastrophic failure and if it possible giving a suggestion on new material when the rail track need to be replaced for the concerned body.

3.1.2. The New Material Selection

Number of Positive Decisions for Rail Track Material Selection

The material selection methods are the cost per unit property and the digital logic method (DLM).These methods have their own way of selecting of material, (1) DLM consider the following parameters: density, yield tensile strength, ultimate tensile strength, module of elasticity and Poisson's ratio and (2) Cost per unit property according to the material strength property [21, 24].

The DLM used to select the material for the wheel and rail rails from the multipoint view are density, tensile strength, yield point, elastic modulus and Poisson's ratio. To select the material, the five positive decisions values have a great impact on the wheel rail track related with regard to strength, and safety of the passengers [21, 24].

Number of Positive Decisions (PD)

Density, yield strength, tensile strength, modulus of elasticity and Poisson's ratio are a factor in choosing the optimal material for wheel and rail tracks. The number of possible decisions depends upon the number

of properties. The number of properties is five (n = 5). The number of possible decisions calculated by Equation 3.1:

$$N = \frac{n(n-1)}{2} \text{----------(3.1)}$$

Therefore; the number of possible decisions, $N = \frac{n(n-1)}{2} = \frac{5(5-1)}{2} = 10$

To compare the two properties, the more important properties assigned 1 and the less important assigned as 10. The number 1 through 0 shows that the importunateness and rank of the material property when value 1 has a larger ranking and 10 has less rank in the material property. The properties and decision numbers are listed in Table 3.3.

Table 3.3 Evaluation of positive factor

Material Properties	Decision Numbers										Positive Decisions (PD)
	1	2	3	4	5	6	7	8	9	10	
Density	1	0	1	0	0	0	1	0	0	0	3
Yield tensile strength	0	0	1	0	1	0	0	0	0	0	2
Ultimate tensile strength	0	1	0	1	0	0	0	0	0	0	2
Module of elasticity	1	0	0	1	0	0	0	0	0	0	2
Poisson's ratio	0	0	0	0	0	0	1	0	0	0	1
Total Number of Decision (N)											10

Weighting Factor (α_w) Analysis

The weighting factor obtained from the PD Table 3.4, in which each of the properties is compared to each another. A weighting factor for each property is obtained by dividing the number of PDs for each property into the total number of possible decisions as seen in Equation 3.2 [21, 24].

Mathematically, $\alpha_w = \frac{PD}{N}$ ----------(3.2)

Table 3.4 Evaluation of weighting factor for wheel and rail track

Material Properties	Positive Decision (PD)	Weighting Factor, $\alpha_w = \frac{PD}{N}$
Density	3	0.3
Yield tensile strength	2	0.2
Ultimate tensile strength	2	0.2
Module of elasticity	2	0.2
Poisson's ratio	1	0.1
Total (N)	10	1.0

Scaled Property Value

To calculate the scaled property value (see Equation 3.3 and Equation 3.4) the following points are needed, beneficial (where higher value is required) and non-beneficial (where a lower value is required) attributes. For the evaluation of the scaled property, materials with a higher modulus of elasticity, a higher tensile strength and a higher yield strength are advantageous, and the highest value is evaluated as 100, and the yield strength, Poisson's ratio and density are not advantageous for wheel and rail rails Therefore, its lowest value is considered 100. Scaled property values are calculated using the following equation [21, 24]:

$$\text{For beneficials: Scaled property value} = \frac{\text{Number value of property}}{\text{Maximum value in the list}} * 100\% \text{----------(3.3)}$$

$$\text{For non-beneficials: Scaled property value} = \frac{\text{Minumum value in the list}}{\text{Number value of property}} * 100\% \text{----------(3.4)}$$

Note: The following material selected from different journals, research papers, and selected as number one candidate material.

Table 3.5 Properties of candidate materials for wheel and rail track [17, 25]

Materials	Number of properties				
	1	2	3	4	5
	Density, Kg/m^3	Yield tensile strength, MPa	Ultimate tensile strength, MPa	Module of elasticity, GPa	Poisson's ratio
54E1 (R350HT)	7800	511	1175	210	0.3
AS60 (AS1085.1)	7800	780	1130	210	0.3
U71Mn (ISCR70)	7800	540	880	210	0.3

The higher value of the tensile strength, the yield strength and the modulus of elasticity are 1175MPa, 780MPa & 210GPa. The lowest value for density and Poisson's ration is 7850Kg/m3 and 0.3. After seating in the above values in the above Equation 3.3 and Equation 3.4 the scaled property evaluated:

Table 3.6 Scaled property of candidate materials for wheel and rail track

Materials	Number of properties				
	1	2	3	4	5
54E1 (R350HT)	100	65.51	100	100	100
AS60 (AS1085.1)	100	100	96.17	100	100
U71Mn (ISCR70)	100	69.23	74.89	100	100

Performance Index

Performance index (γ_{pi}) used in the ranking of the material based on their values and calculated by using Equation 3.5. The performance index is analyzed by summing the values of the weighting factor and the scaled property values for all relevant properties. Then the performance indices become [21, 24]:

$$\gamma_{pi} = \sum_{i}^{n} \alpha_{wi}\beta_i \text{----------(3.5)}$$

Table 3.7 Performance index of candidate materials for wheel and rail track

Materials	Weighting factor (α_w) x Scaled property (β)					Performance index, $\gamma_{pi} = \sum_{i}^{n} \alpha_{wi}\beta_i$
	1	2	3	4	5	
54E1 (R350HT)	30	13.1	20	20	10	93.1
AS60 (AS1085.1)	30	20	19.23	20	10	99.23
U71Mn (ISCR70)	30	13.85	14.9	20	10	88.75

A Figure of Merit (FOM)

The performance index evaluated in the above indicates that the material selection by considering the material strength property without material cost. It is important to consider the cost of material before making any final decision. However, if there are so many mechanical properties to be considered, the cost of material considered separately to modify the material performance index. Therefore, by considering the market price of the material other than the mechanical properties and, the FOM become by using Equation 3.6 [21, 24]:

$$FOM = \frac{\gamma_{pi}}{C_t \rho} \text{----------(3.6)}$$

Where: γ_{pi} – Performance index,

C_t – Total cost of material/unit weight,

ρ – Density of the material

Table 3.8 FOM of candidate materials for wheel and rail track

Material	C_t (US$/Kg)	ρ (Kg/m^3)	γ_{pi}	$FOM = \frac{\gamma_{pi}}{C_t \rho}$
54E1(R350HT)	0.7	7800	93.1	0.0171
AS60 (AS1085.1)	0.7	7800	99.23	0.0182
U71Mn (ISCR70)	0.9	7800	88.75	0.0126

Ranking

Different mechanical and physical properties combined in terms of material cost to select the appropriate material for the wheel and rail track. Therefore, the material that was having higher numerical value will have more influence than lower value by its weighting factor. The ranking of the material with respect to figure of merit evaluated from the performance indices, total cost of the material per unit weight and density of the material values and the ranking take place based on the material FOM descending order as seen in Figure 3.1 [21, 24].

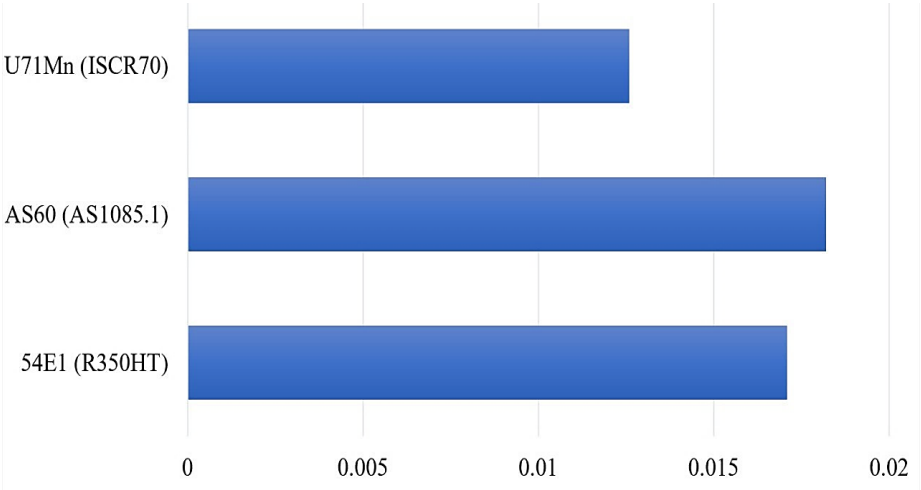

Figure 3.1 Figure of merit for the selected material

Table 3.9 Ranking of candidate material for wheel and rail track

Material	C_t (US$/Kg)	ρ (Kg/m^3)	γ_{pi}	$FOM = \frac{\gamma_{pi}}{C_t \rho}$	Rank
54E1(R350HT)	0.7	7800	93.1	0.0171	2
AS60 (AS1085.1)	0.7	7800	99.23	0.0182	1
U71Mn (ISCR70)	0.9	7800	88.75	0.0126	3

From Table 3.9 and Figure 3.1 shows that AS60 (AS1085.1) has the higher value of the figure of merit, which indicates that the total cost of the material per unit weight is lower, has approximately a lower material density and a lower value for the third performance index. Therefore AS60 (AS1085.1) has a larger figure of merit and used for the wheel and rail track with the following mechanical property as shown in Table 3.10.

Table 3.10 Revision of property of wheel and rail track

Material property	AS60 (AS1085.1)
Density, Kg/m^3	7850
Ultimate tensile strength, MPa	1130
Yield tensile strength, MPa	780
Modulus of elasticity, GPa	210
Bulk modulus, GPa	175
Shear modulus, GPa	80.7
Poisson's ratio	0.3
Elongation at break	9%
Cost (US $/Kg)	0.7
Brinell hardness	340

3.2. Standards Collected Data from the Company

3.2.1. General Ethio-Djibouti Railway Line Wheel-Rail Specifications and Dimensions.

Based on Ethio-Djibouti railway share company standard the real wheel-rail specifications and dimensions are given in the Table 3.11. Which are collected from the company.

Table 3.11 Ethio-Djibouti railway heavy duty line specifications and dimensions

Type of rails for main lines and depot	UIC 54 kg/m
Track gauge	1435 mm
Rail cant	1in 40
Minimum radius of horizontal curve	800 m
Maximum super elevation of curve	120 mm
Wheel rolling diameter	840 mm
Sleeper space / sample rail track length	760 mm
Transverse radii of the rail head	300 mm

(**Source:** Ethio-Djibouti Railway Shear Company, Technical Specifications of Vehicles July 2013.)

3.2.2. General Ethio-Djibouti Heavy Duty Railway Line Vehicle Specification

Based on local conditions in Ethiopia and Djibouti, the line's role in Ethiopia's railway network, the maximum operating speed of passenger trains on the route is suggested to be set at 120km/h, and that of freight train is to be set at 80km/h. in this study we consider the passenger train only for simplicity and here the operating speed of the train is 120km/h. the total weight of vehicle described in the Table 3.12.

Table 3.12 Ethio - Djibouti railway heavy duty line vehicle weight specifications

Loads	Car body weight	Passenger weight	Total weight
Empty vehicle (t)	44	0	44
Rated passenger capacity (t)	44	15.24	59.24
Overload capacity (t)	44	19.02	63.02
Axle load (t)	$\leq$ 25(1+3%) tons		

(**Source:** Ethio-Djibouti Railway Shear Company, Technical Specifications of Vehicles July 2013.)

3.3. Geometric Modelling

The geometric 3D modeling is done with the software SOLIDWORK 2019. This is done by taking the actual data from a selected Ethio-Djibouti Railway wheel and rail track specifications. The specifications are based on S1002 wheel and UIC54 rail track profiles. Thus, the radius of curvature of the rail head is 300 mm. For this model a piecewise rail is taken with length of 760mm that is the standard average

distance between two sleepers. The assembled drawing of wheel and rail track are created using SOLIDWORK 2019 modeling software as from Figure 3.2 and Figure 3.3.

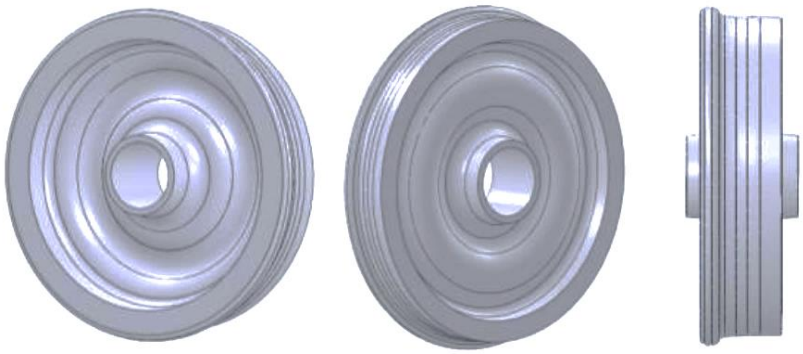

Figure 3.2 The 3D wheel model drawings showing in different views poison in SOLDWORK 2019 software.

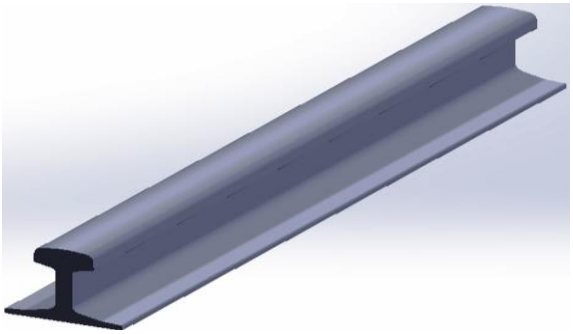

Figure 3.3 The 3D model of rail track in SOLIDWORK 2019 software.

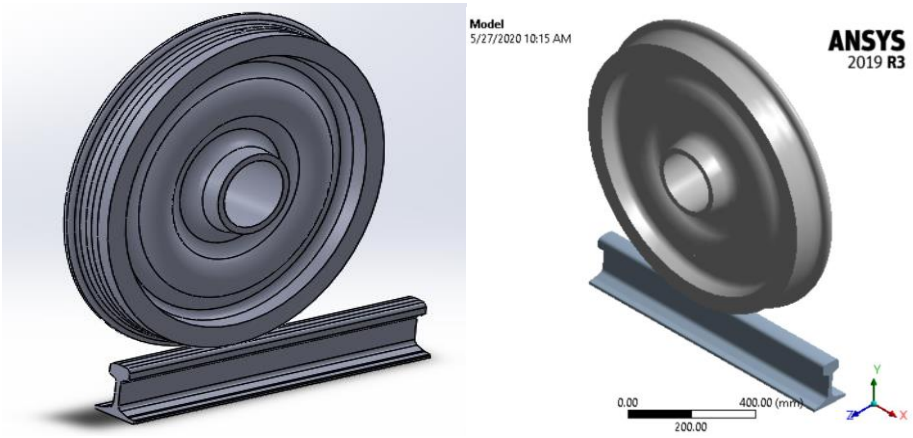

(a) (b)

Figure 3.4 The 3D model of wheel-rail assembly drawing in (a) SOLIDWORK 2019 and (b) ANSYS 2020R1 software.

3.4. Mathematical Modelling

This section is focuses on force analysis of wheel-rail track interference (contact point of wheel-rail track), to analyze rolling contact fatigue failure of rail track using ANSYS 2020R1 simulation under this section normal force, gravitational force, centrifugal force, vertical and lateral (horizontal) forces are calculated considering track condition like curved track specifically in awash curve.

3.4.1. Kinematic Analysis of the Wheelset on Curved Track

The kinematic analysis is concerned with how the forces on a railcar while cornering can cause both maximum and minimum speeds on curved sections of the route. The railroad wheelset features like coning of the tread and flange, affect the dynamics of the railcar on the curved track. Every kinematic analysis of the wheelset and the railcar begins with a description of the geometry of the wheelset. The track geometry is composed by a straight segment, followed by a circular curve with radius R and by a tangent segment. The lengths of the track segments are $L_1 = L_3$ straight segment and L_2 is circular curve length. The dashed lines represent the transition curves length [25].

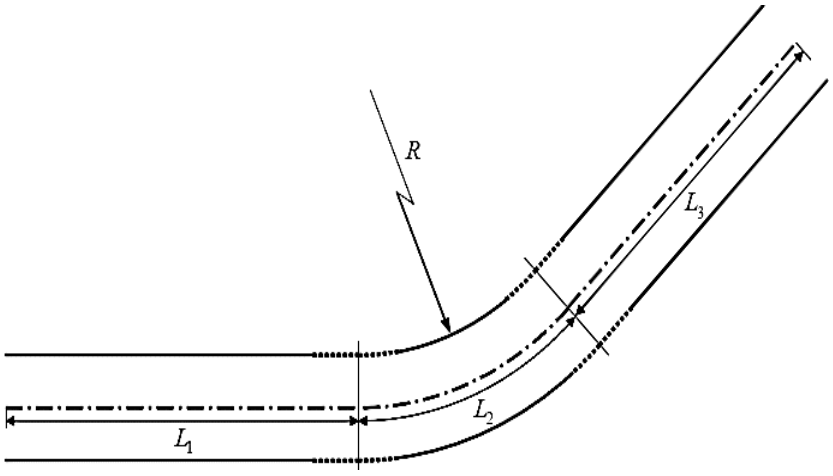

Figure 3.5 Curved track geometry

The effect of a wheel set with conical wheels in a curve was intuitively understood early in the development of the railways [26]. A simple geometric relationship between the outward movement of wheelset ‘y’, the radius of the curve ‘R’, the wheel radius ‘r’, the distance between the contact points ‘2b’ and the conicity ‘γ’ of the wheels can be derived in order to obtain pure rolling:

$$\frac{r+\Delta r}{r-\Delta r} = \frac{R+b}{R-b} \quad \text{---------- (3.6)}$$

Therefore, the required rolling radii difference in wheelset for passing a curve without slippage can be calculated according to the formula.

$$\Delta r = \frac{2br}{R} \text{ ---------- (3.7)}$$

An important feature of the wheel-rail contact is the rolling radius of a wheel at the point of contact [30]. This radius can be different for the right and left wheel when a wheel set is moving along a track.

When a wheel set is in a central position with respect to the track, the rolling radius of the left and right wheels is the same, namely r1 = r2 = r. An instantaneous difference between the rolling radius of the right and left wheels can be defined as a function of the lateral displacement "y" of a wheelset with respect to its central position, as shown in the following figure, according to:

$$\Delta r = 2y\gamma \text{ ---------- (3.8)}$$

Rolling Radius Difference (RRD) is one of the main characteristics of wheel / rail contact, which defines the behavior of a wheelset on a rail. For example, in order to pass a sharply curved track without slip between wheels and rails, a suitable RRD of the wheelset is required. Avoiding slip is important from the point of view of wheel and rail wear.

In general, the rolling radius difference is a nonlinear function of the lateral displacement 'y' of a wheelset, which from geometrical considerations and taking into account equation 3.8 the relationship between the lateral displacement y of the wheelset and the curve radius 'R' can be derived as follows:

$$y = \frac{rb}{\gamma R} \text{ ---------- (3.9)}$$

Where 'γ' is the wheel conicity and the effective or equivalent conicity $'\gamma_e'$ is determined at a certain lateral displacement $y = \bar{y}$. It should be noted that for an innocently conical wheel the corresponding conicity is like to the cone angle of the wheel, i.e. $\gamma_e = \gamma$.

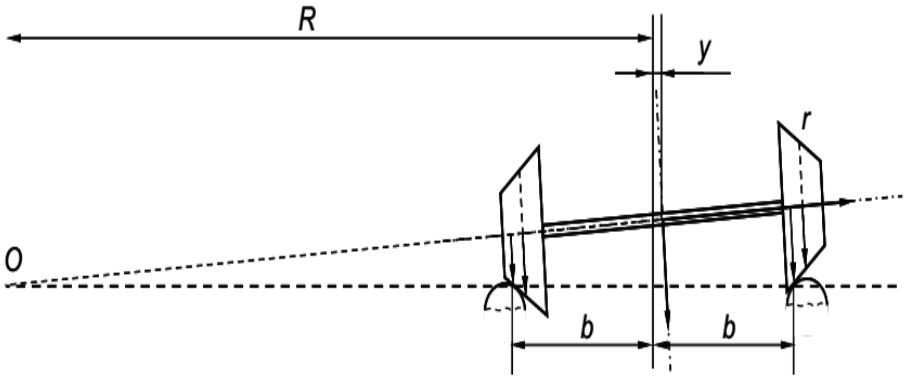

Figure 3.6 Rolling of a coned wheelset in a curve [26].

Therefore, wheelset will be able to move outwards to achieve pure rolling only if either the radius of curvature or the flangeway clearance is sufficiently large. Otherwise, a realistic consideration of curving requires analysis of the forces acting between the vehicle and the track.

Let us consider Equation 3. assuming that the flange play is sufficient and that the distance between the contact points "2b" is equal to the track width 2b = S = 1.5 m. The required values of the RRD for passing curve with radius *R* without slippage are must produce the required RRD within given wheel/rail profile combinations.

Table 3.13 Sample Required RRD (Δr) for curves with radius *R*.

R, m	Δr, mm (r=0.331m)	Δr, mm (r=0.390m)	Δr, mm (r=0.460m)	Δr, mm (r=0.500m)
3000	0.166	0.195	0.230	0.250
2000	0.248	0.293	0.345	0.375
1500	0.331	0.390	0.460	0.500
1000	0.4965	0.585	0.690	0.750
500	0.993	1.170	1.380	1.500
300	1.655	1.950	2.300	2.500
150	3.310	3.900	4.600	5.000
100	4.965	5.850	6.900	7.500
50	9.930	11.700	13.800	15.000
30	16.550	19.500	23.000	25.000
25	19.860	23.400	27.600	30.000
18	27.583	32.500	38.333	41.666

From Equation 3.7 and Table 3.13, it is clear that the wheels with smaller radius require smaller RRD to pass curve in comparison with wheels of larger radius. In the case of Awash curve radius R = 800m and wheel diameter of 840m, r = 0.420mm the required values of the RRD for passing curve using equation 3.7:

$$\Delta r = \frac{2br}{R}$$

$$= \frac{1500*0.420}{800}$$

$$= \frac{630}{800} = \mathbf{0.787}\boldsymbol{mm}$$

3.4.2. Curving and the Role of the Flange

According to Newton's second laws of motion, the motion of the train due to the axle load is an inertial force. When a train accelerates or changes its speed, the acceleration is accompanied by a force according to the following equation:

$$\vec{F} = m\vec{a} \text{ ---------- (3.10)}$$

Where m - Mass of the object,

W - Weight axel,

g - Gravitational acceleration constant = 9.81m/s^2,

In the case of circular curve movement at constant speed, the change in direction of the tangential speed results in an acceleration radially inward to the center of rotation. With this centripetal acceleration (and the associated force) the object remains in motion on a circular path. However, the inertia of the object resists this change and therefore always acts in the opposite direction of the acceleration or in this case radially outward from the center of the circle. With a railcar and attached wheelset going around a curve, it is the inertia of the train that leads to instability and guidance problems such as overturning or derailing. With a stable curvature, lateral forces between the wheels and the rail ensure the same centripetal acceleration [27]:

$$a_c = \frac{V^2}{R} \text{ ---------- (3.11)}$$

Where V - Tangential velocity.

R - Radius of the curve.

The centripetal force associated with centripetal acceleration keeps the train in a circular, or curved path; however, the train's inertia acts in the contrary path of centripetal acceleration. In other words, the centrifugal force is simply the train's inertial resistance to the centripetal acceleration around a curve and can be calculated using Equation 3.11. For a locomotive train, the centrifugal inertial load is given by:

$$F_c = m * a_c = m * \frac{V^2}{R} \text{ ---------- (3.12)}$$

Where F_c - Centrifugal inertial loading/load

m - Mass of axle (25(1+3%)) tons = 25.750 Tone = 25750Kg

a_c - Centrifugal acceleration

V - Operating speed of vehicle

R - Rail track curve radius

Therefore, based on this formula the centrifugal force for single wheelset at the minimum track curve radius in EDR high-performance railway line in Awash area curve, R=800m, is given as:

$$F_C = m * a_c = \frac{V^2}{R}$$

$$F_C = 25750\text{Kg} * \frac{(33.33\,{}^{m}/_{s})^2}{800\text{m}} = \mathbf{35756.74N = 35.74KN}$$

The side forces between the wheels and the rail have to react against the centrifugal inertial load in order to keep the train on the rails. If the centrifugal inertia load is too high, the locomotive begins to tip over. The flange of the wheel locks into the rail and the locomotive begins to turn. Because of this, the flanges are on the inside of the wheels.

3.4.3. Contact Forces During Curve Negotiation with Flange Contact

When passing the curve, the movement of the rail vehicle is controlled by a contact mechanism between the wheel and the rail, so that the vehicle can follow the geometric arrangement of the track. As the vehicle tends to follow its initial running direction the wheelset will move outward to the outer rail as shown in Figure 3.8 (a) [19].

When it comes into the curve track which cause different rolling radius between the inner and outer wheel, due to the conicity of the wheel, the outer wheel has larger rolling radius and the wheelset will naturally turns following the track curve as both wheels are connected by a rigid axle. In the sharp curve the wheelset moving further outward until the flange of the outer wheel touches the outer rail and gives bigger turning force. However, this situation can lead to the derailment accident when the lateral force is big enough to force the flange moving further outward and climbs the outer rail Figure 3.8 (b) [19].

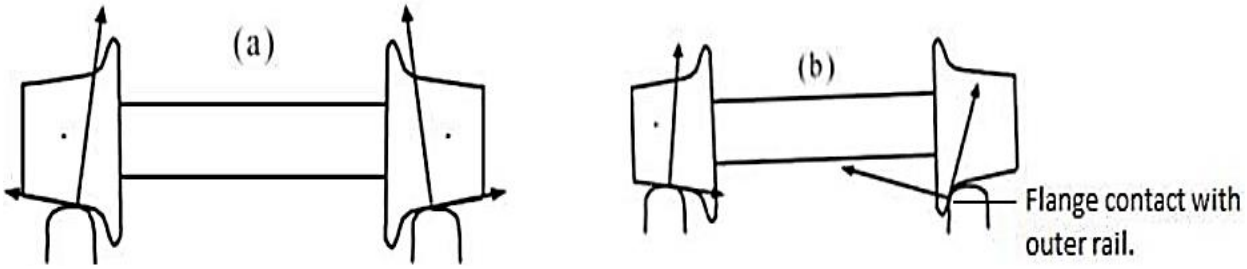

Figure 3.7 (a) Wheelset central position. (b) Wheelset position when passing the curve [19].

In the design phase of a new rail vehicle, it is important to assess the risk of derailment in order to ensure the safety of the vehicle against the derailment accident. Flange climbing derailment is the typical derailment occurred when the rail vehicle passing the curve. The sensitivity of a railway vehicle against flange climbing derailment can be measured by Nadal's criterion [10, 11]. If the derailment coefficient is lower than critical value calculated using Nadal's equation, then the derailment is justified to be "unlikely happen". The derailment coefficient is given in the form of the lateral force (Y) generated at the point of contact between the wheel flange and the rail, divided by the vertical force (Q) at the same point as shown in Figure 3.9.

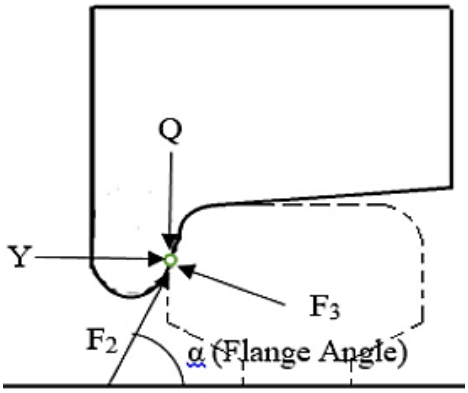

Figure 3.8 Forces at flange contact point [26].

According to the Nadal's formulation the critical value of Y/Q is defined by the flange contact angle and the wheel-rail friction coefficient as shown in the Equation (3.13).

$$\left(\frac{Y}{Q}\right)_{crit} = \frac{\tan\alpha - \mu}{1 + \mu\tan\alpha} \text{ ---------- (3.13)}$$

For standard wheel profile in Indonesia, which has 67° flange contact angle, and friction coefficient of 0.3 the critical value of Y/Q is 1.2. However, for the design purpose maximum value of 1.0 is commonly chosen [19].

The railroad tracks generally consist of straight (or tangential) sections, transition curves and circular curves. The horizontal curves have a constant radius and are defined in the tracks described in the horizontal plane. The radius of the curve used is defined in relation to the track center line. The old infrastructure had yet to be upgraded to allow for faster speeds and higher traffic flows after the accident occurred on a flat curve. In modern industrial practice, many tracks are designed so that rails are not flat on curves. Instead, the curve is banked so that the outside rail on a curve is elevated higher than the inside rail. In addition, when traveling in horizontal curves, rail vehicles are influenced by centrifugal forces which act in a direction away from the center of the curve to tip the vehicle over. The sum of a vehicle's weight and its centrifugal forces produced a resulting force that was directed towards the outer rail. To counteract this force, the outer rail is raised in a curve. The difference in height between the outer and inner rail level is called the cant or cant "S". This superelevation (or cross level in the US) is usually characterized by the height difference between the tops of the rails, but can also be measured in terms of angle or cant. The relationship between the cant angle and superelevation height, 'S' is dictated by the rail contact distance according to simple right-triangle geometry [19].

$$\text{Sin}\varphi = \frac{s}{2b} = \frac{120\text{mm}}{1505\text{mm}} = 0.0797342 \text{ ---------- (3.14)}$$

Where, the maximum superelevation is, S = 120mm, and track gauge plus rail head width (i.e., distance between contacts) is, 2b = 1505mm (1435mm + 70mm).

Therefore, $\boldsymbol{\varphi = 4.573^{o}}$

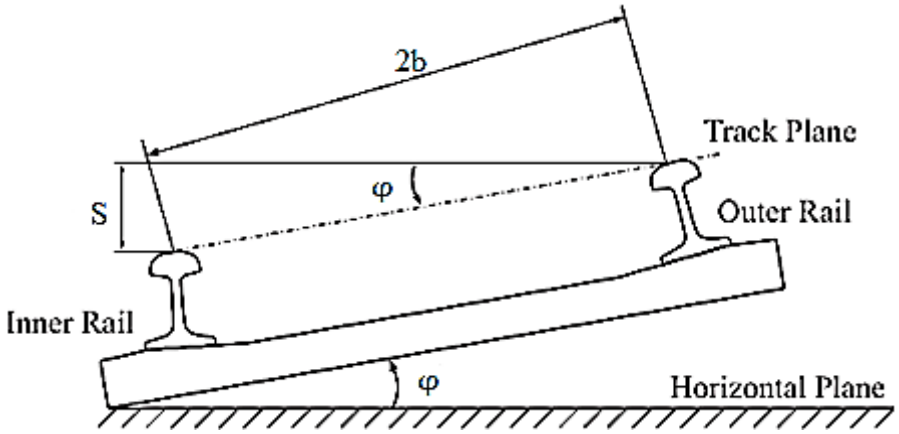

Figure 3.9 Cant and Cant Angl [28]

A raised outside rail rotates the train toward the inside of the curve and helps fight off the overturning rotation toward the outside of the curve caused by the centrifugal inertial loading. Note that when entering a curve, the wheel set is shifted as far as necessary to the side of the outer rail so that the difference in the rolling radii corresponds to the difference in the length covered on the outer and inner rails. Since a sufficient difference in the rolling radii is not achieved, flange contact occurs in the outer wheel during curve negotiation [28].

The flange contact occurrences on both wheels, which are observed when driving on the tangent path segment after the circular curve, result from the instability of the wheelset chase. According to the stability theory of rail vehicles, a wheel set that is not suspended is always unstable [28]. As a result, when the wheelset enters the straight lane, it will have an initial lateral displacement with respect to the lane centerline resulting from the curve negotiation. Such misalignment originates a hunting motion.

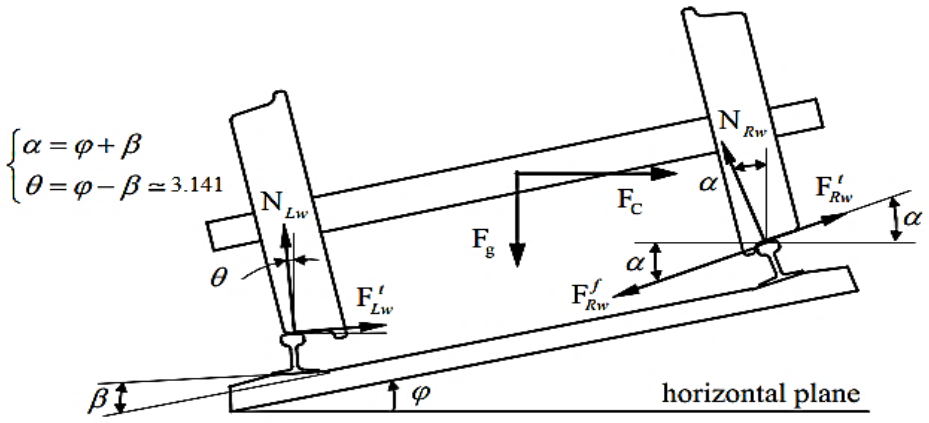

Figure 3.10 Wheelset forces during curve negotiation with flange contact on the outer wheel [28].

Figure 3.11. represents the forces that act on the wheel set when it moves in the circular curve and flange contact occurs on the right wheel. The quantities $\mathbf{N}_{Lw}$ and $\mathbf{N}_{Rw}$ represent the normal contact forces on the left and right wheels, $\mathbf{F}^t_{Lw}$ and $\mathbf{F}^t_{Rw}$ are the lateral contact forces on the treads of the wheels, $\mathbf{F}^f_{Rw}$ is the lateral flange force on the right wheel and $\mathbf{F}_g$ and $\mathbf{F}_C$ are those acting on the wheelset Gravitational and centrifugal forces. The angle ϕ represents the track cant angle, β is the rail inclination angle and θ and α are the angles associated to the sets of forces acting on the left and right wheels, respectively. An equilibrium of forces in the horizontal direction can be written in the form:

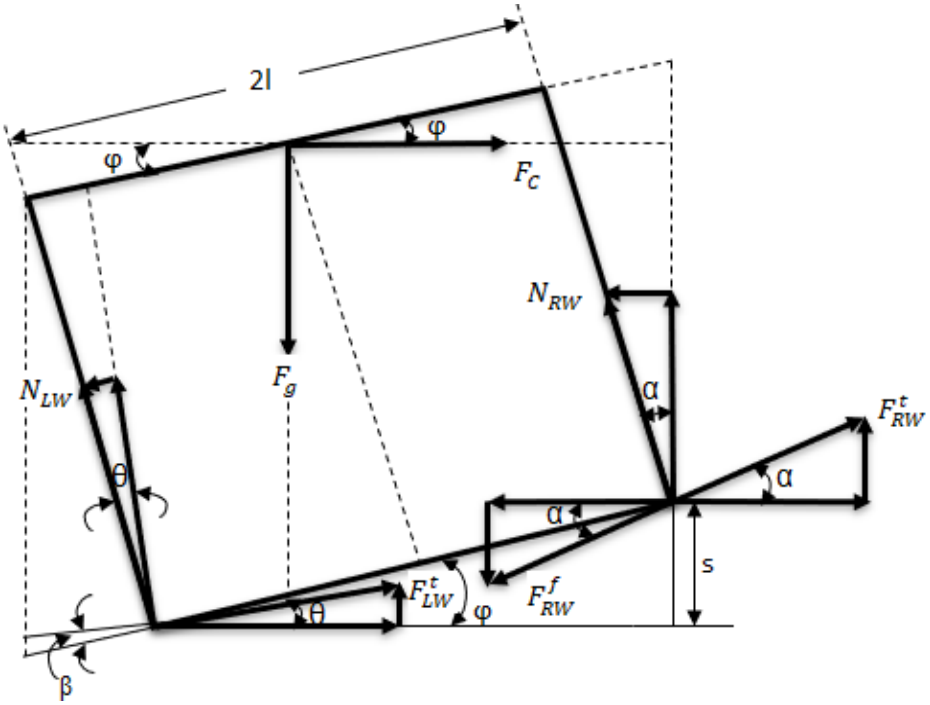

Figure 3.11 Free body diagram of the wheel-rail contacts forces and axle load.

Vertical Forces:

$$\sum F_y = 0 \text{ ---------- (3.15)}$$

$$N_{RW}\cos\alpha + N_{RL}\cos\theta + F^t{}_{RW}\sin\alpha - F^f{}_{RW}\sin\alpha - F^t{}_{LW}\sin\theta - F_g = 0$$

$$\therefore F_g = N_{RW}\cos\alpha + N_{LW}\cos\theta + F^t_{RW}\sin\alpha - F^f{}_{RW}\sin\alpha + F^t{}_{LW}\sin\theta \text{ ---------- (3.16)}$$

$$\mathbf{0.998N_{LW} + 0.055F^t_{LW} - 0.105F^f_{RW} + 0.994N_{RW} + 0.105F^t_{RW} = 252607.5N} \quad \mathbf{(1)}$$

Lateral Forces:

$$\sum F_x = 0 \text{ ---------- (3.17)}$$

$$-N_{RW}\cos\alpha - N_{LW}\sin\theta - F^f{}_{RW}\cos\alpha + F^t{}_{RW}\cos\alpha + F^t{}_{LW}\cos\theta + F_C = 0$$

$$\therefore F_C = N_{RW}\sin\alpha + N_{LW}\sin\theta + F^f{}_{RW}\cos\alpha - F^t{}_{RW}\cos\alpha - F^t{}_{LW}\cos\theta \text{ ---------- (3.18)}$$

$$\mathbf{0.055N_{LW} - 0.998F^t_{LW} + 0.995F^f_{RW} + 0.105N_{RW} - 0.995F^t_{RW} = 35756.74N} \quad \mathbf{(2)}$$

To calculate the unknown force values, we can formulate additional three equations from moment equation at the contact point of left and right wheel and at the center of axel or at the position of axel load.

Moment at left rail (M_{LW}):

$$\sum M_{LW} = 0 \text{ ---------- (3.19)}$$

$$F_g\left(l\cos\varphi - \frac{D_W}{2}\sin\theta\right) + F_C\left(\frac{D_W}{2}\cos\theta + l\sin\varphi\right) + F^f_{RW}\sin\alpha(2l\cos\varphi) - F^f_{RW}\cos\alpha(2l\sin\varphi) - F^t_{RW}\sin\alpha(2l\cos\varphi) + F^t_{RW}\cos\alpha(2l\sin\varphi) - N_{RW}\sin\alpha(2l\sin\varphi) - N_{RW}\cos\alpha(2l\cos\varphi) = 0$$

$$F_g\left(l\cos\varphi - \frac{D_W}{2}\sin\theta\right) + F_C\left(\frac{D_W}{2}\cos\theta + l\sin\varphi\right) = -F^f_{RW}\sin\alpha(2l\cos\varphi) + F^f_{RW}\cos\alpha(2l\sin\varphi) + F^t_{RW}\sin\alpha(2l\cos\varphi) - F^t_{RW}\cos\alpha(2l\sin\varphi) + N_{RW}\sin\alpha(2l\sin\varphi) + N_{RW}\cos\alpha(2l\cos\varphi) \text{ ---------- (3.20)}$$

$$\mathbf{0N_{LW} + 0F^t_{LW} - 0.04F^t_{RW} - 1.503N_{RW} + 0.039F^f_{RW} = -201464.4Nm} \quad \mathbf{(3)}$$

Moment at right rail (M_{RW}):

$$\sum M_{RW} = 0 \text{ ---------- (3.21)}$$

$$-F_g\left(l\cos\varphi + \frac{D_W}{2}\sin\alpha\right) + F_C\left(\frac{D_W}{2}\cos\alpha - l\sin\varphi\right) - F_{LW}^t\cos\theta(2l\sin\varphi) + F_{LW}^t\sin\theta(2l\cos\varphi) + N_{LW}\sin\theta(2l\sin\varphi) + N_{LW}\cos\theta(2l\cos\varphi) = 0$$

$$F_g\left(l\cos\varphi + \frac{D_W}{2}\sin\alpha\right) + F_C\left(\frac{D_W}{2}\cos\alpha - l\sin\varphi\right) = F_{LW}^t\cos\theta(2l\sin\varphi) + F_{LW}^t\sin\theta(2l\cos\varphi) + N_{LW}\sin\theta(2l\sin\varphi) + N_{LW}\cos\theta(2l\cos\varphi) \text{ ---------- (3.22)}$$

$$\mathbf{1.504N_{LW} + 1.468F_{LW}^t + 0F_{RW}^f + 0N_{RW} + 0F_{RW}^t = 187877.9Nm} \quad \mathbf{(4)}$$

Moment center of axel (M_{CA}):

$$\sum M_{CA} = 0 \text{ ---------- (3.23)}$$

$$N_{LW}\left[\sin\theta\left(\frac{D_W}{2}\cos\theta + l\sin\varphi\right) + \cos\theta(l\cos\varphi - \frac{D_W}{2}\sin\theta)\right] + F_{LW}^t\left[-\cos\theta\left(\frac{D_W}{2}\cos\theta + l\sin\varphi\right) + \sin\theta(l\cos\varphi - \frac{D_W}{2}\sin\theta)\right] + F_{RW}^f\left[\cos\alpha\left(\frac{D_W}{2}\cos\alpha - l\sin\varphi\right) + \sin\alpha(l\cos\varphi - \frac{D_W}{2}\sin\alpha)\right] + N_{RW}\left[\sin\alpha\left(\frac{D_W}{2}\cos\alpha - l\sin\varphi\right) + \cos\alpha(l\cos\varphi + \frac{D_W}{2}\sin\alpha)\right] + F_{RW}^t\left[-\cos\alpha\left(\frac{D_W}{2}\cos\alpha - l\sin\varphi\right) - \sin\alpha(l\cos\varphi + \frac{D_W}{2}\sin\alpha)\right] = 0$$

$$N_{LW}\left[\sin\theta\left(\frac{D_W}{2}\cos\theta + l\sin\varphi\right) + \cos\theta(l\cos\varphi - \frac{D_W}{2}\sin\theta)\right] + F_{LW}^t\left[-\cos\theta\left(\frac{D_W}{2}\cos\theta + l\sin\varphi\right) + \sin\theta(l\cos\varphi - \frac{D_W}{2}\sin\theta)\right] + F_{RW}^f\left[\cos\alpha\left(\frac{D_W}{2}\cos\alpha - l\sin\varphi\right) + \sin\alpha(l\cos\varphi - \frac{D_W}{2}\sin\alpha)\right] + N_{RW}\left[\sin\alpha\left(\frac{D_W}{2}\cos\alpha - l\sin\varphi\right) + \cos\alpha(l\cos\varphi + \frac{D_W}{2}\sin\alpha)\right] + F_{RW}^t\left[-\cos\alpha\left(\frac{D_W}{2}\cos\alpha - l\sin\varphi\right) - \sin\alpha(l\cos\varphi + \frac{D_W}{2}\sin\alpha)\right] = 0 \text{ ---------- (3.24)}$$

$$\mathbf{0.544N_{LW} - 0.44F_{LW}^t + 0.2923F_{RW}^f - 0.2923N_{RW} - 0.418F_{RW}^t = 0} \quad \mathbf{(5)}$$

Where: $F_g = W = mg = 25000 * 9.81 = 245250N$

$$F_C = m * \frac{V^2}{R} = 25000 * \frac{(33.33)^2}{800} = 34715.278N$$

$\alpha = (\varphi + \beta) = 6.005°$

$\theta = (\varphi - \beta) = 3.141°$

β is 1.432° and φ is 4.573°

W is axle weight ($m * g$)

V is vehicle speed (33.33m/s)

R is radius of curvature (800m)

μ is coefficient of friction. For this analysis we assume that 0.3 at wheel-rail contact.

Therefore, by solving the Equation (3.16), Equation (3.18), Equation (3.20), Equation (3.22) and Equation (3.24) using matrix notation we can obtain the normal loads at the right wheel (N_{RW}). The unknown's values of the forces using matrix notation:

$$\begin{bmatrix} 0.055 & -0.998 & 0.995 & -0.995 & 0.105 \\ 0.998 & 0.055 & -0.105 & 0.105 & 0.994 \\ 0 & 0 & 0.039 & -0.04 & -1.503 \\ 1.504 & 1.468 & 0 & 0 & 0 \\ 0.544 & -0.44 & 0.2923 & -0.418 & -0.2923 \end{bmatrix} \begin{Bmatrix} N_{LW} \\ F_{LW}^{t} \\ F_{RW}^{f} \\ F_{RW}^{t} \\ N_{RW} \end{Bmatrix} = \begin{Bmatrix} 35756.74 \\ 252607.5 \\ -201464.44 \\ 187877.9 \\ 0 \end{Bmatrix}$$

Finally, N_{RW} = 112493.5242N

Now the vertical forces applied at the outer wheel (at the right wheel) is given as;

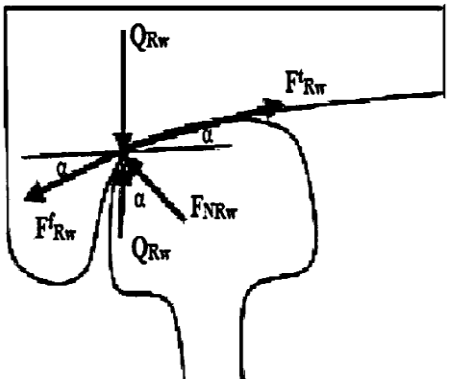

Figure 3.12 Vertical forces on the outer right wheel

$$\therefore Q_{RW} = F_{NRW}\cos\alpha = 112493.5242 * \cos(6.005) = 111876.2463\text{N}$$

3.4.4. Transition Curve Track Contact Forces

Transition curves are curves in which the radius gradually changes from infinity to a particular value R. The effect of this is to gradually increase the radial force for, from zero to its maximum value. To announce a centrifugal force a uniformly along the length of the transition curve and proportional to the length of the transition curve, L. The transition curve is necessary to smoothly change the direction of a moving vehicle.

However, as the vehicle enters or leaves a curve (a Simple Circular Curve) sudden change of direction implies sudden change of radial acceleration, causing inconveniences to the passengers. This can be avoided by introducing a special curve called a Transition Curve between the straight section (initial section) and the beginning of circular curve followed by another transition curve between the final section and the end of circular curve as shown in Figure.3.14.

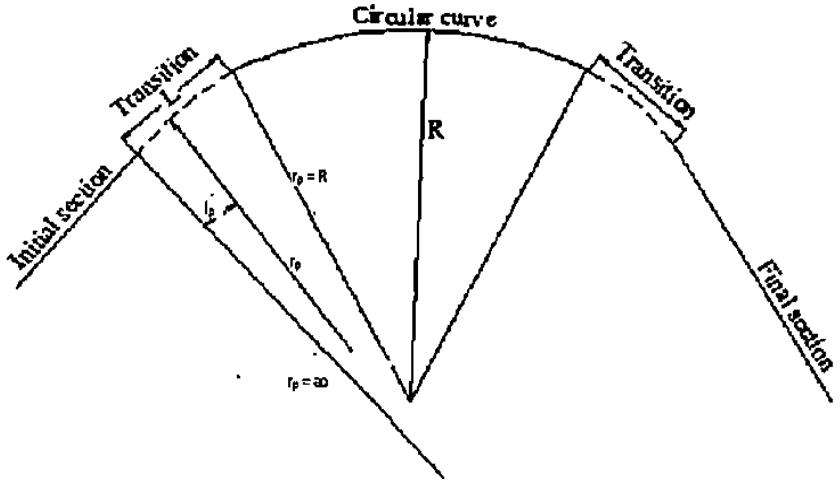

Figure 3.13 Formation of transition curves between straight and circular curve section [22].

Note that the centrifugal force at any point on the transition curve is proportional to the distance from the start point of the curve. Therefore, at constant mass and speed of the train, the centrifugal force, is given by:

$$F_C \propto l_p \propto \frac{1}{r_p} \quad \text{---------- (3.25)}$$

$$l_p \propto \frac{1}{r_p} \text{ i.e. } l_p r_p = K \text{ (contant)} \quad \text{---------- (3.26)}$$

Therefore, for each transition curve the radius R and the length L can be designed to equal to K (constant) over the whole length of the curve [19].

$$\text{At } l_p = L$$

$$\text{and } r_p = R, \text{and then } RL = K \text{ ---------- (3.27)}$$

$$\therefore l_p r_p = LR = K \text{ ---------- (3.28)}$$

$$r_p = \frac{LR}{l_p} \text{ ---------- (3.29)}$$

According to Ethio-Djibouti heavy duty railway line in awash area the minimum horizontal design radius is R=800m and the transition length, L=80m is selected. For this analysis assume, l_p is 1/80 of the length of the total transition curve length. Therefore, l_p will be 1m and then r_p will be 64000m. Then, at r_p = 64000m of the transition curve length, the centrifugal force is given as:

$$F_C = m * \frac{v^2}{r_p} \text{ ---------- (3.30)}$$

$$F_C = 25750 * \frac{33.33^2}{64000} = 25750 * \frac{1110.8889}{64000} = 25750 * 0.01735764 = 446.96 \text{ N}$$

Where, m - Axle load.

V - Design vehicle speed.

r_p - Radius of curve at any point of the transition curve length.

l_p - Transition length at any point of the transition curve radius.

Here, the superelevation height, S or track cant angle, φ at the transition curve is inversely proportional to r_p. since, r_p varies linearly with l_p. Therefore, the superelevation angle or track cant angle, φ from Equation 3.31 is obtained from the relation as Figure.3.15.:

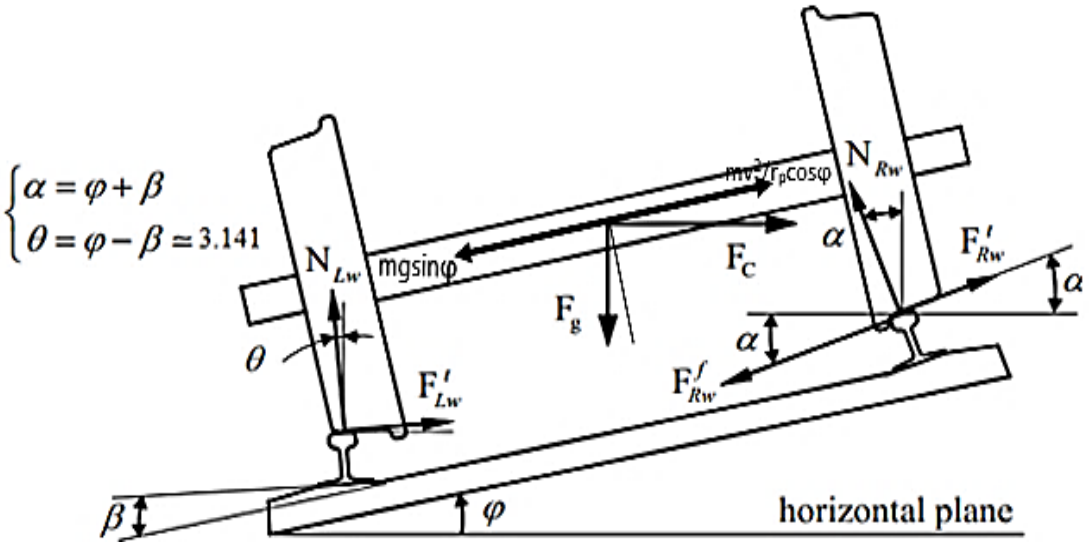

Figure 3.14 Forces acting on a vehicle at a transition curve on super elevated track.

Known, $F_g = W = m * g = 25750 * 9.81 = 252607.5$ N

$$F_C = m * \frac{v^2}{r_p} = 25750 * \frac{33.33^2}{64000} = 446.96 \text{ N}$$

$$m * \frac{v^2}{r_p}\cos\varphi = m * g * \sin\varphi \quad \text{---------- (3.31)}$$

$$\therefore \tan\varphi \ \frac{33.33^2}{64000 * 9.81} = \frac{1110.8889}{626840} = 0.00176938$$

$$\varphi = 0.1014°$$

Known, $\alpha = \varphi + \beta = 0.1014° + 1.432° = 1.5334°$

$$\theta = \varphi - \beta = 0.1014° - 1.432° = -1.3306°$$

$$S = 2l * \tan\varphi = 1505 * \tan(0.1014°) = 1505 * 0.00176938 = 2.663\text{mm}$$

Therefore, from force and moment equation at equilibrium;

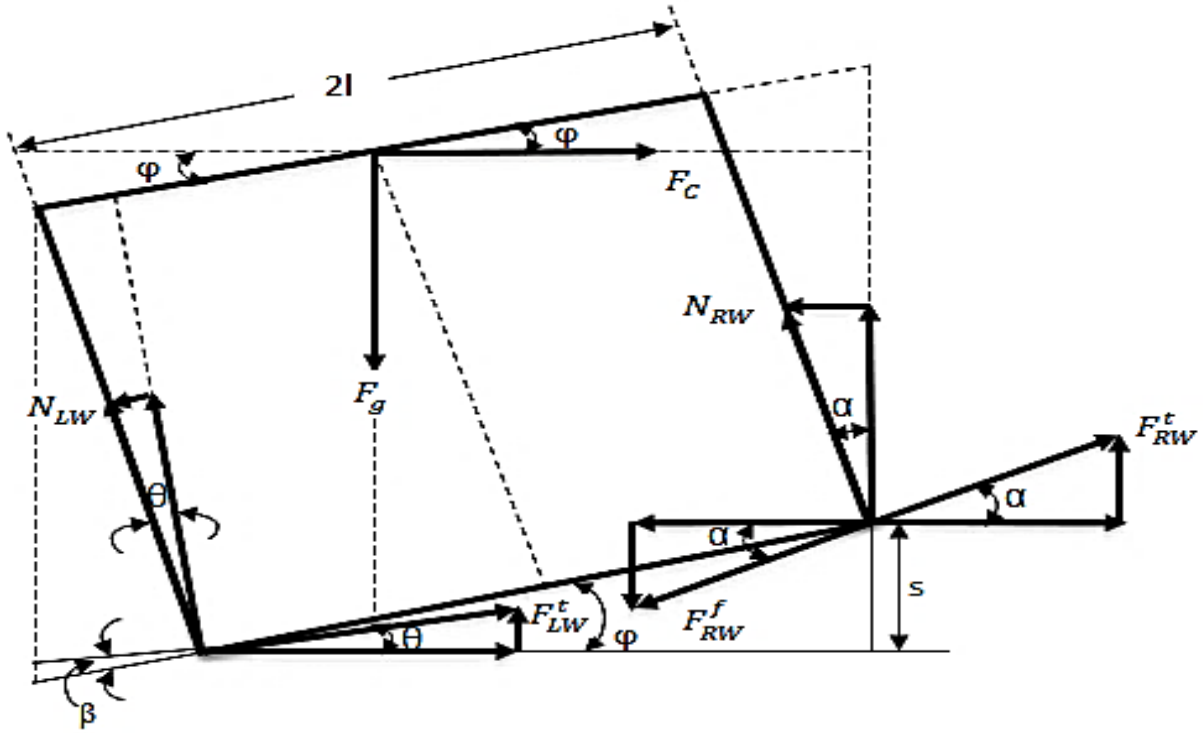

Figure 3.15 Free body diagram on right wheel and rail for transition curve

$$F_g = N_{RW}cos\alpha + N_{LW}cos\theta - F^t{}_{RW}sin\alpha - F^f{}_{RW}sin\alpha + F^t{}_{LW}sin\theta \quad \text{---------- (3.32)}$$

$$\mathbf{0.999N_{LW} - 0.023F^t_{LW} - 0.0268F^f_{RW} + 0.999N_{RW} + 0.0268F^t_{RW} = 252607.5N}$$

$$F_C = N_{RW}sin\alpha + N_{LW}sin\theta + F^f{}_{RW}cos\alpha - F^t{}_{RW}cos\alpha - F^t{}_{LW}cos\theta \quad \text{---------- (3.33)}$$

$$\mathbf{-0.023N_{LW} - 0.999F^t_{LW} + 0.999F^f_{RW} + 0.0268N_{RW} - 0.999F^t_{RW} = 446.96N}$$

$$F_g\left(l\cos\varphi - \frac{D_W}{2}\sin\theta\right) + F_C\left(\frac{D_W}{2}\cos\theta + l\sin\varphi\right) = -F^f_{RW}\sin\alpha(2l\cos\varphi) + F^f_{RW}\cos\alpha(2l\sin\varphi) + F^t_{RW}\sin\alpha(2l\cos\varphi) - F^t_{RW}\cos\alpha(2l\sin\varphi) + N_{RW}\sin\alpha(2l\sin\varphi) + N_{RW}\cos\alpha(2l\cos\varphi) \text{---------- (3.34)}$$

$$\mathbf{0N_{LW} + 0F^t_{LW} - 0.0377F^t_{RW} - 1.502N_{RW} + 0.03764F^f_{RW} = -192525.376Nm}$$

$$F_g\left(l\cos\varphi + \frac{D_W}{2}\sin\alpha\right) + F_C\left(\frac{D_W}{2}\cos\alpha - l\sin\varphi\right) = F^t_{LW}\cos\theta(2l\sin\varphi) + F^t_{LW}\sin\theta(2l\cos\varphi) + N_{LW}\sin\theta(2l\sin\varphi) + N_{LW}\cos\theta(2l\cos\varphi) \text{---------- (3.35)}$$

$$\mathbf{1.502N_{LW} - 0.032F_{LW}^{t} + 0F_{RW}^{f} + 0N_{RW} + 0F_{RW}^{t} = 186869.024Nm}$$

$$N_{LW}\left[\sin\theta\left(\frac{D_W}{2}\cos\theta + l\sin\varphi\right) + \cos\theta(l\cos\varphi - \frac{D_W}{2}\sin\theta)\right] + F_{LW}^{t}\left[-\cos\theta\left(\frac{D_W}{2}\cos\theta + l\sin\varphi\right) + \sin\theta(l\cos\varphi - \frac{D_W}{2}\sin\theta)\right] + F_{RW}^{f}\left[\cos\alpha\left(\frac{D_W}{2}\cos\alpha - l\sin\varphi\right) + \sin\alpha(l\cos\varphi - \frac{D_W}{2}\sin\alpha)\right] + N_{RW}\left[\sin\alpha\left(\frac{D_W}{2}\cos\alpha - l\sin\varphi\right) + \cos\alpha(l\cos\varphi + \frac{D_W}{2}\sin\alpha)\right] + F_{RW}^{t}\left[-\cos\alpha\left(\frac{D_W}{2}\cos\alpha - l\sin\varphi\right) - \sin\alpha(l\cos\varphi + \frac{D_W}{2}\sin\alpha)\right] = 0 \text{ ---------- (3.36)}$$

$$\mathbf{0.75097N_{LW} - 0.438F_{LW}^{t} + 0.437845F_{RW}^{f} + 0.77341N_{RW} - 0.41818F_{RW}^{t} = 0}$$

By substituting, these values to Equation 3.32, Equation 3.33, Equation 3.34, Equation 3.35, and Equation 3.36 solving simultaneously to get the normal contact forces at the outer wheel.

$$\begin{bmatrix} 0.999 & -0.023 & -0.0268 & 0.0268 & 0.999 \\ -0.023 & -0.999 & 0.999 & -0.999 & 0.0268 \\ 0 & 0 & 0.03764 & -0.03764 & -1.5021 \\ 1.502 & -0.03726 & 0 & 0 & 0 \\ 0.75097 & -0.438 & 0.437845 & -0.41818 & 0.7734 \end{bmatrix} \begin{Bmatrix} N_{LW} \\ F_{LW}^{t} \\ F_{RW}^{f} \\ F_{RW}^{t} \\ N_{RW} \end{Bmatrix} = \begin{Bmatrix} 252607.5 \\ 446.96 \\ -192523.5 \\ 186869.024 \\ 0 \end{Bmatrix}$$

Therefore, N_{Rw} will be 275071.579 N, and then the vertical force at the right wheel, Q_{Rw} will be 275071.579* cos1.5334°N = 274973.0746N

3.5. Finite Element Method and Analysis

In this paper, structural analysis is performed on a simple Finite Element (FE) model of a real single wheelset wheel-rail assembly to obtain the fatigue life of the Wheel-Rail track, Total deformation (equivalent von-mises elastic strain) of the Wheel-Rail track, and the Von Mises stress in Wheel-Rail track interface by utilizing the ANSYS 2020R1 FE software. Sensitivity study on rotation of the Wheel-Rail track, load pattern and coefficient of friction is also performed.

Von-Mises stress (σ_{vm}) is an equivalent or effective stress at which yielding (σ_y) is predicted to occur in ductile materials. According to the von Mises failure criterion, the material results under multiaxial loading if the von Mises stress is equal to or greater than the critical value for the material. [29] Numerically: $\sigma_{vm} > \sigma_y$

$$\sigma_{vm} = \sqrt{\frac{(\sigma_x - \sigma_y)^2 + (\sigma_y - \sigma_z)^2 + (\sigma_z - \sigma_x)^2 + 6(\tau^2_{xy} + \tau^2_{yz} + \tau^2_{zx})}{2}}, \sigma_z = \tau^2_{yz} = \tau^2_{zx} = 0$$

$$\sigma_{vm} = \sqrt{(\sigma_x)^2 + (\sigma_y)^2 + (\sigma_z)^2} \quad \text{---------- (3.37)}$$

where, $\sigma_x = \sigma_1, \sigma_y = \sigma_2, \sigma_z = \sigma_3$

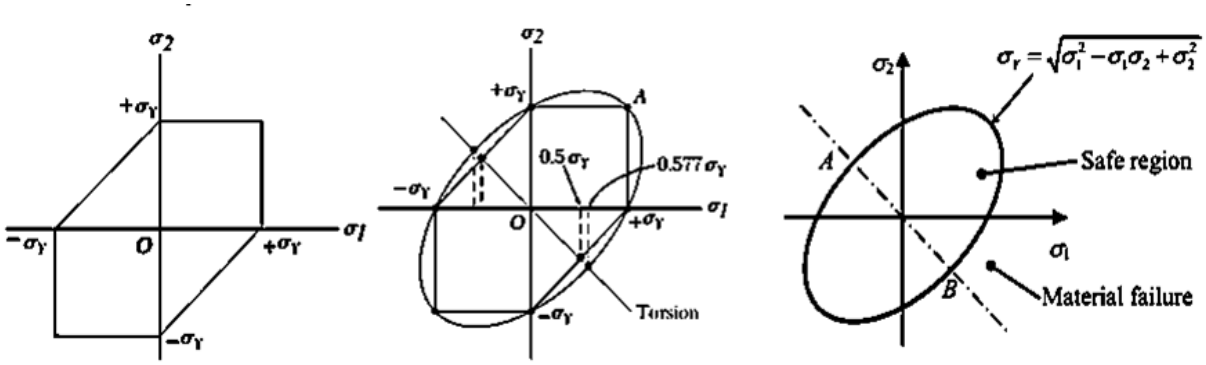

Figure 3.16 Failure envelope of the distortion energy theory [39].

Equivalent von-mises elastic strain of the wheel/rail of homogeneous, isotropic materials can be described relatively simply by using the Young's and Shear module. The Cartesian strains resulting from a state of plane stress ($\sigma_z = 0$) are:

$$\varepsilon_x = \frac{1}{E}(\sigma_x - v\sigma_y)$$

$$\varepsilon_y = \frac{1}{E}(\sigma_y - v\sigma_x)$$

$$\gamma_{xy} = \frac{1}{G}\tau_{xy} \quad \text{---------- (3.38)}$$

Using matrix notation, these relations can be written as: -

$$\begin{bmatrix} \varepsilon_x \\ \varepsilon_y \\ \gamma_{xy} \end{bmatrix} = \begin{bmatrix} \frac{1}{E} & \frac{-v}{E} & 0 \\ \frac{-v}{E} & \frac{1}{E} & 0 \\ 0 & 0 & \frac{1}{E} \end{bmatrix} \begin{bmatrix} \sigma_x \\ \sigma_y \\ \sigma_z \end{bmatrix} \text{---------- (3.39)}$$

In the above relations there are three elastic constants: The Young's modulus (E), Poisson's ratio (ν), and the shear modulus (G). relationship between each of this constant can be obtained from the relation using Equation 3.40:

$$v = \frac{E}{2G} - 1 \text{ ---------- (3.40)}$$

Fatigue Life

Fatigue life usually refers to the number of stress or strain cycles structures and components can withstand before failure. The rating of the service life determines the service life of components that are exposed to certain load conditions. The fatigue life can be determined from experimental work, the formulation or simulation being obtained using specific software [30]. In the design phase, a thorough understanding of the material behavior is critical to ensure the safety and integrity of the component. The life of the component can be estimated from the number of charging cycles before cracks form. Fatigue crack growth rates (FCG) are the main parameters that need to be considered [31]. the total fatigue life is a combination of the number of cycles before cracks form and propagate to ultimate failure.

Three basic approaches are commonly used to calculate fatigue damage: the stress-life approach, the strain-life approach, and the crack propagation method. The stress life approach has been used as the standard method for assessing life since the 19th century. This method uses cyclic stress as a control variable, which is different from other types of fatigue analysis. The stress life analysis is suitable for fatigue phenomena with a high cycle, in which only slight plastic deformation occurs due to the cyclic loading. The elongation life approach is beneficial for the analysis of the fatigue life exposed to the VAL, where the load sequence effect is significant. This approach takes into account both the elastic and the plastic strain behavior of the material. In contrast to stress-life and strain-life approaches to fatigue, fracture mechanics assumes that cracks are present in materials and structures. The crack propagation approach is based on the stress intensity factor range [32].

In general, the stress-life approach is directly related to the operating load in order to ensure a safe lifetime based on a linear representation of the accumulated damage [33]. The Stress Life (S-N) curve is useful for estimating fatigue life by reporting the number of cycles as failure data at certain stress levels. The S-N curve is usually recorded on a semi-log or log-log scale containing experimental constant amplitude stress (CAL) data. Fatigue data is obtained by testing a smooth specimen, which is often done at zero mean stress.

$$\frac{\Delta\sigma}{2} = \sigma_a = \sigma_f(2N_f)^b \Rightarrow \sigma_a = \sigma_f(2N_f)^b \text{ ---------- (3.40)}$$

Where, $\frac{\Delta\sigma}{2} = \sigma_a$ is stress amplitude.

σ_f is the fatigue strength coefficient.

N_f is the number of cycles to failure.

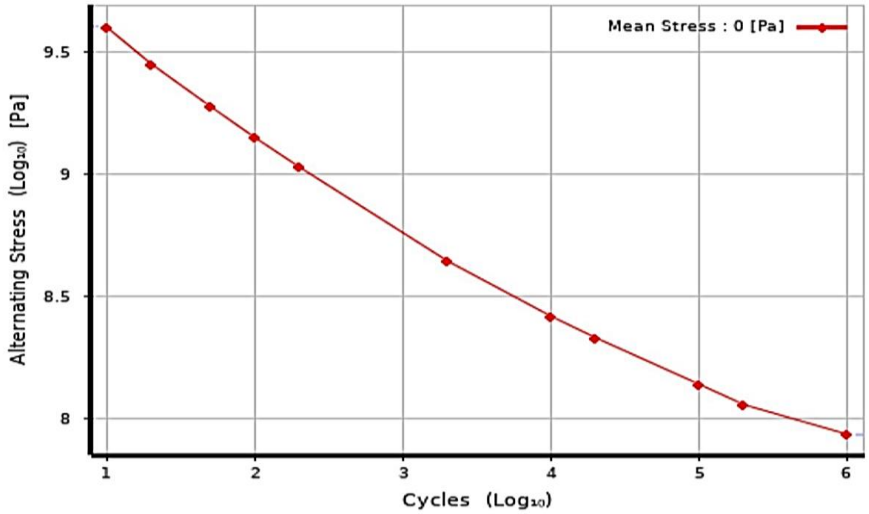

Figure 3.17 Stress life (S-N) curve diagram

Loading Type

Since the load created on the wheel is assumed quasi-static loads, then constant amplitude and proportional loading is used. Loading is of constant amplitude because only one set of FE stress results along with a loading ratio is required to calculate the alternating and mean values. The loading ratio is defined as the ratio of the second load to the first load. Loading is proportional since only one set of FE results are needed (principal stress axes do not change over time). Since loading is proportional, looking at a single set of FE results can identify critical fatigue locations.

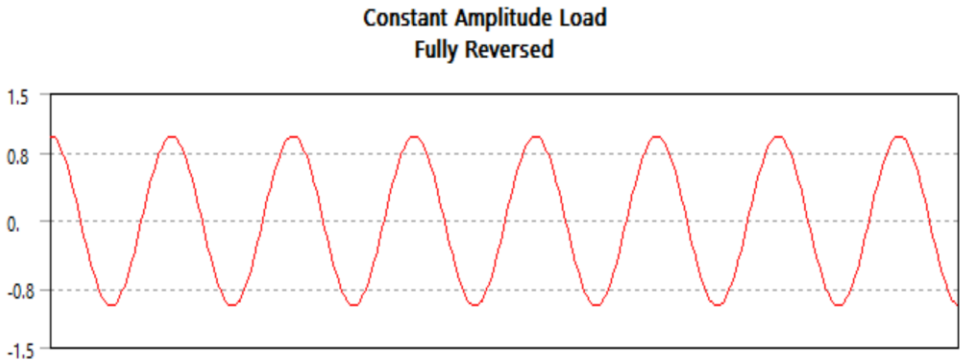

Figure 3.18 Zero-based loading response.

Mean stress Correction for Stress Life

Loads other than fully reversed have a non-zero mean stress/voltage. Mean stress correction methods have been developed to avoid fatigue testing stress at various mean stresses. The influence of the local mean stress can be characterized as the influence of the stress ratio R, the ratio of a local minimum stress to a local maximum stress in a fatigue load cycle. The *S-N* curve is developed based on a constant stress range σ_r or constant stress amplitude σ_{an} applied on the specimen until final failure. The mean stress σ_m can significantly influence the service life of the material. Figure 3.20 shows a typical service life behavior with different mean loads, the fatigue strength of a material decreases significantly with increasing mean tensile stress, but increases with increasing mean compressive stress.

Fatigue data at each endurance can be cross-plotted to demonstrate the effect of mean load on fatigue strength at the chosen duration. At an average stress that corresponds to the ultimate strength of a material, it is suggested that the allowable stress amplitude is zero because the material is at the point of breakage. Hence, in general, there are many theories that are used to study the influence of mean stress [33]. In this article two theories have been used that are commonly used to predict life span under fluctuating loads. The stress effect can be defined analytically by the modified Goodman and Gerber equations given in equations (3.26) and (3.27), respectively [30,33].

$$\frac{\sigma_a}{\sigma_e} + \frac{\sigma_m}{s_u} = 1 \text{ ---------- (3.41)}$$

$$\frac{\sigma_a}{S_e} + (\frac{\sigma_m}{s_u})^2 = 1 \text{ ---------- (3.42)}$$

Where, σ_a - Stress amplitude

S_e -Stress amplitude at zero mean stress

σ_m - Mean stress

S_u - Ultimate tensile strength

The mean stress must therefore be taken into account when predicting the service life of components, in particular of components, as it has a noticeable influence on the service life behavior.

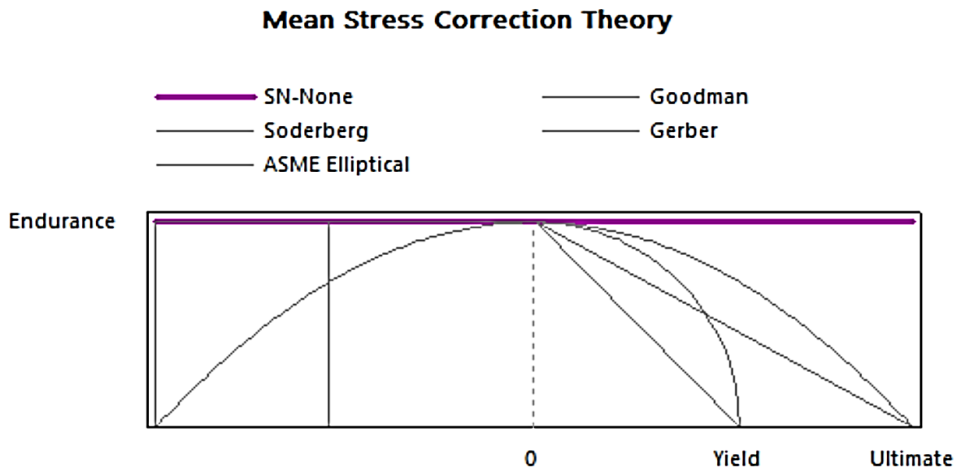

Figure 3.19 Schematic of the Goodman and Gerber mean stress correction

3.5.1. Finite Element Analysis

Finite Element Analysis FEA is the mathematical modeling of products and the numerical solution of very complex structural, fluid and multi-phase problems in a short time. Due to the complexity of the material properties, the boundary conditions and the structure itself, analytical solutions are not suitable for many technical problems [34].

3.5.2. Methods of Finite Element Analysis

a) Building the Model/Pre-processor:

Is the stage of defining the problem which will be analyzed by FEM. The importing SOLIDWORK file, element type and material properties are defined under this section.

b) Solution/Analysis:

The preprocessor is used as input to the finite element code itself, which constructs and solves a system of linear or nonlinear algebraic equations [K] [U] = [F], with K, U and F coefficient matrix, displacements and external applied Forces at the nodes respectively. Meshing and assigning constraints are sated under this section.

c) Obtaining and Reviewing the Results/Post-processing:

Further processing and reviewing of the results such as; Temperature distribution**,** Deformation**,** Weight and Stress. [34, 35]. In our case, the results are the rail track fatigue life, checking the equivalent alternate stress, equivalent alternate strain, and total deformation.

Structural Analysis: Seven types of structural analyzes are available in ANSYS 2020R1. The following types of structural analysis can be performed. (1) Static analysis, (2) Modal analysis, (3) Harmonic analysis, (4) Transient analysis, (5) Spectrum analysis, (6) Buckling analysis, and (7) Explicit dynamic analysis.

Static Analysis: A static analysis calculates the effects of a stable load condition on a structure by ignoring time-varying loads. However, a static analysis can include constant inertial loads such as gravity and rotational speed, as well as time-varying loads, which can be approximated as static equivalent loads commonly defined in many building codes. Method for static finite element analysis with the workbench software ANSYS 2020R1 for wheel-rail-tracks the contact is shown in the table. Figure 3.21.

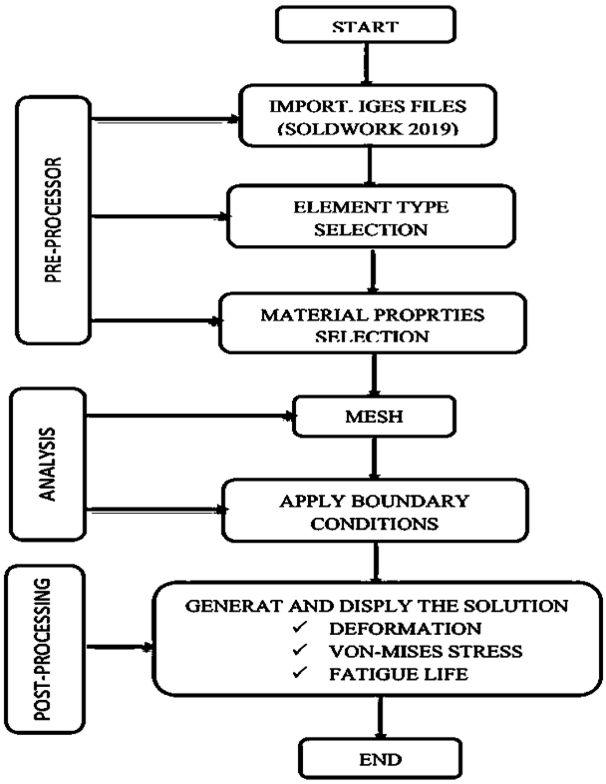

Figure 3.20 Finite Element A Procedure chart

3.5.2.1. Importing the Model Geometry

To achieve the objective and scope of this paper, a 3D Elasto-plastic finite element model is needed. The geometric 3D modeling of the wheel-rail contact is carried out with the SOLDWORK 2019 software. This 3D elastoplastic model should be imported in IGES format into the ANSYS 2020R1 Workbench, which was created with the ANSYS 2020R1 software package for the finite element Analysis is compatible.

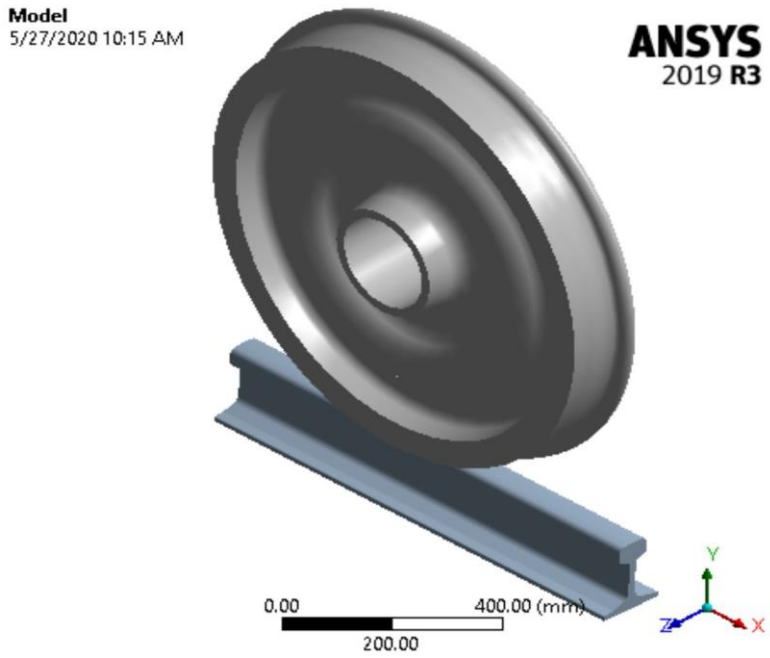

Figure 3.21 Imported model of wheel-rail in ANSYS 2020R1 workbench.

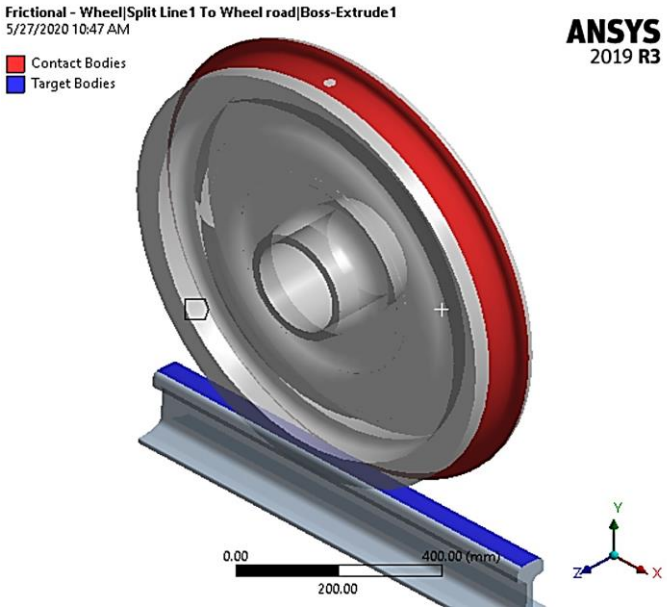

Figure 3.22 Contact region between wheel and wheel road

3.5.2.2. Input Material

The material type and its properties such as density, Young's modulus, Poisson's ratio etc. are specified under engineering data as shown in Figure.3.24, Figure 3.25 and Figure 3.26 for the existing, wheel, and newly selected material respectively. by using the same material for both wheel and rail track as stated in EDR specification. The mechanical properties of wheel and rails are given in Table 3.14.

Table 3.14 Existing and newly selected material properties for wheel-rail materials used for FEA.

S.No.	Properties	Value		Units
		Structural steel (grade 9000A)	Structural steel (grade AS60)	
1	Young modulus	207	210	GPa
2	Density	7800	7800	kg/m^3
3	Tensile Yield strength	>580	780	MPa
4	Ultimate tensile strength	900	1130	MPa
5	Poison Ration	0.3	0.3	NA

Properties of Outline Row 3: 9000A

	A	B	C	D	E
1	Property	Value	Unit		
2	Material Field Variables	Table			
3	Density	7800	kg m^-3		
4	Isotropic Secant Coefficient of Thermal Expansion				
5	Coefficient of Thermal Expansion	1.2E-05	C^-1		
6	Isotropic Elasticity				
7	Derive from	Young's Modulus an...			
8	Young's Modulus	2.07E+05	MPa		
9	Poisson's Ratio	0.3			
10	Bulk Modulus	1.725E+11	Pa		
11	Shear Modulus	7.9615E+10	Pa		
12	Strain-Life Parameters				
13	Display Curve Type	Strain-Life			
14	Strength Coefficient	9.2E+08	Pa		
15	Strength Exponent	-0.106			
16	Ductility Coefficient	0.213			
17	Ductility Exponent	-0.47			
18	Cyclic Strength Coefficient	1E+09	Pa		
19	Cyclic Strain Hardening Exponent	0.2			
20	S-N Curve	Tabular			
21	Interpolation	Log-Log			
22	Scale	1			
23	Offset	0	Pa		
24	Tensile Yield Strength	580	MPa		
25	Compressive Yield Strength	580	MPa		
26	Tensile Ultimate Strength	900	MPa		
27	Compressive Ultimate Strength	900	Pa		

Figure 3.23 Existing Workbench UIC54Kg/m mechanical property specification (Engineering data)

Properties of Outline Row 4: Structural Steel RT7

	A	B	C	D	E
1	Property	Value	Unit		
2	Material Field Variables	Table			
3	Density	7850	kg m^-3		
4	Isotropic Secant Coefficient of Thermal Expansion				
5	Coefficient of Thermal Expansion	1.2E-05	C^-1		
6	Isotropic Elasticity				
7	Derive from	Young's Modulus and P...			
8	Young's Modulus	2E+05	MPa		
9	Poisson's Ratio	0.3			
10	Bulk Modulus	1.6667E+11	Pa		
11	Shear Modulus	7.6923E+10	Pa		
12	Strain-Life Parameters				
13	Display Curve Type	Strain-Life			
14	Strength Coefficient	9.2E+08	Pa		
15	Strength Exponent	-0.106			
16	Ductility Coefficient	0.213			
17	Ductility Exponent	-0.47			
18	Cyclic Strength Coefficient	1E+09	Pa		
19	Cyclic Strain Hardening Exponent	0.2			
20	S-N Curve	Tabular			
21	Interpolation	Log-Log			
22	Scale	1			
23	Offset	0	Pa		
24	Tensile Yield Strength	520	MPa		
25	Compressive Yield Strength	520	MPa		
26	Tensile Ultimate Strength	940	MPa		
27	Compressive Ultimate Strength	940	Pa		

Figure 3.24 Wheel Workbench UIC60Kg/m mechanical property specification (Engineering data)

Properties of Outline Row 3: AS60 (AS1085.1)

	A	B	C	D	E
1	Property	Value	Unit		
2	Material Field Variables	Table			
3	Density	7800	kg m^-3		
4	Isotropic Secant Coefficient of Thermal Expansion				
5	Coefficient of Thermal Expansion	1.2E-05	C^-1		
6	Isotropic Elasticity				
7	Derive from	Young's Modulus and ...			
8	Young's Modulus	2.15E+05	MPa		
9	Poisson's Ratio	0.3			
10	Bulk Modulus	1.7917E+11	Pa		
11	Shear Modulus	8.2692E+10	Pa		
12	Strain-Life Parameters				
13	Display Curve Type	Strain-Life			
14	Strength Coefficient	9.2E+08	Pa		
15	Strength Exponent	-0.106			
16	Ductility Coefficient	0.213			
17	Ductility Exponent	-0.47			
18	Cyclic Strength Coefficient	1E+09	Pa		
19	Cyclic Strain Hardening Exponent	0.2			
20	S-N Curve	Tabular			
21	Interpolation	Log-Log			
22	Scale	1			
23	Offset	0	Pa		
24	Tensile Yield Strength	780	MPa		
25	Compressive Yield Strength	780	MPa		
26	Tensile Ultimate Strength	1130	MPa		
27	Compressive Ultimate Strength	1130	Pa		

Figure 3.25 Newly Workbench AS60 mechanical property specification (Engineering data)

3.5.2.3. Meshing the Object

In FEA, the basic concept is to analyze structure, which is an arrangement of discrete parts called elements that are connected together at a finite number of points called nodes. A network between these elements is called networking. Meshing / networking is the mechanism of dividing the complex geometry model into small elements to solve easily with accuracy. In a finite analysis, more time is spent creating elements and nodal data. With the preprocessor, the user can automatically generate nodes and elements at the same time and thus control the size and number of elements by meshing the geometry.

One of the fundamental parts of solving contact stress problems using FEM is to reliably and efficiently locate potential contact areas. Furthermore, once the possible contact areas are identified, further refinement has to be done in the vicinity of the stress concentration areas to achieve accurate results.

The meshing process can be performed only after the specification of element type (Pre-processing). ANSYS 2020R1 offers several convenient options to assist in meshing. These include Automatic Meshing, Smart Sizing, and Mapped Meshing. One of the best features of ANSYS 2020R1 is automatic mesh generation. With automatic meshing, the user can still provide specific preferences for mesh density and shape. If no preferences are specified by the user, ANSYS 2020R1 uses the default preferences. [34,35].

The meshing is done as seen in Figure.3.27. by using a triangulated linear structural mesh and the refinement is done, specifically in the wheel and rail track contact zone because the fatigue life varies significantly due to the high stress concentrations and larger deformation for this region the element size is 1.5mm,

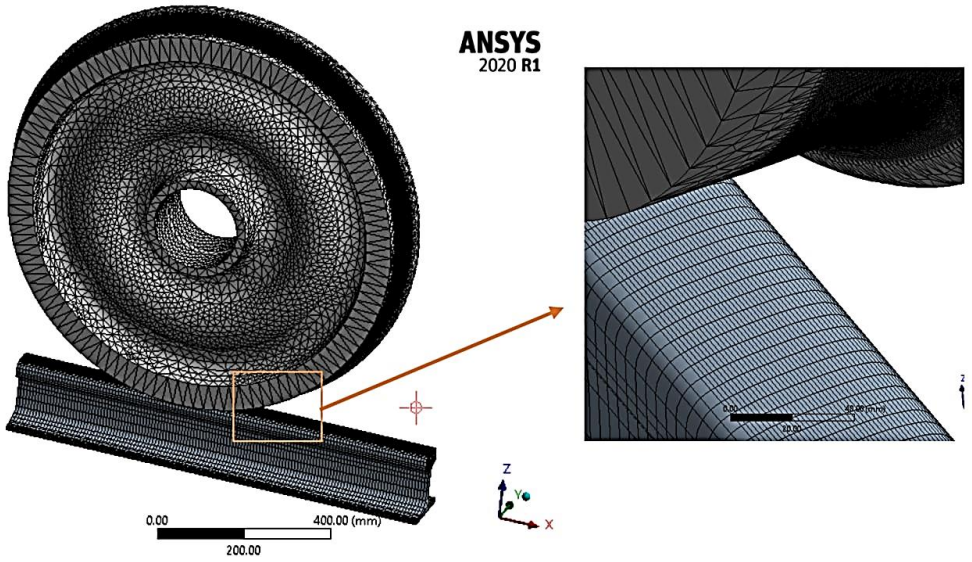

Figure 3.26 Finite element model meshing of wheel-rail contact for all track conditions

The general statistical network / mesh data for the straight, transition and circular curve of the wheel-rail track after the imported models have meshed are shown in Figure 3.28.

⊞ Quality	
⊞ Inflation	
⊞ Advanced	
⊟ Statistics	
Nodes	1370217
Elements	792862

Figure 3.27 Mesh statistical data of wheel-rail.

3.5.2.4. Applying Boundary Conditions:

The next step of FEA involves applying appropriate boundary conditions and loading mechanism. There are two ways to apply the boundary conditions and loading to the model in ANSYS 2020R1; either apply the conditions to the solid model (key point, lines and areas), or the conditions can be imposed directly on the nodes and elements. In this research work, the first approach is preferable; because if it is decided to change the meshing, there will not need to reapply the boundary conditions and the loads to the new FEM. In this study the geometrical boundary conditions and loadings are applied based on physical characters and real conditions of the Ethio-Djibouti heavy duty railway line specifically in Awash. For this FEA by considering the outer or right wheel exclusively.

Deformation, Stress and Fatigue Life Analysis of Rail Track: The rail is exposed to loads due to the contact force between the wheel and the rail. This leads to deformations on both bodies. To achieve this, the bodies should be tested for structural strength. The fatigue life rating determines the life of the rail, which will be subjected to certain stress conditions using cycles of stress or strain that the rail will withstand before failure. This analysis is done in ANSYS 2020R1 Workbench for after choosing the Static Structural analysis (a quasi-static load) is in the wheel-rail interface, is time dependent but is "slow" enough such that inertial effects can be ignored. This analysis consists of following step by step procedures.

Loading Conditions: There are mechanical stresses subjected to the wheel-rail contact surface/point. The loads acting on the wheelset by the electric locomotive are mainly composed of the axle load of 25 (1 + 3%) tones, which acts on the middle of the wheelset at each end of the wheelset, the centrifugal force, which acts on the middle of the wheelset at the right end (away from the center of curvature) of the wheelset and the drive torque induced by the traction motor, which can be converted into a circle of tangential forces that are evenly distributed at the nodes on the axle surface. The coefficient of friction between wheel and rail is 0.3. The vertical contact forces are: 126,303.75 N, 111876.2463 N and 274973.0746 N on a straight, transition curve or circular curve path. In addition, the lateral forces are 446.9 N and 35756.74 N on the transition or circular curve path.

Constraints: A commercial FE software, namely ANSYS 2020R1 is fully utilized to simulate the structural fatigue life, equivalent alternative stress, equivalent alternative strain, and total deformation of rail track. Boundary conditions are imposed on the models as shown in Figure.3.29. The slope of the rail

on international railways can be either 1:20 or 1:40. In this study, is considered the 1:40 slope, since it can be adjusted easily with sleepers' slope [29]. UIC54Kg/m and AS60Kg/m rail materials are used and the length of the rail is the average distance between two slippers, i.e., 760 mm, and the rail is attached to the bottom of the rail; because the rails on the raised track (around awash area) are completely supported or attached to concrete. The wheel is constrained to both directions (longitudinally and laterally) and its rolling diameter is 840mm. All the loads are applied at the center or hub of the wheel. The mechanical material properties are assumed to be the same for both rail and wheel. Using vehicle data as given under Loading Conditions and Equations (21)-(25), fatigue life, equivalent alternative stress, equivalent alternative strain, and total deformation.

Generate Solutions: Finally, the solution of each dependent parameter can be displayed individually. Once the solution is generated, each dependent parameter is solved and ready to be seen and interpreted. This will be clearly discussed in the next chapter.

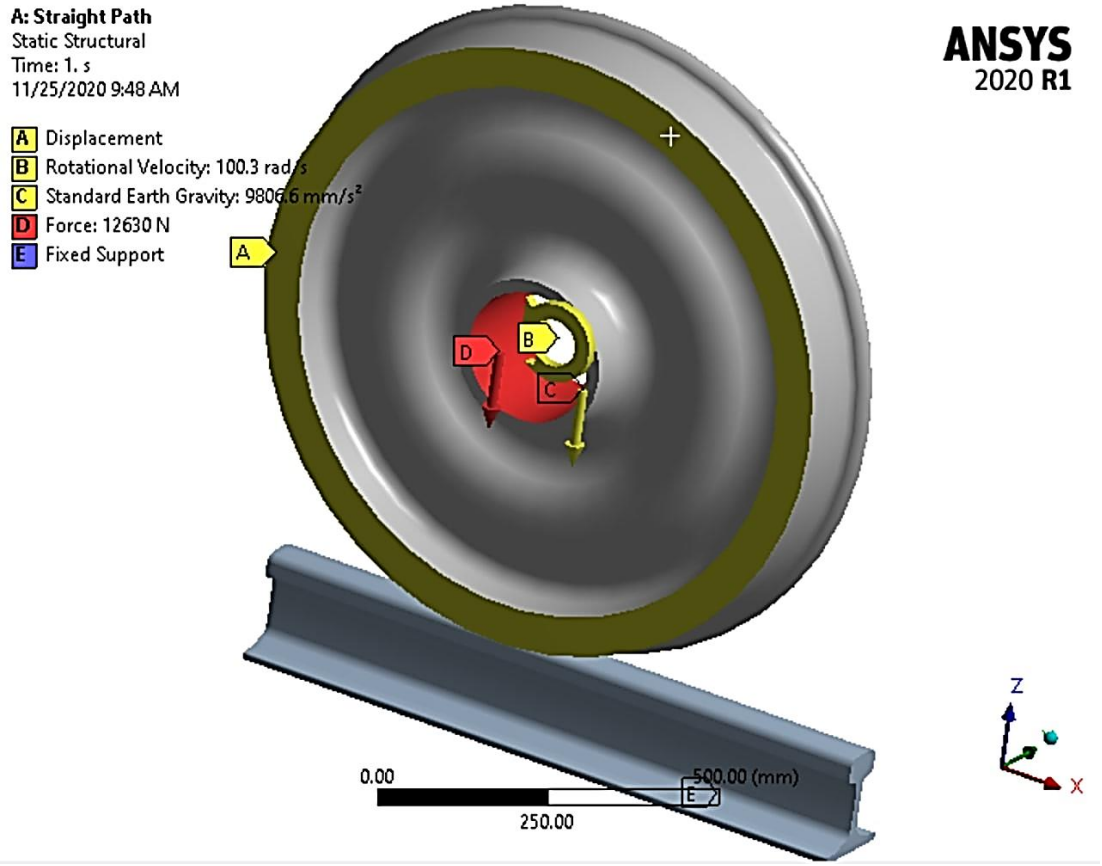

(a)

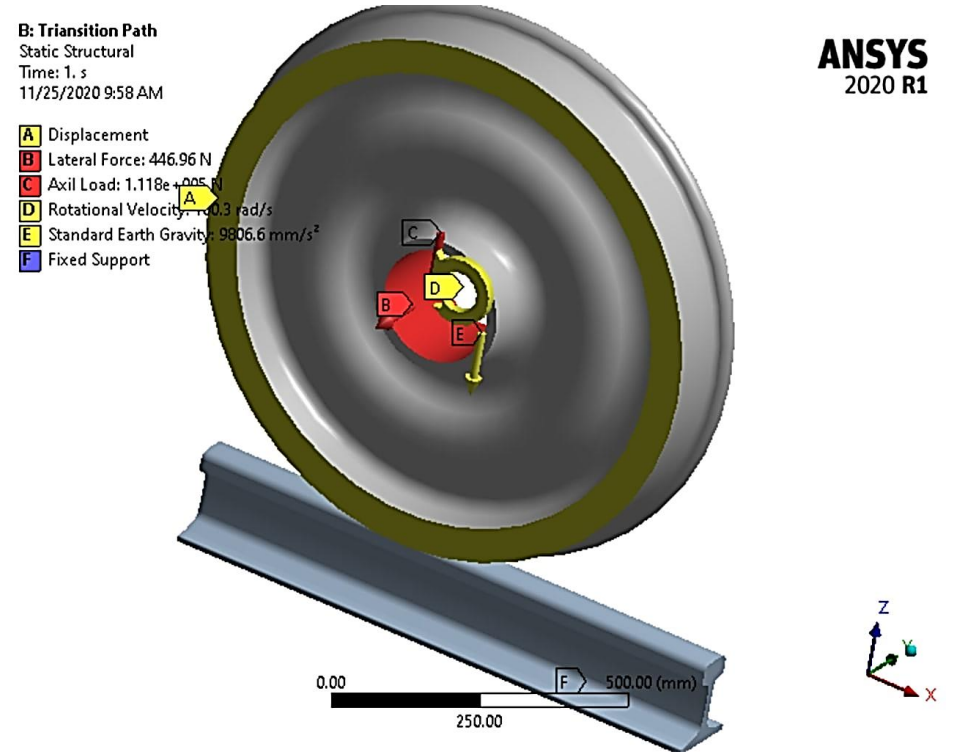

(b)

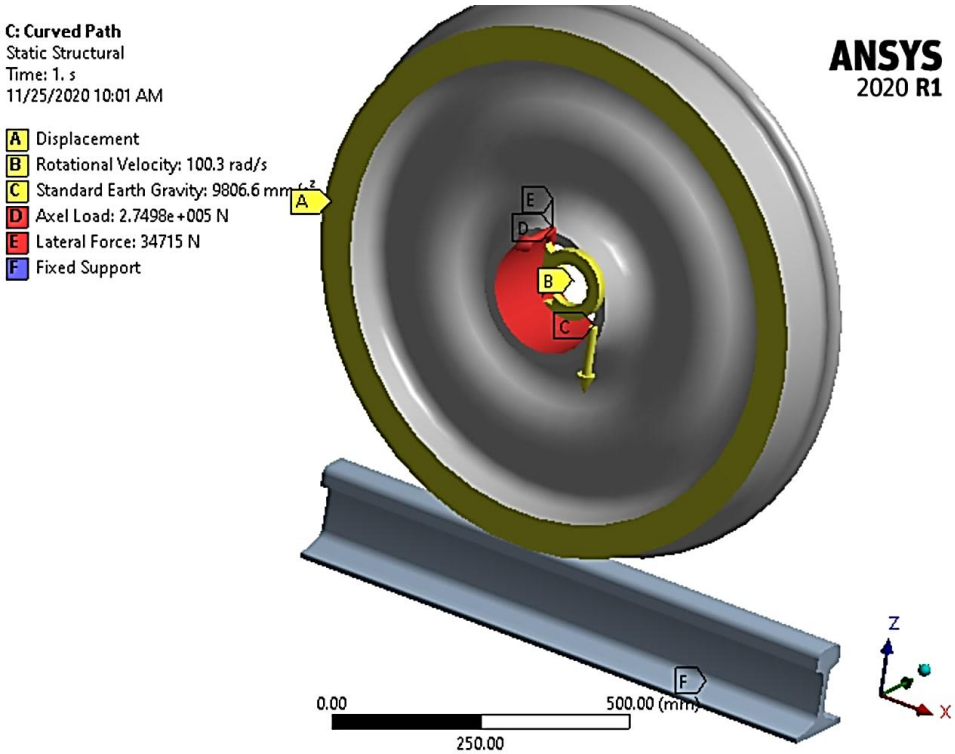

(c)

Figure 3.28 Loading and boundary conditions at the wheel-rail contact. (a) at straight track, (b) at transition curve track, and (c) at circular curve track path.

Chapter Four

Results and Discussions

This chapter describes results obtained from FEA of the rail track after completion of the structural static analysis in ANSYS 2020R1 Workbench. Basically, the significant types of results were recorded from the analysis of the imported model. The results are presented for all categories namely: fatigue life, equivalent alternative stress, equivalent alternative strain, and total deformation of rail track. Therefore, in this chapter we will discusses in software analysis proses, software results and finally result discussions.

4.1. Analysis

The analysis performed using FEM by using ANSYS 2020R1 Workbench for the purpose of obtaining the maximum and minimum fatigue life, equivalent alternate stress, equivalent alternate strain and complete deformation of the EDR rail track at the contact interface caused by applying appropriate boundary conditions to the existing EDR structural steel material and the newly selected structural steel material for this study as shown in Figure 4.1 (a) and (b).

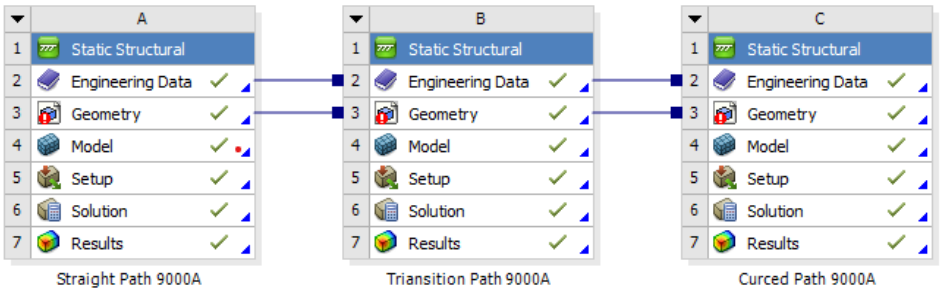

(a)

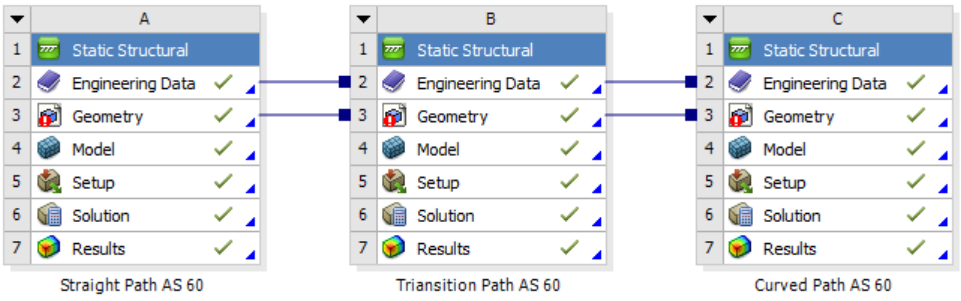

(b)

Figure 4.1 ANSYS 2020R1 Workbench Static structural analysis system (a) Existing material (grade 9000A) (b) selected material (grade AS60).

4.2. Results

4.2.1. Fatigue Life

This result contour plot shows the available life for the given fatigue analysis for existing EDR of structural steel of grade 9000A and selected of structural steel of grade AS60 materials respectively. When the load is of constant amplitude, it indicates the number of cycles until the part fails due to fatigue loading.

(a). The contour plot of ANSYS 2020R1 Workbench shows the fatigue life for both material at the straight track path condition as shown in the Figure 4.2. (a) and (b).

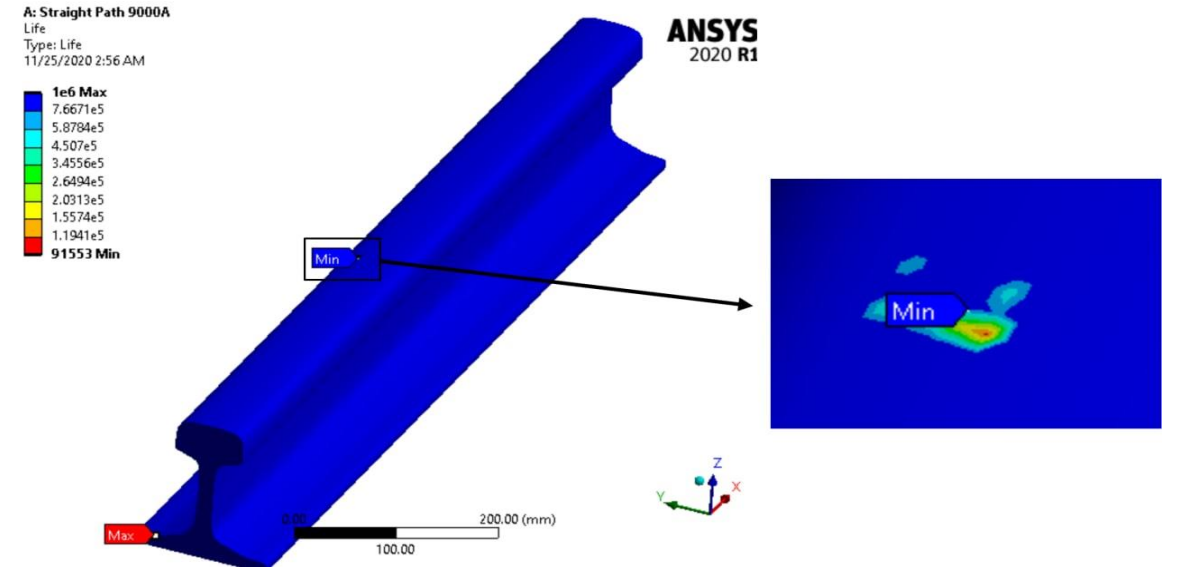

(a)

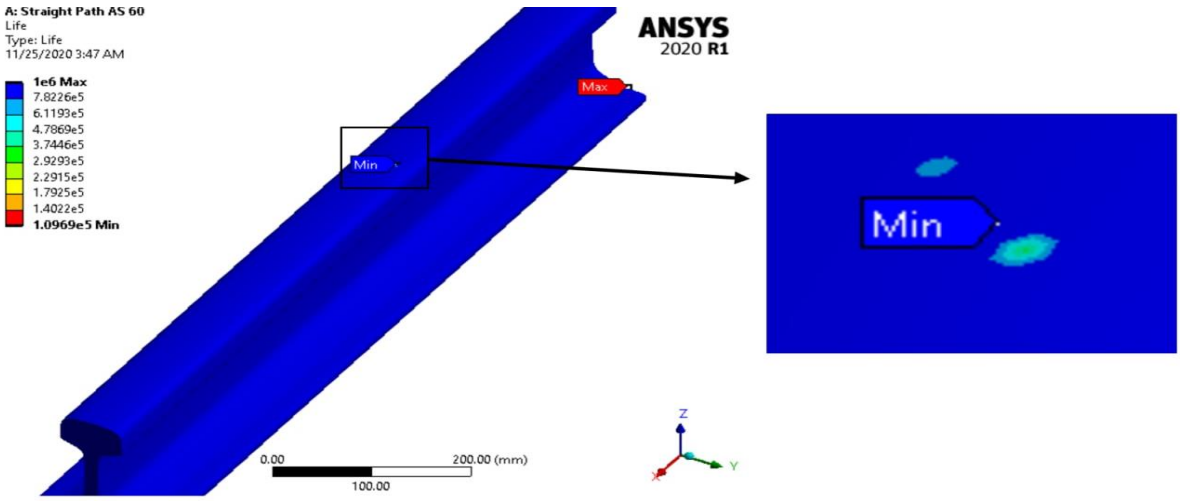

(b)

Figure 4.2 Counter plot of fatigue life for existing and selected material of wheel-rail rolling contact at the straight track path, (a) 9000A and (b) AS60.

(b). The contour plot of ANSYS 2020R1 Workbench shows the fatigue life for both materials at the transition curve rail track path condition in Figure 4.3. (a) and (b).

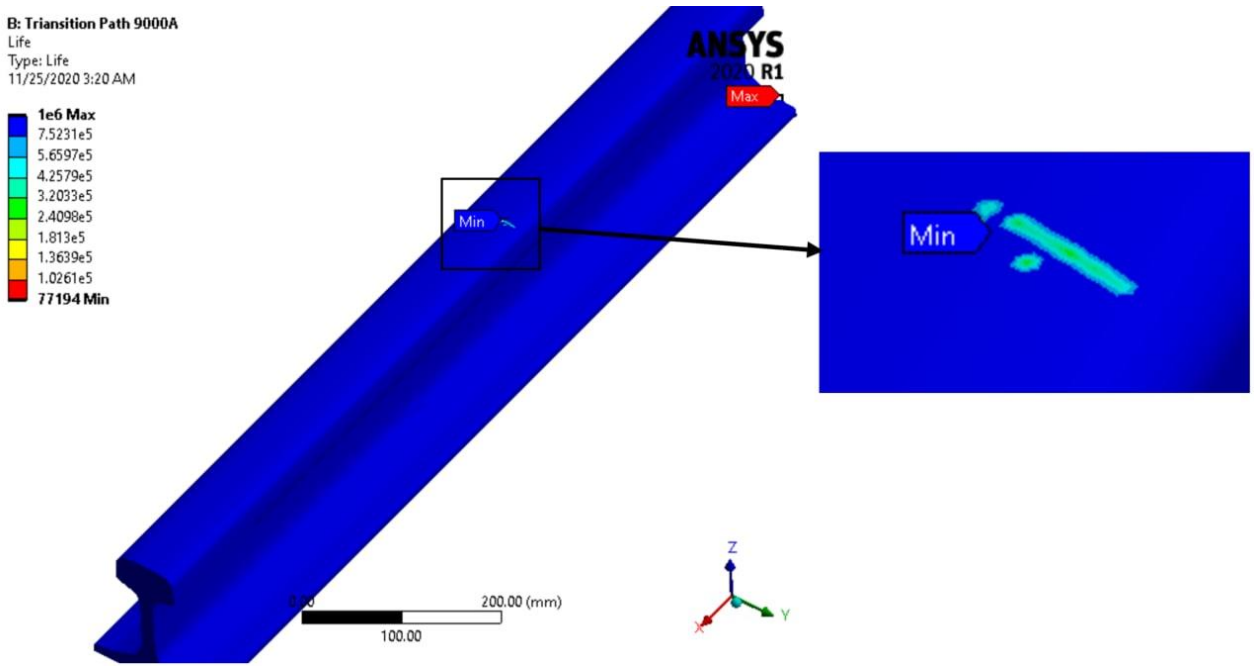

(a)

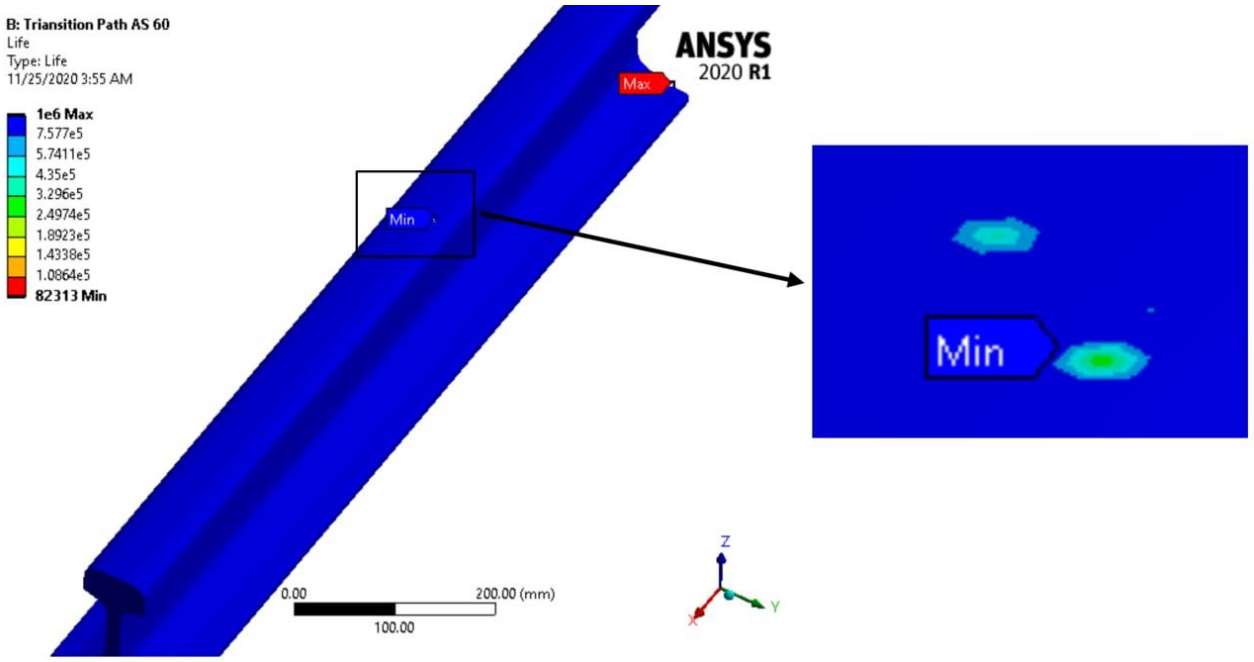

(b)

Figure 4.3 Counter plot of fatigue life for existing and selected material of wheel-rail rolling contact at the transition curve rail track path, (a) UIC54kg/m and (b) AS60kg/m.

(c). The contour plot of ANSYS 2019R3 Workbench shows the fatigue life for both materials at the circular curve rail track path condition in Figure 4.4. (a) and (b).

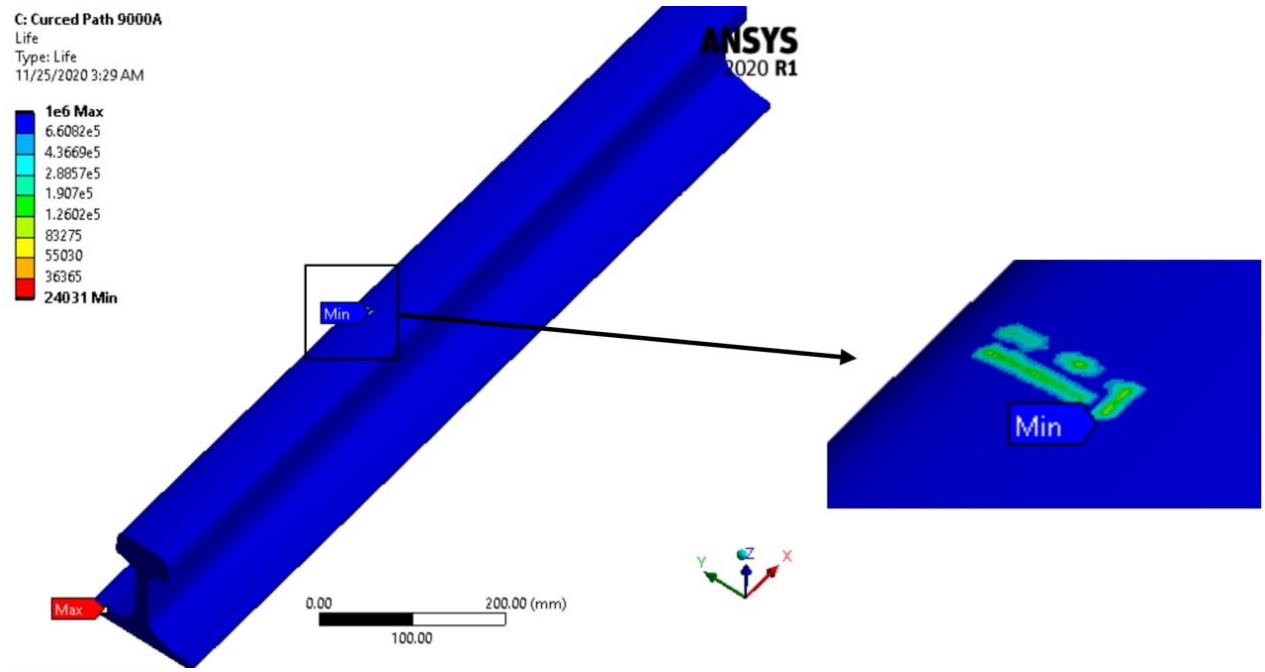

(a)

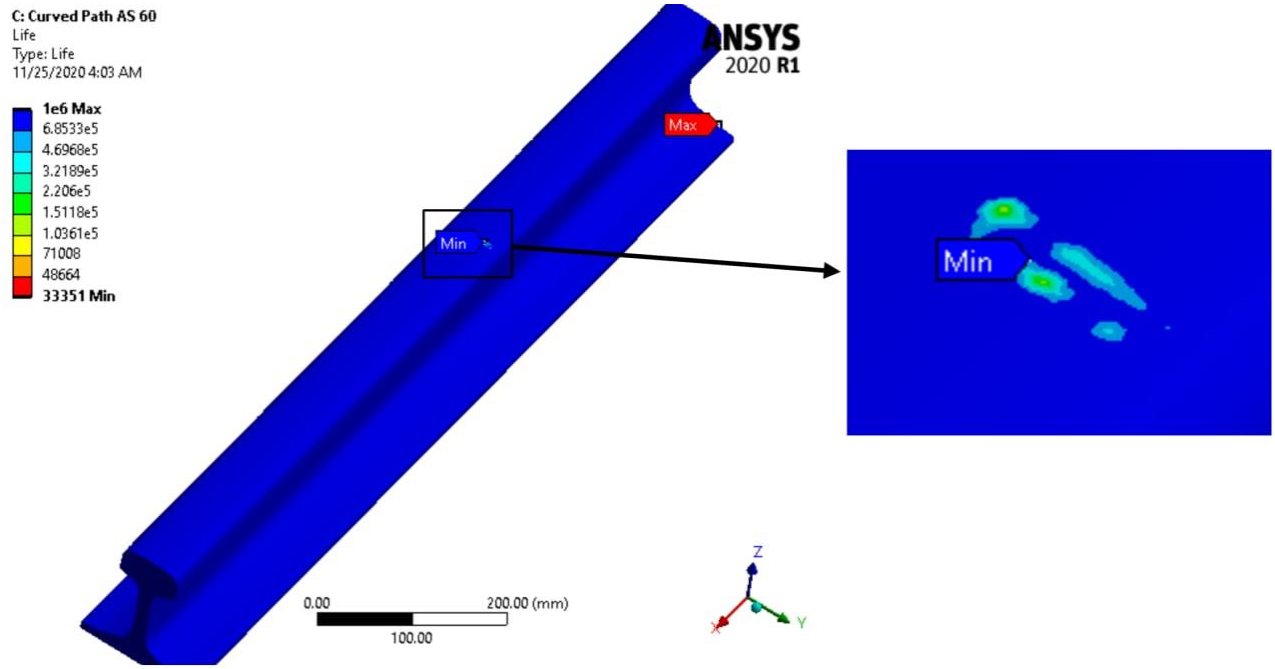

(b)

Figure 4.4 Counter plot of fatigue life for existing and selected material of wheel-rail rolling contact at the circular curve rail track path, (a) UIC54 and (b) AS60.

4.2.2. Equivalent Alternating Stress

The equivalent alternating stress contour plot is the voltage for interrogating the S-N curve. So, in a tiredness During the analysis, the equivalent alternating voltage/stress can be viewed as the last calculated quantity before determination of the service life. The usefulness of this result is that in general it contains all of the fatigue related calculations independent of any fatigue material properties. Some mean stress theories use static material properties such as tensile strength so Equivalent Alternating Stress may not be totally of material properties. This result does not apply to the strain or stress life if the amplitude fatigue load is not constant due to the fact that there are several S-N queries per location required and thus there is no single equivalent alternating voltage (stress).

(a). The contour plot of ANSYS 2020R1 Workbench shows the equivalent alternating stress for both materials at the straight rail track path condition which is shown in the Figure 4.5. (a) and (b).

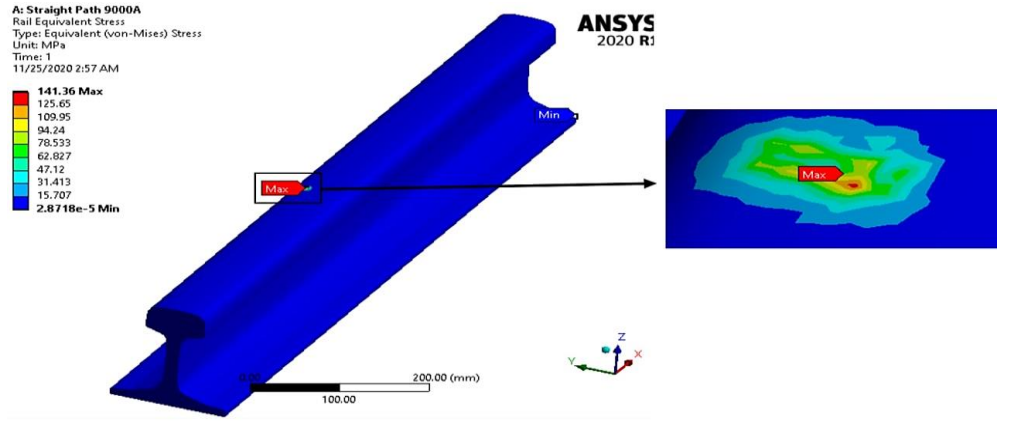

(a)

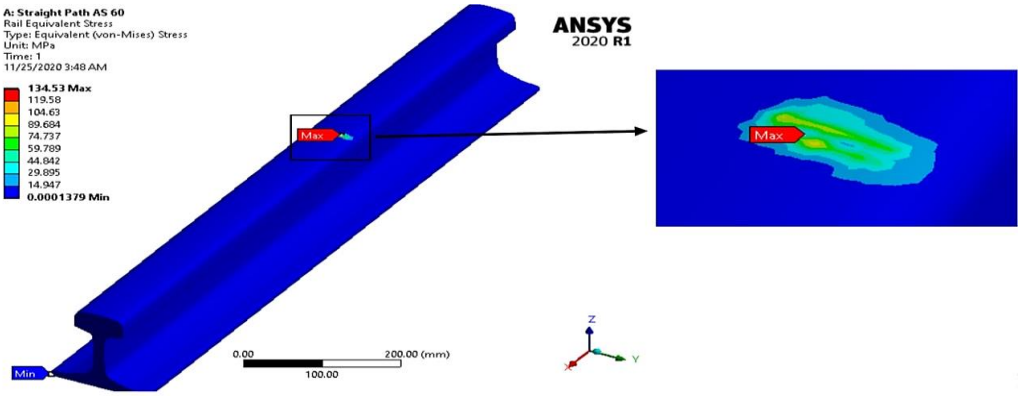

(b)

Figure 4.5 Counter plot of equivalent alternating stress for existing and selected material of wheel-rail rolling contact at the straight rail track path, (a) UIC54kg/m and (b) AS60kg/m.

(b). The contour plot of ANSYS 2019R3 Workbench shows the equivalent alternating stress for both materials at the transition curve rail track path condition which is shown in the Figure 4.6. (a) and (b).

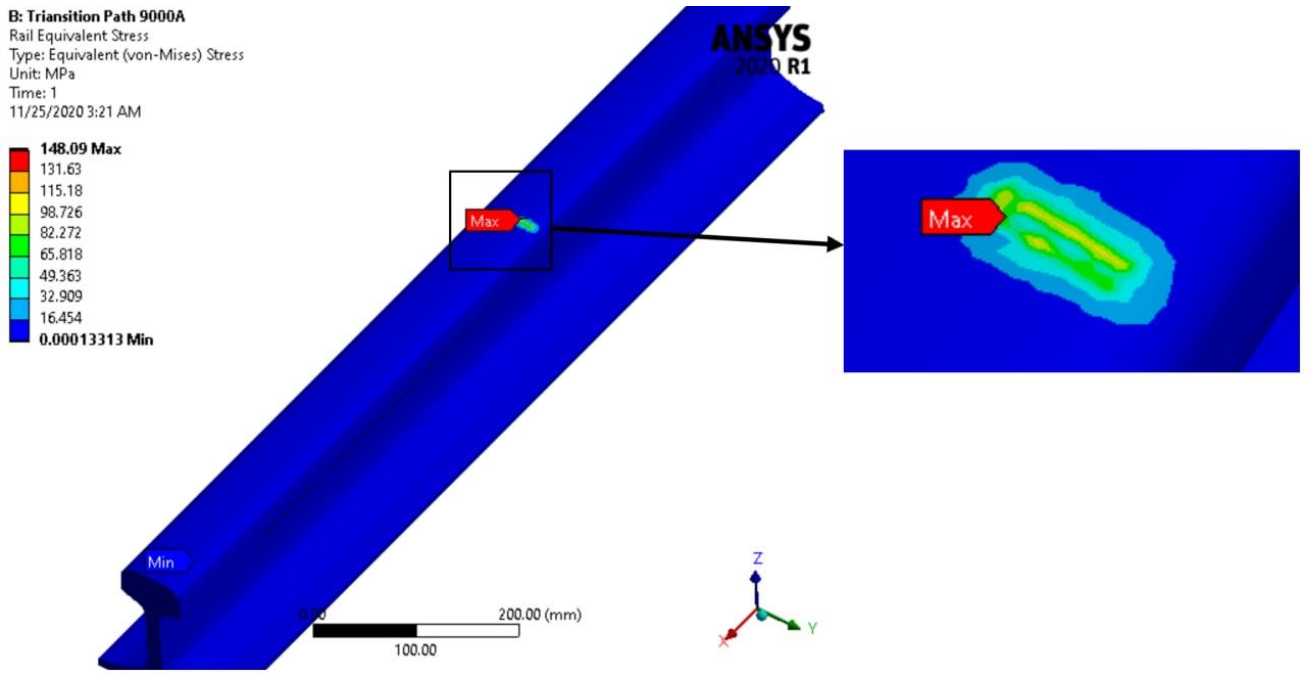

(a)

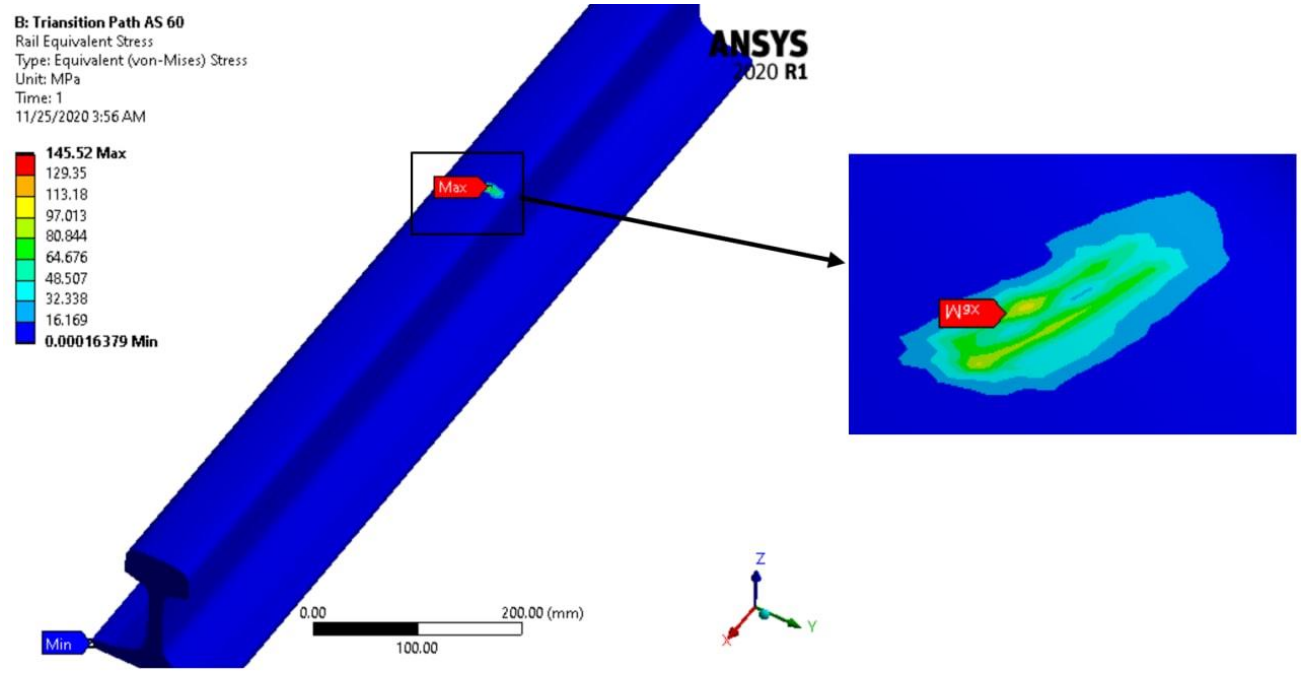

(b)

Figure 4.6 Counter plot of equivalent alternating stress for existing and selected material of wheel-rail rolling contact at the transition rail track path, (a) UIC54kg/m and (b) AS60kg/m.

(c). The contour plot of ANSYS 2020R1 Workbench shows the equivalent alternating stress for both materials at the circular curve rail track path condition which is shown in the Figure 4.7. (a) and (b).

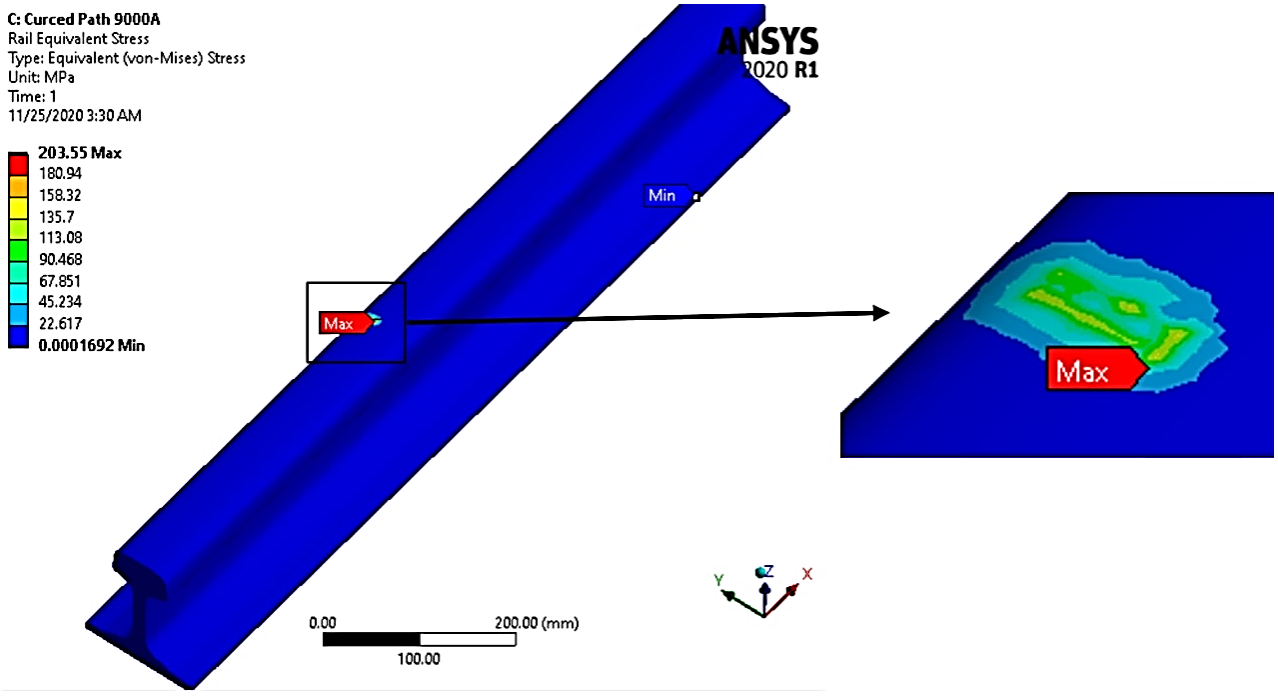

(a)

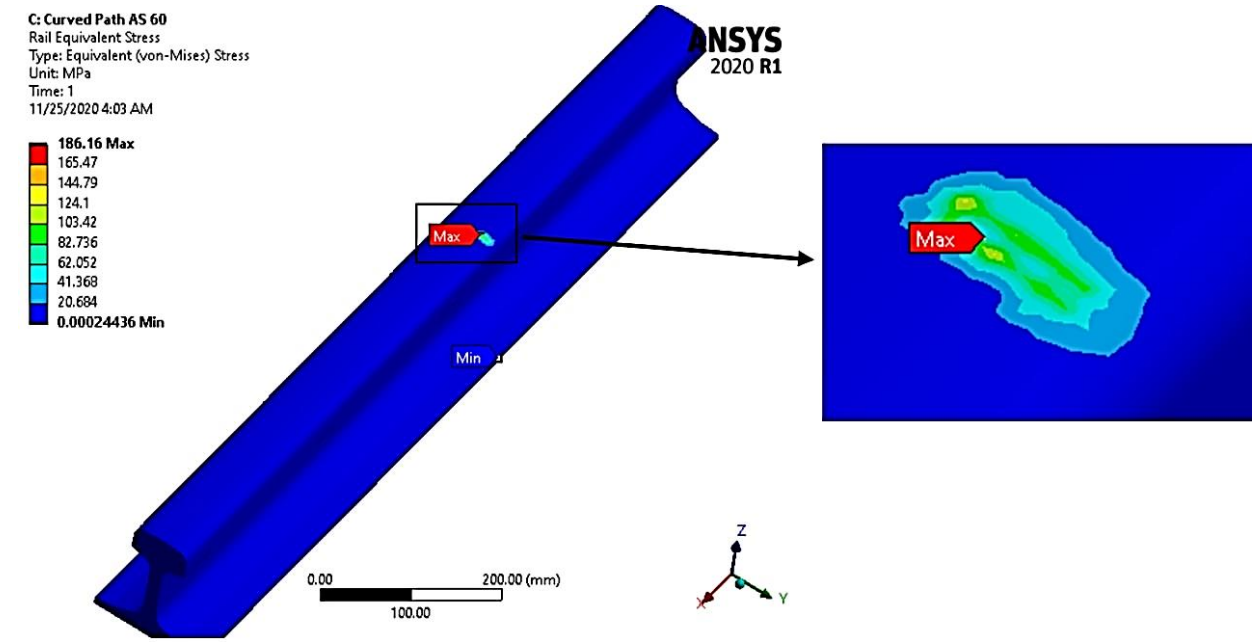

(b)

Figure 4.7 Counter plot of equivalent alternating stress for existing and selected material of wheel-rail rolling contact at the circular curve rail track path, (a) UIC54kg/m and (b) AS60kg/m.

4.2.3. Equivalent Elastic Strain

In 1910, Basquin observed that stress-life data could be modeled using a performance relationship, resulting in a straight line on a log-log chart. This observation corresponds to the elastic material behavior in the strain-life approach. The Basquin equation can be expressed in terms of true elastic strain amplitude. In the 1950s, Coffin and Manson independently discovered that plastic strain-life data could also be modeled using a performance relationship. Therefore, the elongation life curve can be formed by summing the elastic and plastic components, i.e., $\varepsilon_t = \varepsilon_e + \varepsilon_p$. For this paper we consider in the simulation results the elastic strain case only because which shows same fatigue results with the *Stress-Life approach*. And also, the counter plots of strain show the deformation of the rail steel material at the rolling contact interface. This contour plots inducts the maximum and minimum strain values for a constant applied axle load (a quasi - static axle load) at the three rail track conditions of EDR in the Awash area. These rail track conditions are straight, transition and circular curve, respectively.

(a). The contour plot of ANSYS 2020R1 Workbench shows the equivalent elastic strain for both materials at the straight rail track path condition as shown in Figure 4.8. (a) and (b).

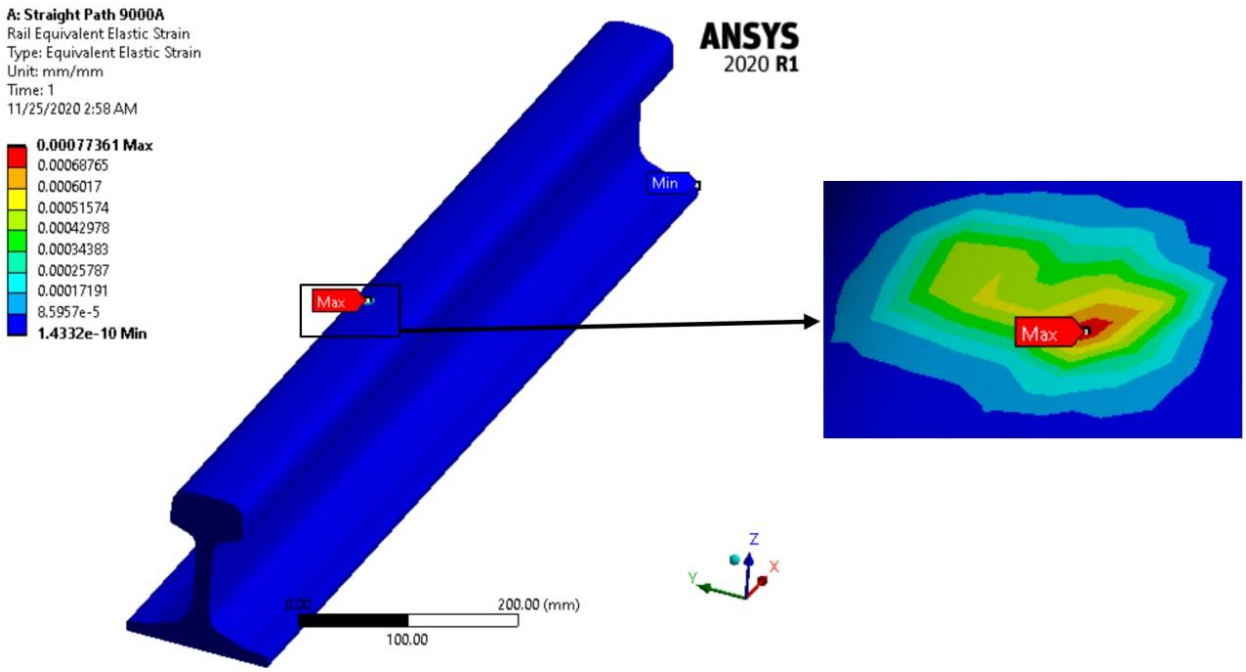

(a)

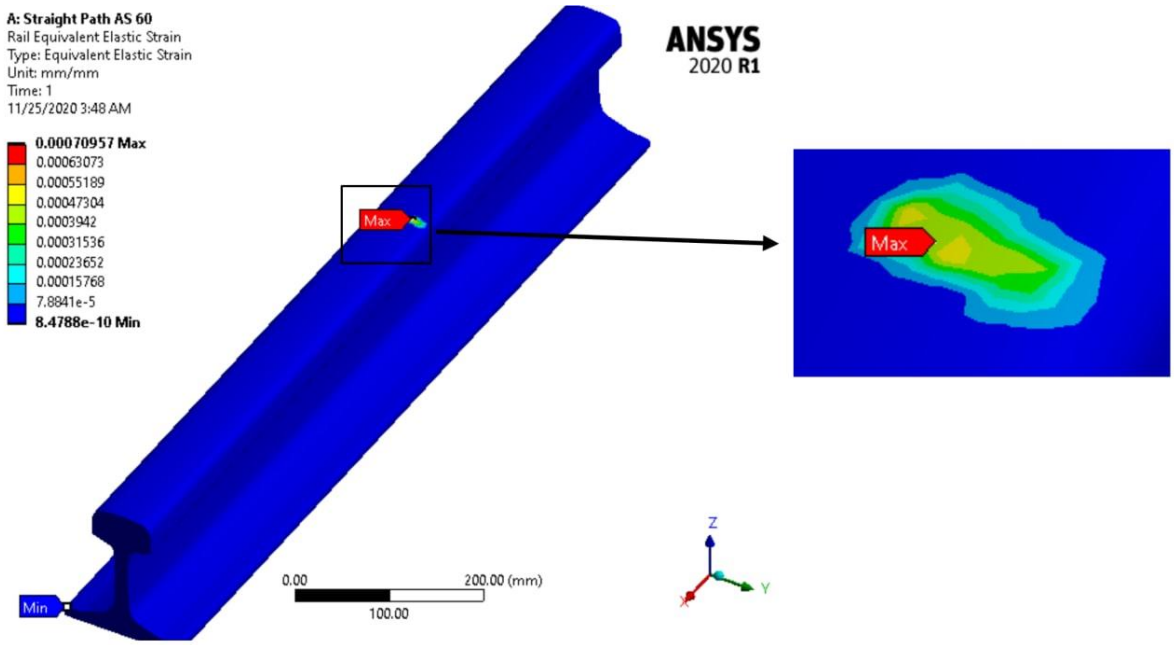

(b)

Figure 4.8 Counter plot of equivalent elastic strain for existing and selected material of wheel-rail rolling contact at the straight rail track path, (a) UIC54kg/m and (b) AS60kg/m

(b). The contour plot of ANSYS 2020R1 Workbench shows the equivalent elastic strain for both materials at the transition curve rail track path condition which is shown in the Figure 4.9. (a) and (b).

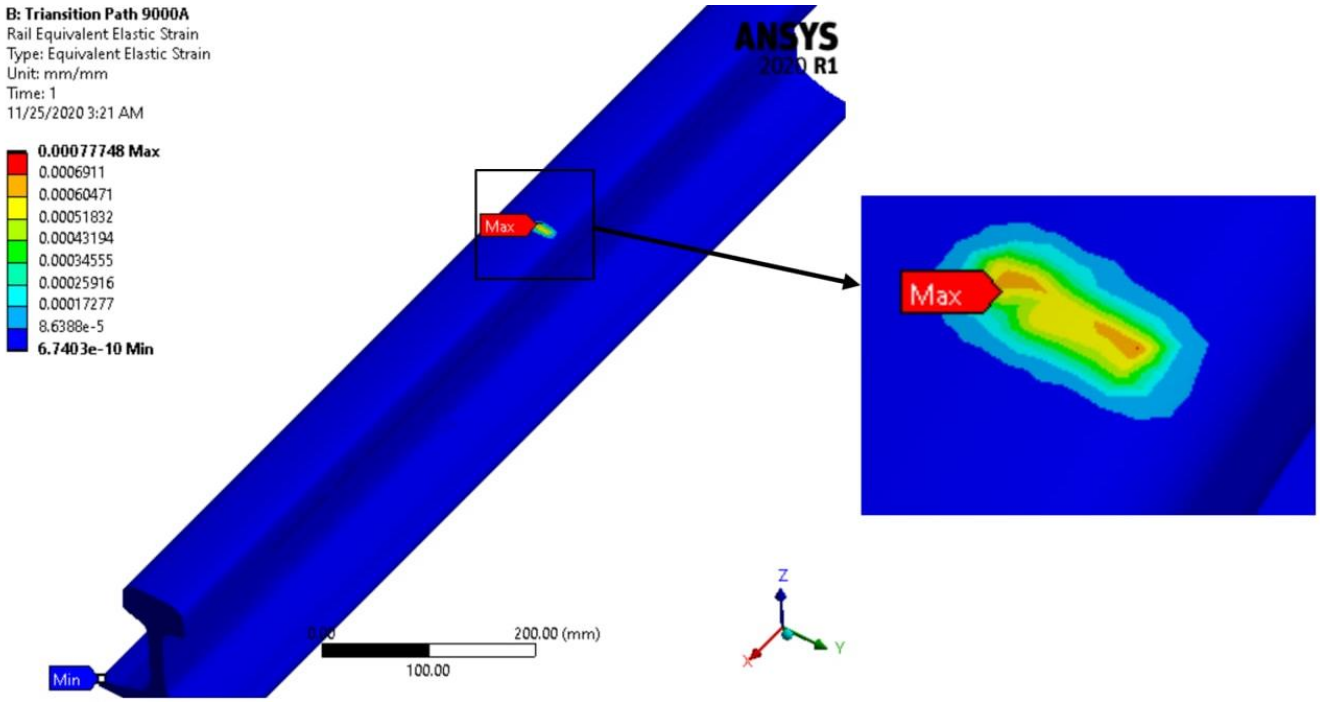

(a)

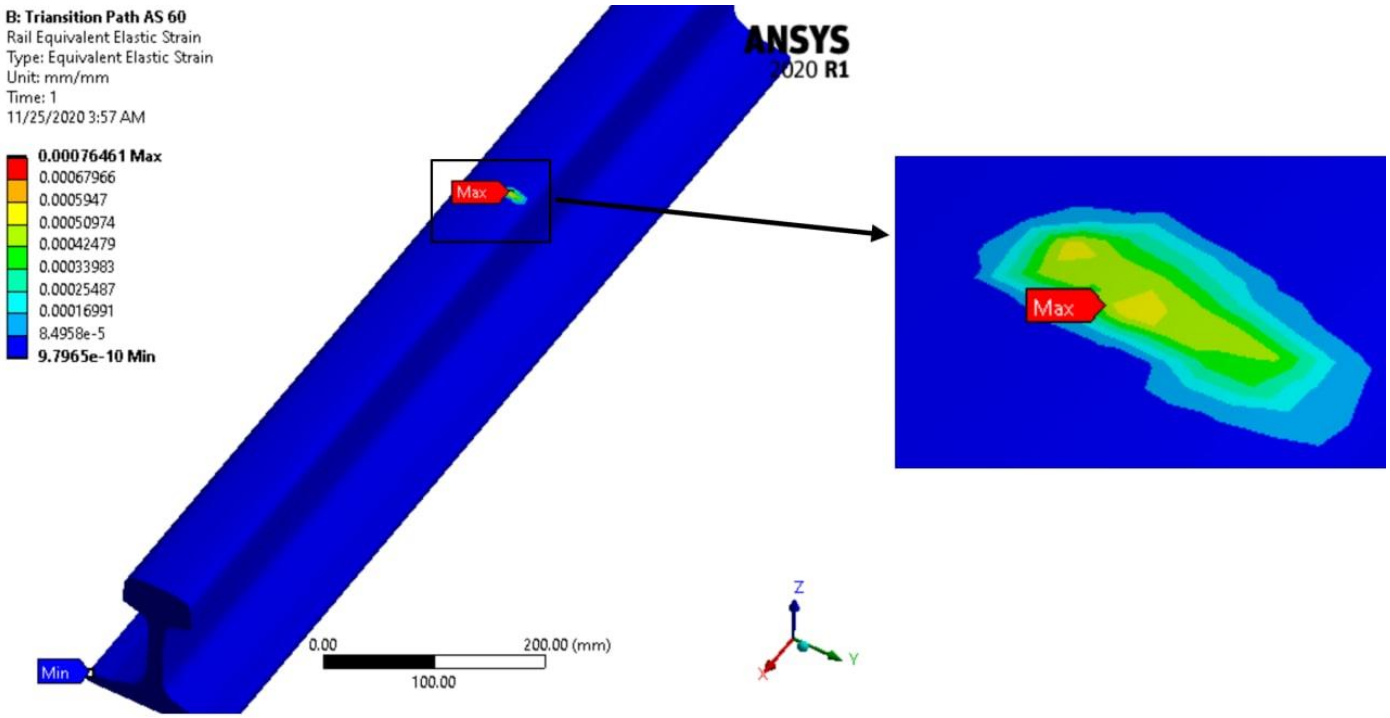

(b)

Figure 4.9 Counter plot of equivalent elastic strain for existing and selected material of wheel-rail rolling contact at the transition curve rail track path, (a) UIC54kg/m and (b) AS60kg/m.

(c). The contour plot of ANSYS 2020R1 Workbench shows the equivalent elastic strain for both materials at the circular curve rail track path condition as shown in Figure 4.10. (a) and (b).

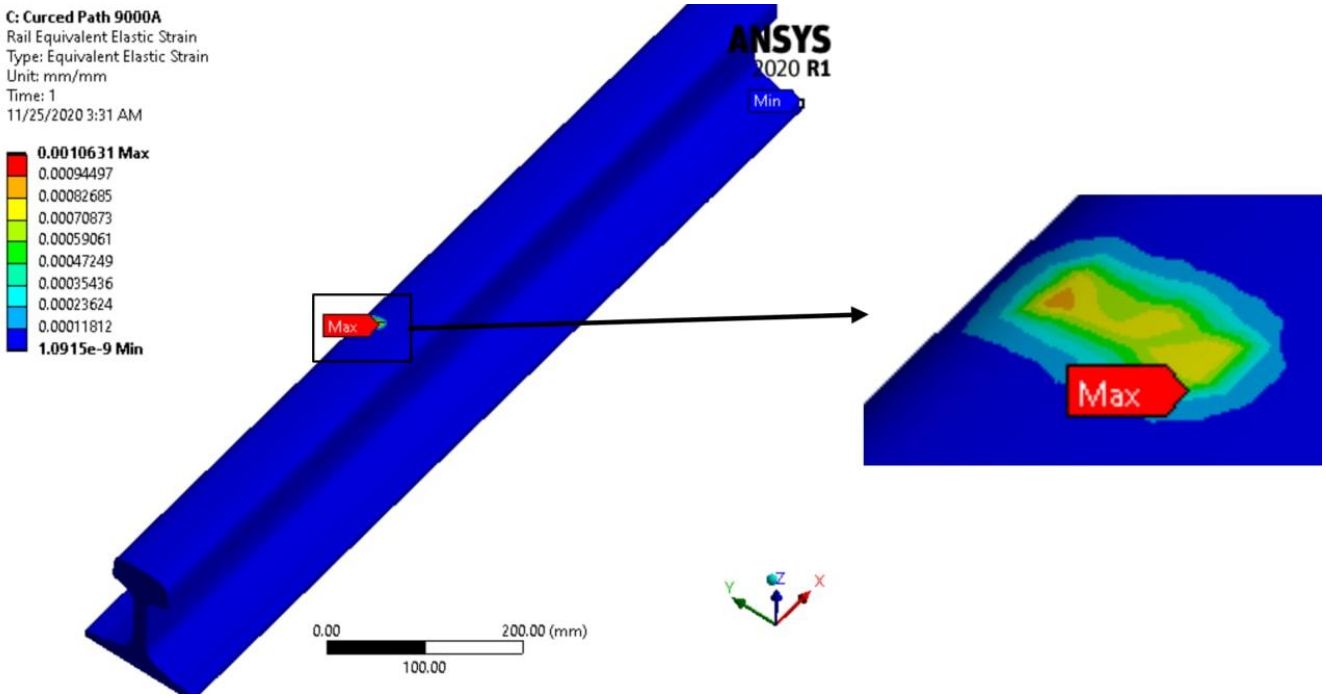

(a)

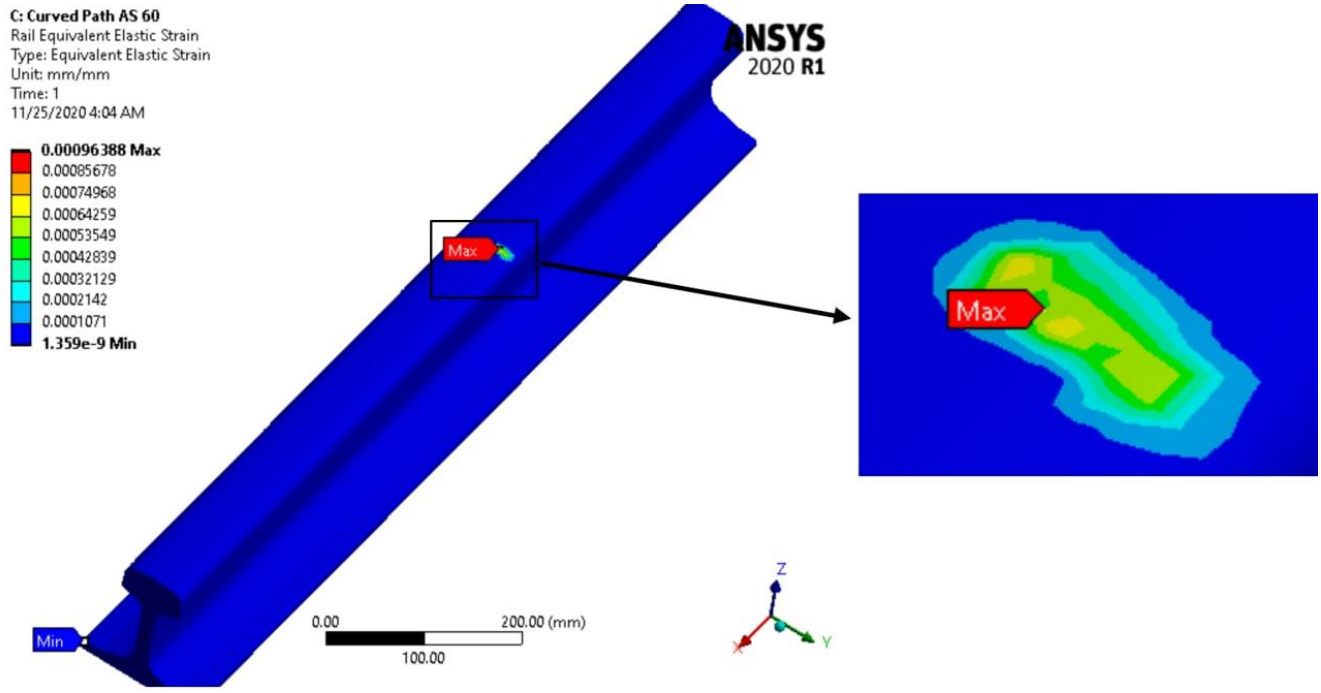

(b)

Figure 4.10 Counter plot of equivalent elastic strain for existing and selected material of wheel-rail rolling contact at the circular curve rail track path, (a) UIC54kg/m and (b) AS60kg/m.

4.2.4. Total Deformation

(a). The contour plot of ANSYS 2020R1 Workbench shows the total deformation for both materials at the straight rail track path condition which is shown in the figure 4.11. (a) and (b).

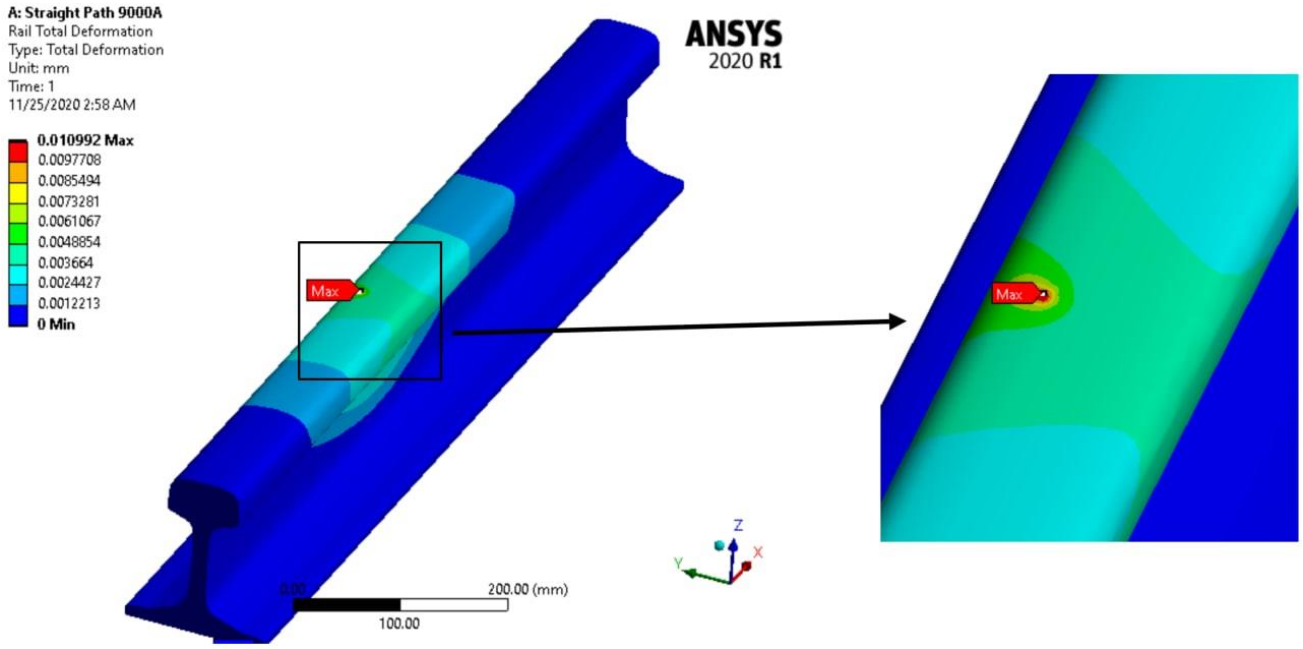

(a)

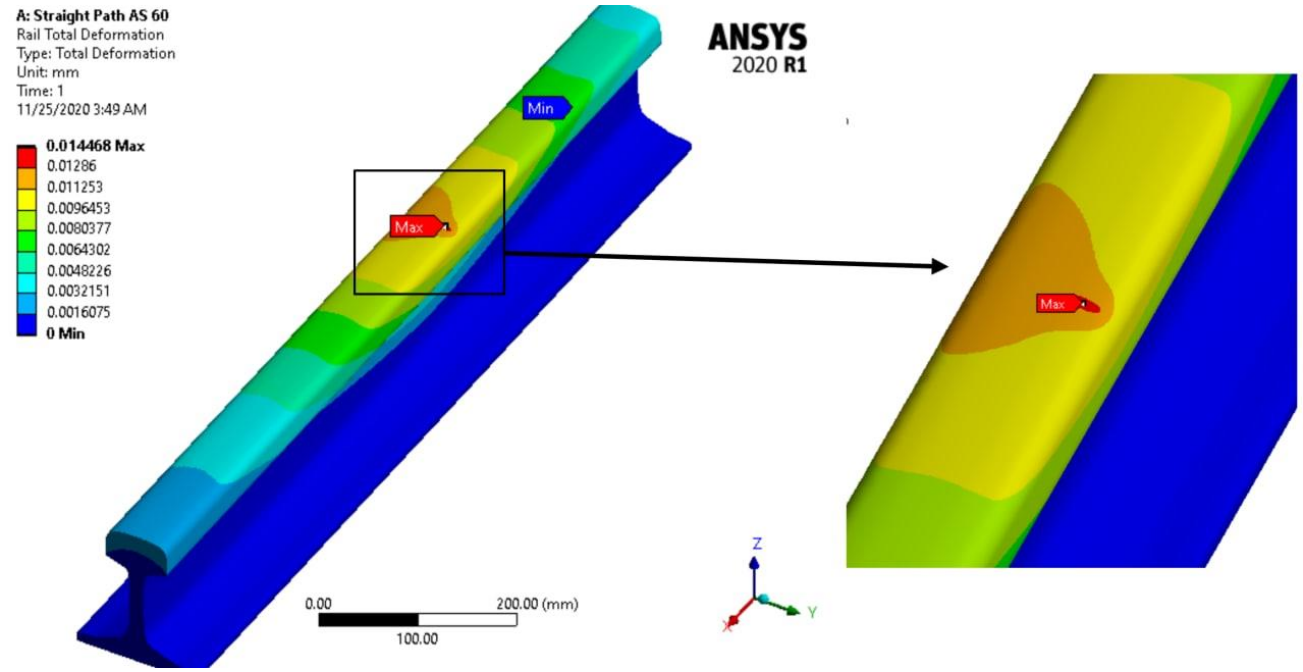

(b)

Figure 4.11 Counter plot of total deformation for existing and selected material of wheel-rail rolling contact at the straight rail track path, (a) UIC54kg/m and (b) AS60kg/m.

(b). The contour plot of ANSYS 2020R1 Workbench shows the total deformation for both materials at the transition curve rail track path condition which is shown in the Figure 4.12. (a) and (b).

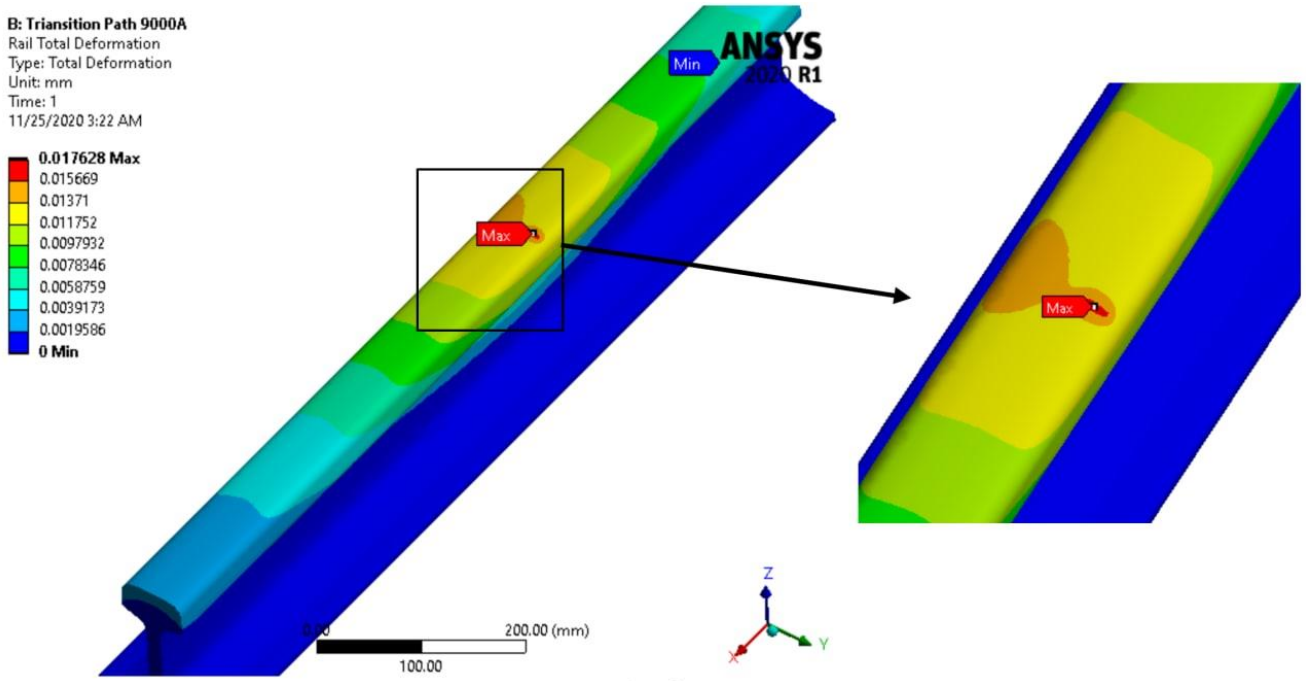

(a)

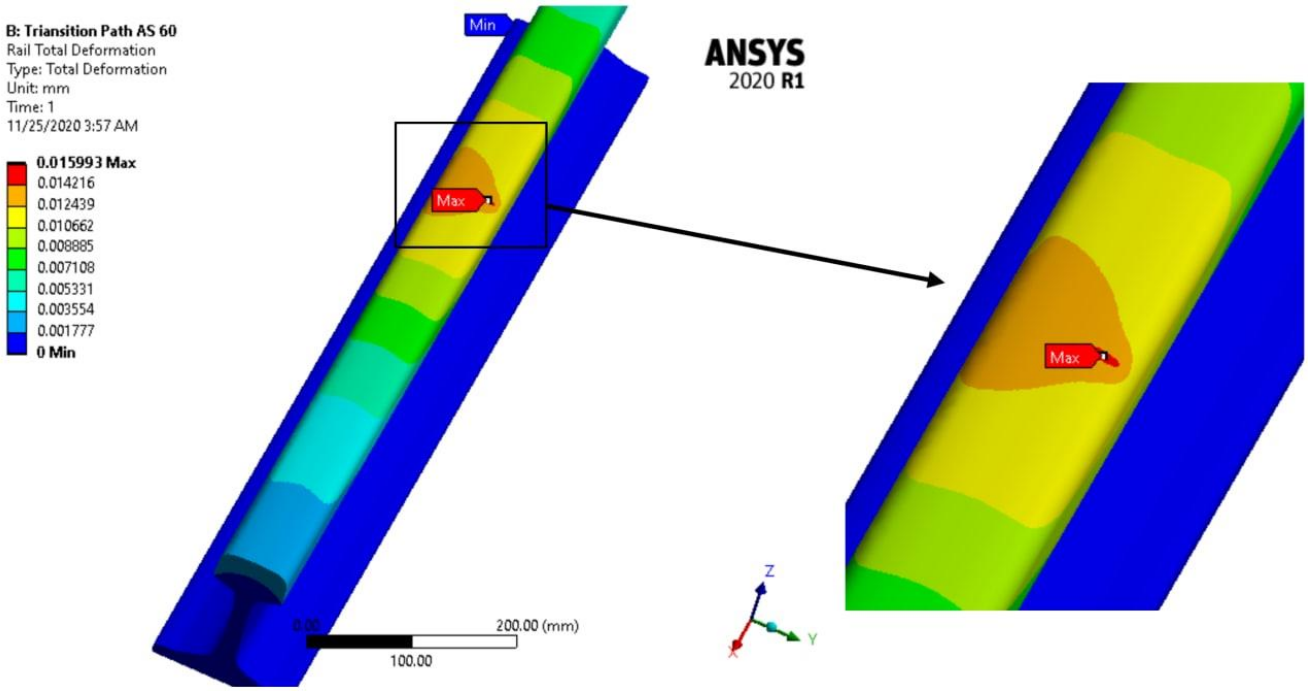

(b)

Figure 4.12 Counter plot of total deformation for existing and selected material of wheel-rail rolling contact at the transition curve rail track path, (a) UIC54kg/m and (b) AS60kg/m.

(c). The contour plot of ANSYS 2020R1 Workbench shows the total deformation for both materials at the circular curve rail track path condition which is shown in the Figure 4.13. (a) and (b).

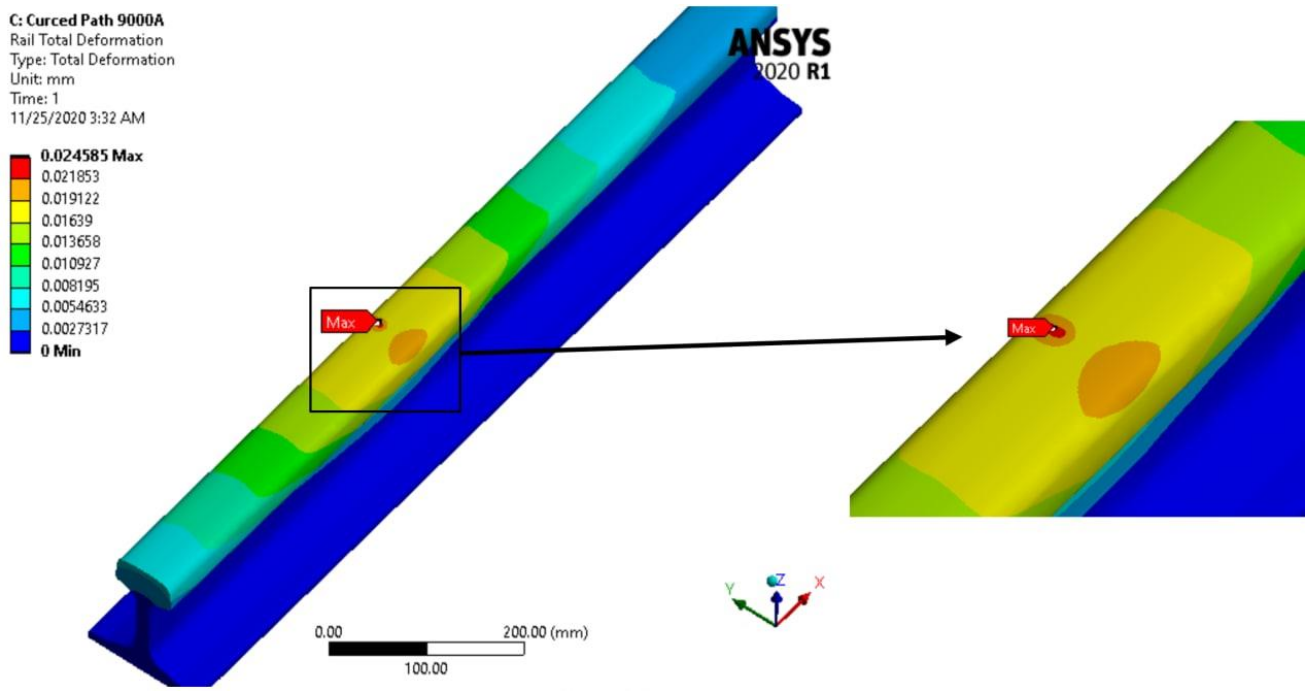

(a)

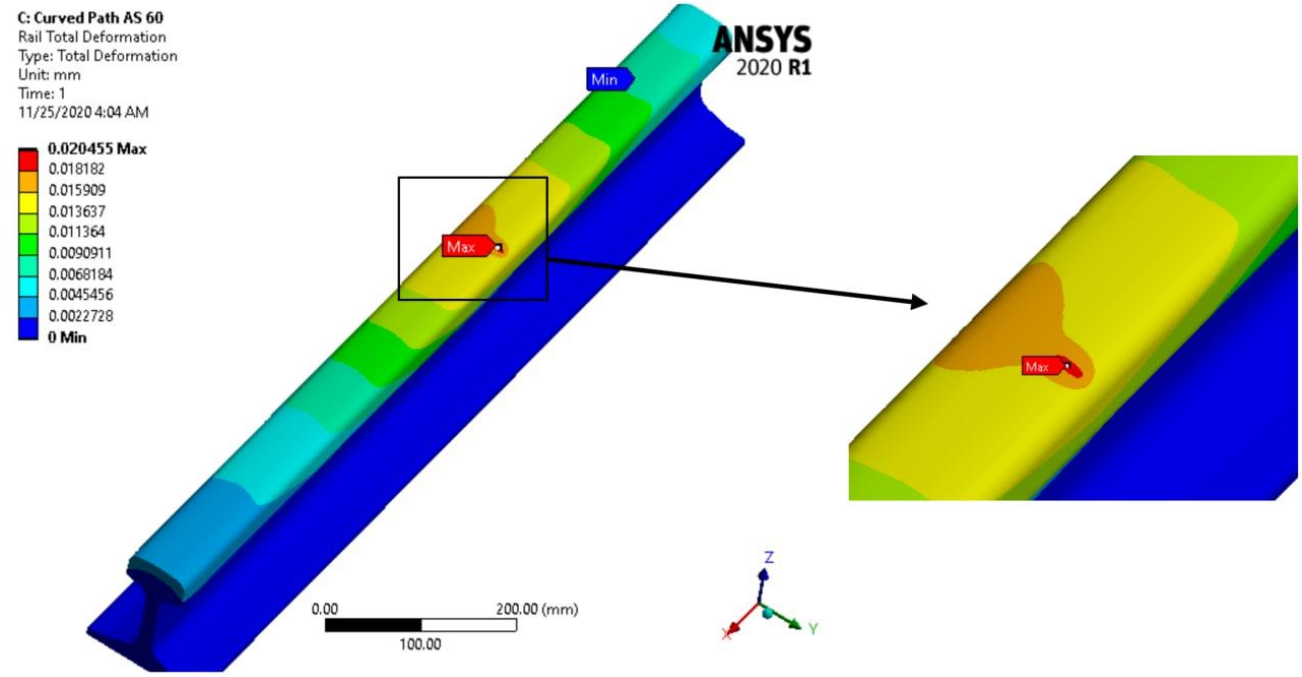

(b)

Figure 4.13 Counter plot of total deformation for existing and selected material of wheel-rail rolling contact at the transition curve rail track path, (a) UIC54kg/m and (b) AS60kg/m.

4.2.5. Fatigue Sensitivity

This diagram shows how the fatigue results change depending on the load at the critical points on the area. Sensitivity to service life, damage or safety factor can be determined for both materials. After seating the lower and upper fatigue sensitivity limits to 50% and 150% respectively, and our scale factor is 1, this result will plot the data points along a scale ranging from a 0.5 to a 1.5 scale factor based on elastic strain and stress-life approach as seen in Figure 4.14. for stress approach and Figure 4.15. for Elastic Strain.

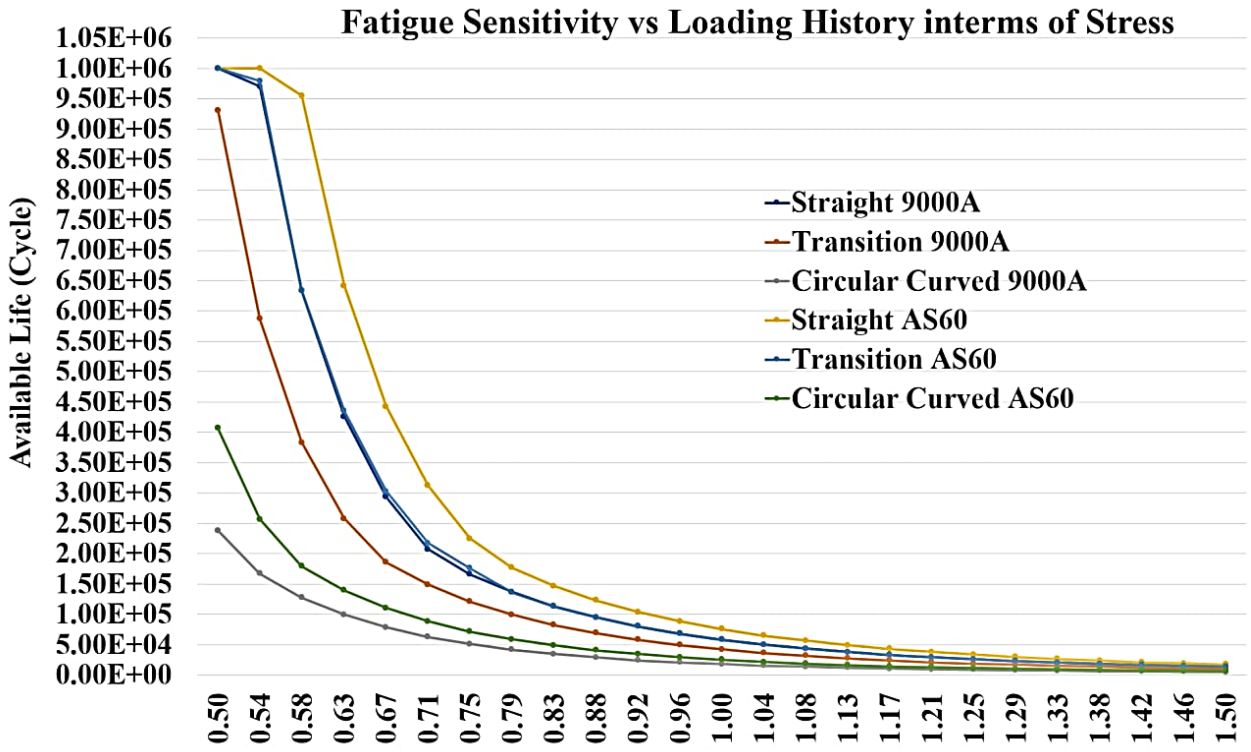

Figure 4.14 Fatigue sensitivity for existing and selected material of wheel-rail rolling contact at the straight, transition curve and circular curve rail track conditions for UIC54kg/m and AS60kg/m.

The fatigue sensitivity tells us from the soft wear results (ANSYS 2020R1) the loading history and the critical locations (straight, transition and circular curve) respectively has direct relation on fatigue life of the body. That means as loading history increases the fatigue life time of the object decreases. And the more critical location like sever curve decreases its failure time with the same applied load.

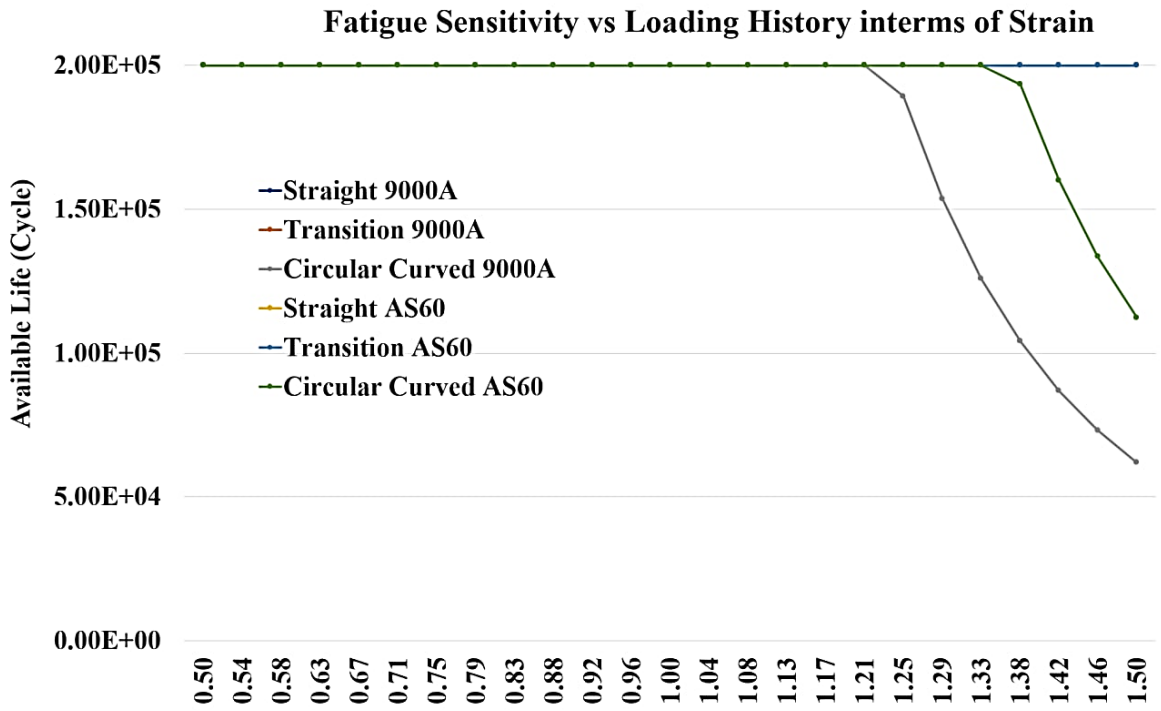

Figure 4.15 Fatigue sensitivity for existing and selected material of wheel-rail rolling contact at the straight, transition curve and circular curve rail track conditions for UIC54kg/m and AS60kg/m.

4.3. Discussions

This paper focuses on the wheel-rail contact interface the rail fatigue life and the fatigue life comparison between the EDR rail existing material and newly selected material of ANSYS results on straight, transition and circular curve of rail track. And the above results can be discussed using fatigue life versus equivalent alternating stress and effect of rail track conditions to compare for both materials.

4.3.1. Equivalent Alternating Stress Versus Fatigue Life

In a Stress Life fatigue analysis, one always needs to query the S-N curve to relate the fatigue life to the stress state. Thus, the "equivalent stress" is the stress used to query the fatigue S-N curve after considering the fatigue stress type, mean stress effects, multiaxial effects, and all other factors in fatigue analysis. From ANSYS 2020R1, the workbench simulation also shows as the usual S-N curve for this case that the alternating stress / voltage increases and the service life of the rails for both materials decreases, as shown in Figure 4.16.

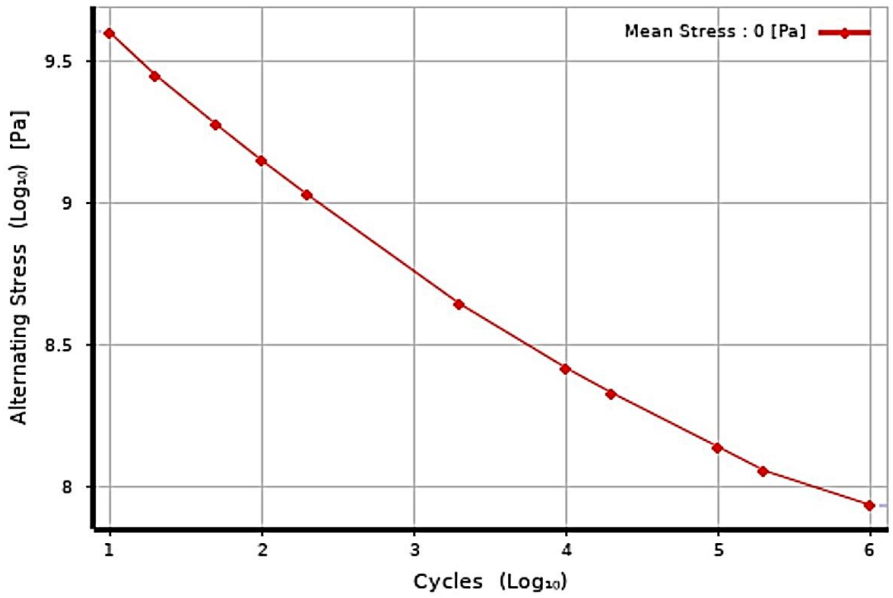

Figure 4.16 Fatigue life N-S curve.

Based on a real condition of ANSYS 2020R1 results of Equivalent Alternative stress cycle and life cycle for each structural steel relates with the Excel graph at the critical condition of rail is shows in the Figure 4.17.

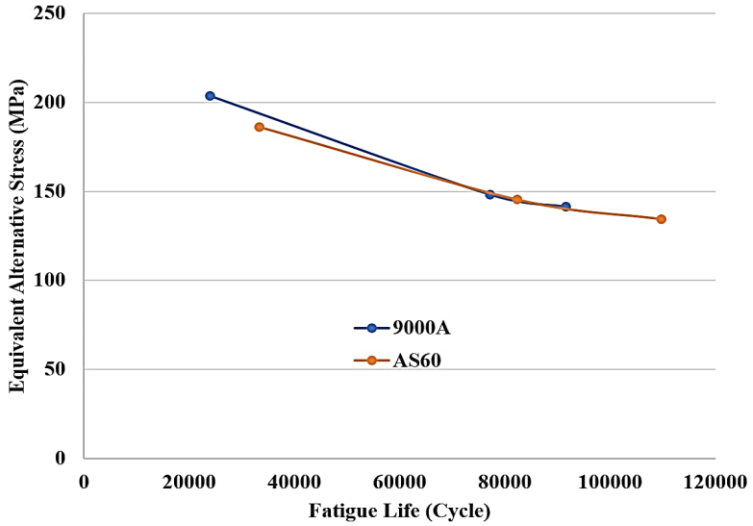

Figure 4.17 Equivalent Alternative stress versus fatigue life cycle both material grade of 9000A and AS60.

From the graph above the fatigue crack initiation life cycle at the early stage for circular curve rail track but for material grade 9000A much early stage than material grade AS60. This effect happen during the stress factor effect is increasing.

The equivalent alternating stress results of ANSYS 2020R1 Workbench for both materials, that means the existing (9000A) and newly selected (AS60) are summarized in the Table 4.1.

Table 4.1 Summery FEA results of the rail track for 9000A & AS60 materials

Track Conditions	Equivalent Alternating Stress	
	9000A / Mpa	AS60 / Mpa
Straight Rail Track	141.36	135.53
Transition Curve Rail Track	148.09	145.52
Circular Curve Rail Track	203.55	186.16

From the stress result in the Table 4.1 the AS60 rail material has lower stress value in the three tack conditions this shows that the newly selected material has a better fatigue life from the existing material of EDR.

4.3.2. Equivalent Alternating Strain Versus Fatigue Life

Based on Basquin and Coffin and Monson equation the elongation life curve can be formed by summing the elastic and plastic components, i.e., $\varepsilon_t = \varepsilon_e + \varepsilon_p$. The influence of the elastic and plastic components on the strain-life curve is shown in Figure 4.18. For this paper we consider in the simulation results the elastic strain case only because which shows same fatigue results with the *Stress-Life approach*.

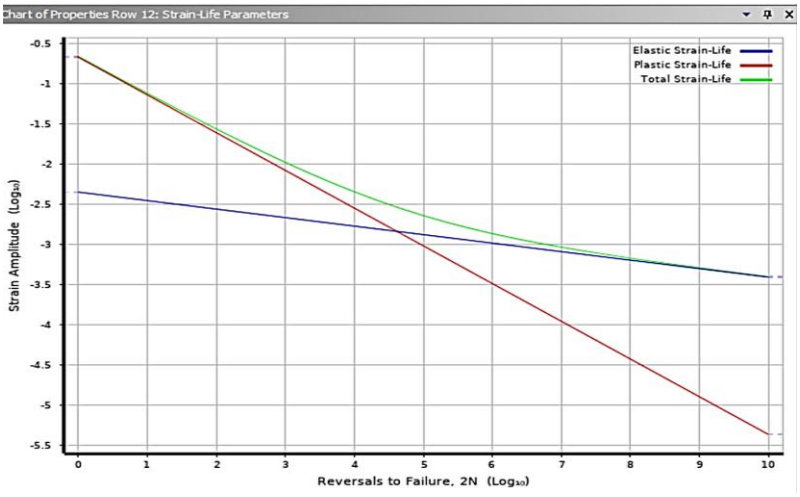

Figure 4.18 The general material property fatigue life of strain amplitude verses reversals to failure, 2N (Strain -Life Curve)

The transition life 2Nt represents the life at which the elastic and plastic strain ranges are equivalent. From the graph above elastic strains have a greater influence on fatigue lives above the transition life. Plastic strains have a greater influence below the transition life. Thus, the transition life provides a convenient delineation between low-cycle and high-cycle fatigue regimes.

Therefore, from the ANSYS simulation results for the case of elastic strain and Awash real condition the elastic strain-life curve (E-N curve) shows the strain value versus fatigue life cycle for straight, transition curve and circular curve as inducted Figure 4.19. for existing material of 9000A and for SA60 selected material. And as the strain value of ANSYS 2020R1 Workbench increases the fatigue life decreases.

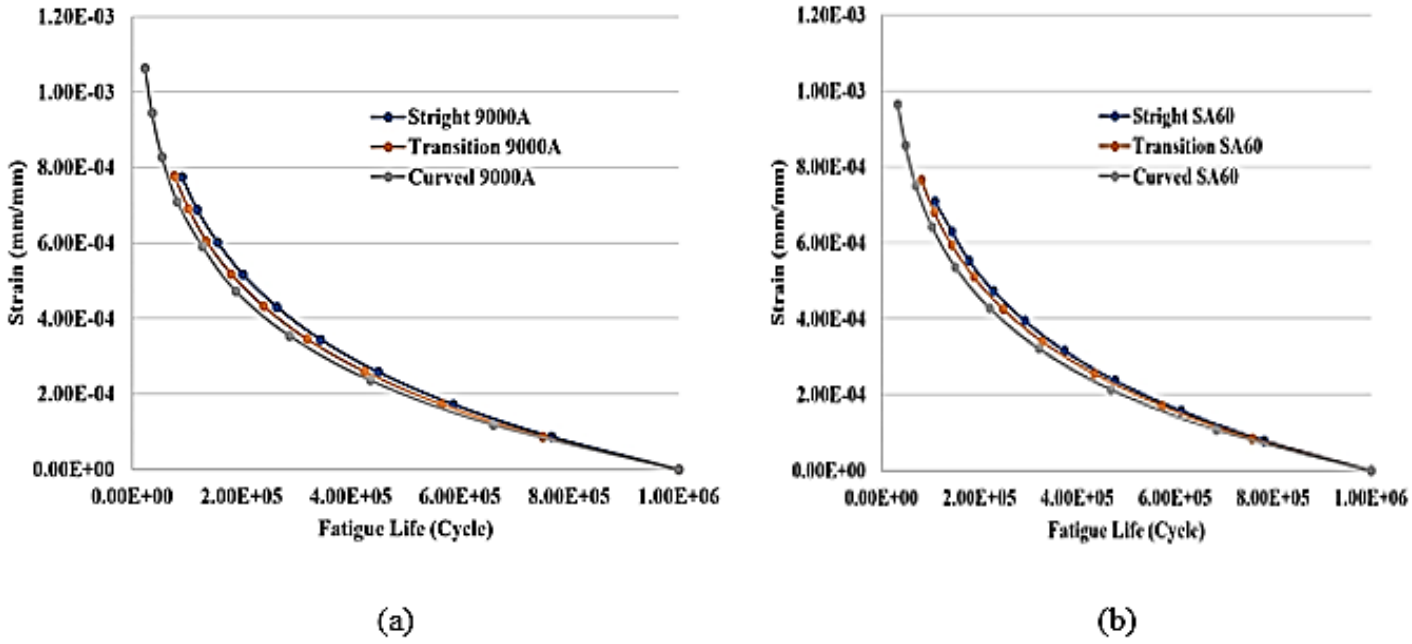

Figure 4.19 Elastic strain versus fatigue life (cycle) material graph on Awash real condition (a) for 9000A material and (b) for SA60 material.

From the above Excel line graph of elastic strain vs fatigue life of both materials as general the fatigue life of material decreases as increases the strain value for each critical location of track path. Based on strain approach theories the crack initiation cycle of 9000A material is much earlier than that of material SA60. For example, in the circular curve track condition of 9000A material the crack initiation cycle is starts much before 1.00E-03mm strain value where as SA60 material initiation cycle is starts after the strain value of 1.00E-03mm.

Summery for equivalent alternating strain versus fatigue life:

Based on a real conditions Awash area the ANSYS 2020R1 results of Equivalent Alternative strain cycle and life cycle for each structural steel relates with the Excel graph at the critical condition of rail that means straight, transition curve and circular curve track condition for each material is shows in the Figure 4.20.

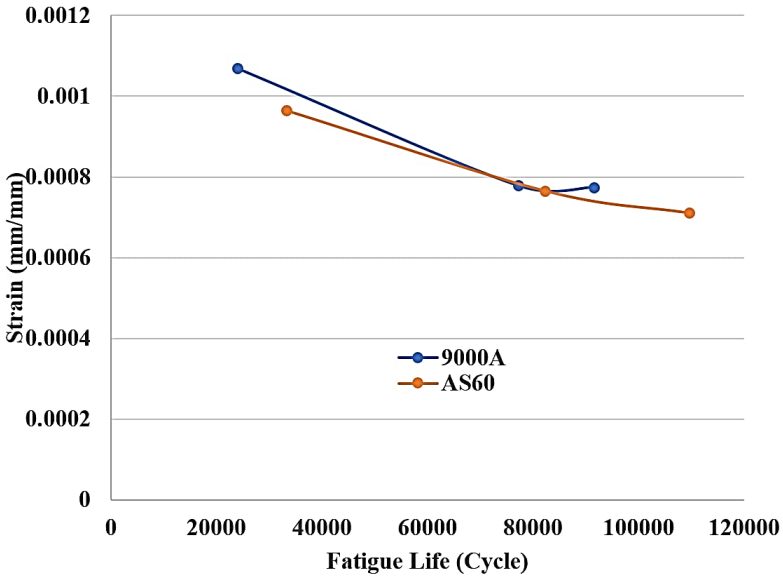

Figure 4.20 Equivalent Alternative strain versus fatigue life cycle both material grade of 9000A and AS60.

In the same manner of stress, the strain Figure 4.20 shows the fatigue crack initiation life cycle at the early stage for circular curve rail track but for material grade 9000A much early stage than material grade AS60. This happen during the strain factor effect is increasing. With numerical value of strain at the circular curve the crack initiation cycle starts between 0.0012 and 0.001mm strain value for existing material of EDR whereas the new material starts after the strain value of 0.001mm.

4.3.3. Effect of Track Conditions on RCF at the Wheel-Rail Contact

The effect of track conditions can be discussed using bar graphs for both materials as a comparison by using total deformation, equivalent alternating stresses and fatigue life of each track conditions straight, transition curve and circular curve. Therefore, the track conditions of rail track can be affected by deformation, equivalent alternating stresses and equivalent alternating elastic strain.

Total Deformation:

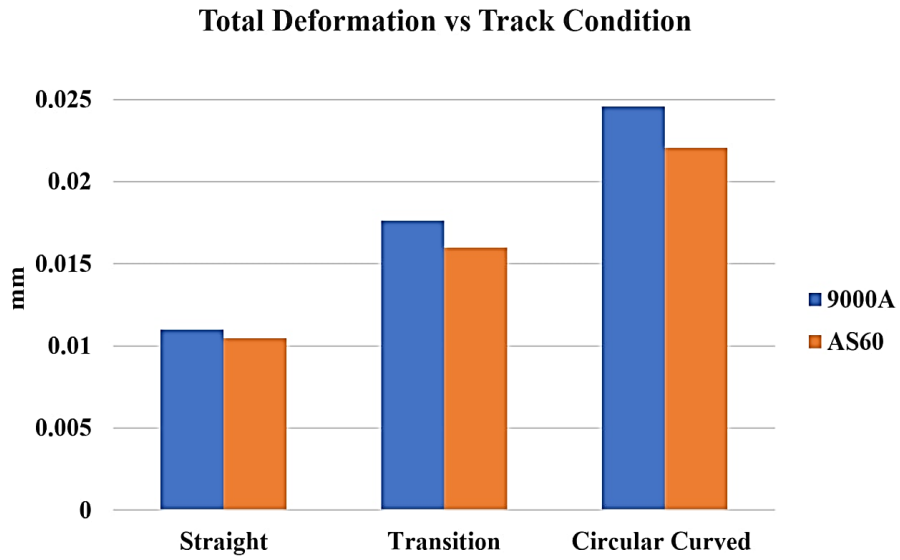

Figure 4.21 Total deformation of rail track for UIC54 and AS60 rail material.

From the Figure 4.21 the total deformation of AS60 lower than 9000A exsiting material of EDR at rolling cotact point of wheel-rail in the straight, transition curve and circular curve of Ethio-Djibouti raliway line. The total deformation of AS60 rail material decreases by 12.7%, 13.26% and 24.43% at the straight, transition curve and circular curve repectively and this inducts that the fatigue life for selected material is better than the existing one.

Equivalent Alternating Stress:

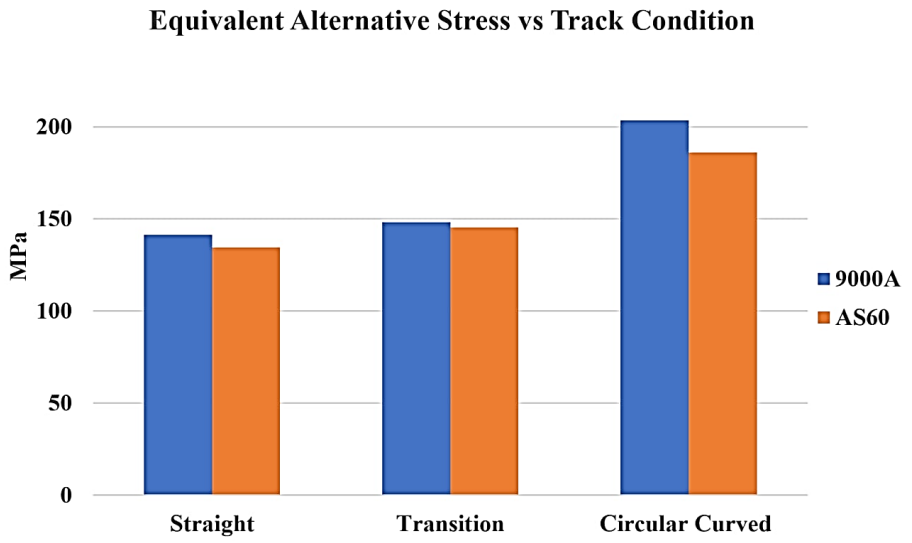

Figure 4.22 Equivalent alternating stress of rail track for 9000A and AS60 rail material.

From the Figure 4.22 the equivalent alternating stress of AS60 lower than 9000A exsiting material of EDR at rolling cotact point of wheel-rail in the straight, transition curve and circular curve of Ethio-Djibouti raliway line. The equivalent alternating stress of AS60 rail material decreases by 5.69%, 10.3% and 13.11% at the straight, transition curve and circular curve respectively and this also inducts that the fatigue life for selected material is better than the existing one.

Fatigue life:

From the stress-life fatigue analysis, the obtained fatigue results at constant coefficient of friction and constant axle load indicate the track condition is greatly affected the wheel-rail rolling contact fatigue. For both materials the minimum fatigue life of rail rolling contact at straight, transition curve and circular curve track paths are presented here in Table 4.1.

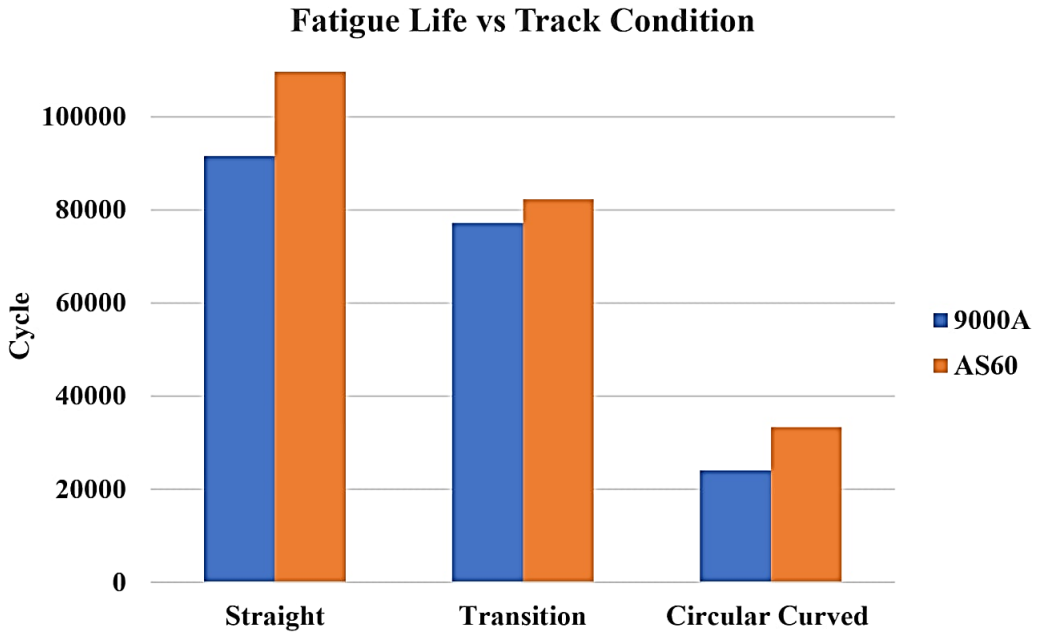

Figure 4.23 Fatigue life of rail track for 9000A and AS60 rail material.

Table 4.2 Effect of track conditions on fatigue life at the rail rolling contact.

Fatigue Results	At Straight Track	At Transition Curve	At Circular Curved Track
Life of existing rail track	91557 Cycles	77194 Cycles	24031 Cycles
Life of new rail track	109695 Cycles	82313 Cycles	33351 Cycles

Figure 4.23 and Table 4.2 indicated that the minmum fatigue life/the crack initiation cycle of the given rail materials. Therfore the grade AS60 rail steel greater than the grade 9000A rail steel which is currently

exsiting material of EDR. This tell us the fatigue life of AS60 rail material shows the crack intiation cycle increases by 16.5% for the straigth path, 22.03% for the tranisition track path and 27.95% for the circular curve track path which indicates that the fatigue life for selected material is better than the existing one.

Chapter Five

Conclusion, Recommendation and Future Work

5.1. Conclusion

The thesis presents an analysis of the rolling contact fatigue at the wheel-rail interface for both rail materials, i.e., for the existing and the newly selected material using the digital logic method. A three-dimensional FEA is used for the wheel-rail track rolling contact fatigue analysis. The wheel-rail assembly geometry is created in SOLIDWORK 2019 and the FEA is performed by using ANSYS 2020R1 workbench. The material used for the wheel and track are the same which is the existing UCI54Kg/m and the new AS60Kg/m and the boundary conditions are employed in the wheel and rail in terms of the different track loading conditions: straight, transition, and curved path. The fatigue analysis is based on the stress life approach and takes into account a constant coefficient of friction (0.3) for all three track conditions

From the stress-life fatigue analysis, the obtained fatigue results at constant coefficient of friction, lateral and axle weight load indicates the track condition is greatly affected the wheel-rail rolling contact fatigue life. In the case of straight tracks, the minimum service life of the rolling contact is in the middle of the rail head and the center of the wheel profile. While on the transition and circular curve path, the minimum service life of the rolling contact is formed on the rail corner gauge and on the wheel root flange.

The ANSYS 2020 R1 Workbench result pointed that the maximum equivalent alternating stresses and minimum fatigue life at the wheel-rail rolling contact are: for existing material 141.36Mpa, 148.09Mpa and 203.55Mpa and 91557 cycles, 77194 cycles and 24031.5 cycles and for newly selected material 134.53MPa, 145.MPa and 186.16MPa and 109695 cycles, 82313 cycles and 33351 cycles for straight, transition and circular curve respectively. Based on the ANSYS 2020R1 Workbench results manifests the existing material (grade of 9000A) has low minimum crack initiation fatigue life at all three track conditions, that means at the straight, transition curve and circular curve whereas the newly selected material (grade of AS1085.1) has improved the crack initiation fatigue life cycle.

Finally, these results are practicable in fatigue resistance design and pre-inspections before much distractions may happen for Ethio-Djibouti heavy duty rail line because the fatigue life predication indicated that there is a reduction of track life with an increasing of stress and deformation.

5.2. Recommendation

Based on the results of the FEA methods with constant coefficient of friction ($\mu = 0.3$) and applied load (axle and centrifugal force) due to the total axle load of 25 tons and the speed of the train 120 km / h. The fatigue life at the rail rolling contact with straight, circular transition curves reduces the rail life cycles for both existing and newly selected material. Based on the fatigue analysis results I recommend the EDR shear company to use the newly selected material (AS60) because:

1. AS60 has better fatigue life at each track condition for this reason, I recommended to be used in the EDR future rail track may failure happen.
2. In circular curve the rolling fatigue failures may happen before the straight and transition curve area; the maximum standard length of rail tack is 25m and it is disassembled and assembled easily because it assembled using flash plate like bolt system. So due to high installation coast of rail through line during failure happen they can replace only the critical area which increase the fatigue life of the circular curve from the existing rail track.

5.3 Future Work

The following research areas are recommended for future studies:

- ✓ Repeat the analysis taking into account the different rolling contact coefficient of friction using FEA and should check this experimentally with a suitable testing machine.
- ✓ Thermomechanical fatigue analysis of the railway wheel in slide-roll motion with FEM. This helps to study the effect of thermal loads on the service life of the wheel profile during slipping or sliding.
- ✓ With the same analysis, develop a new, more effective material with inexpensive and good RCF failure resistance of wheel and rail.

Appendix

(a). The rail tracks standard dimension based on Ethio-Djibouti Railway (EDR) data.

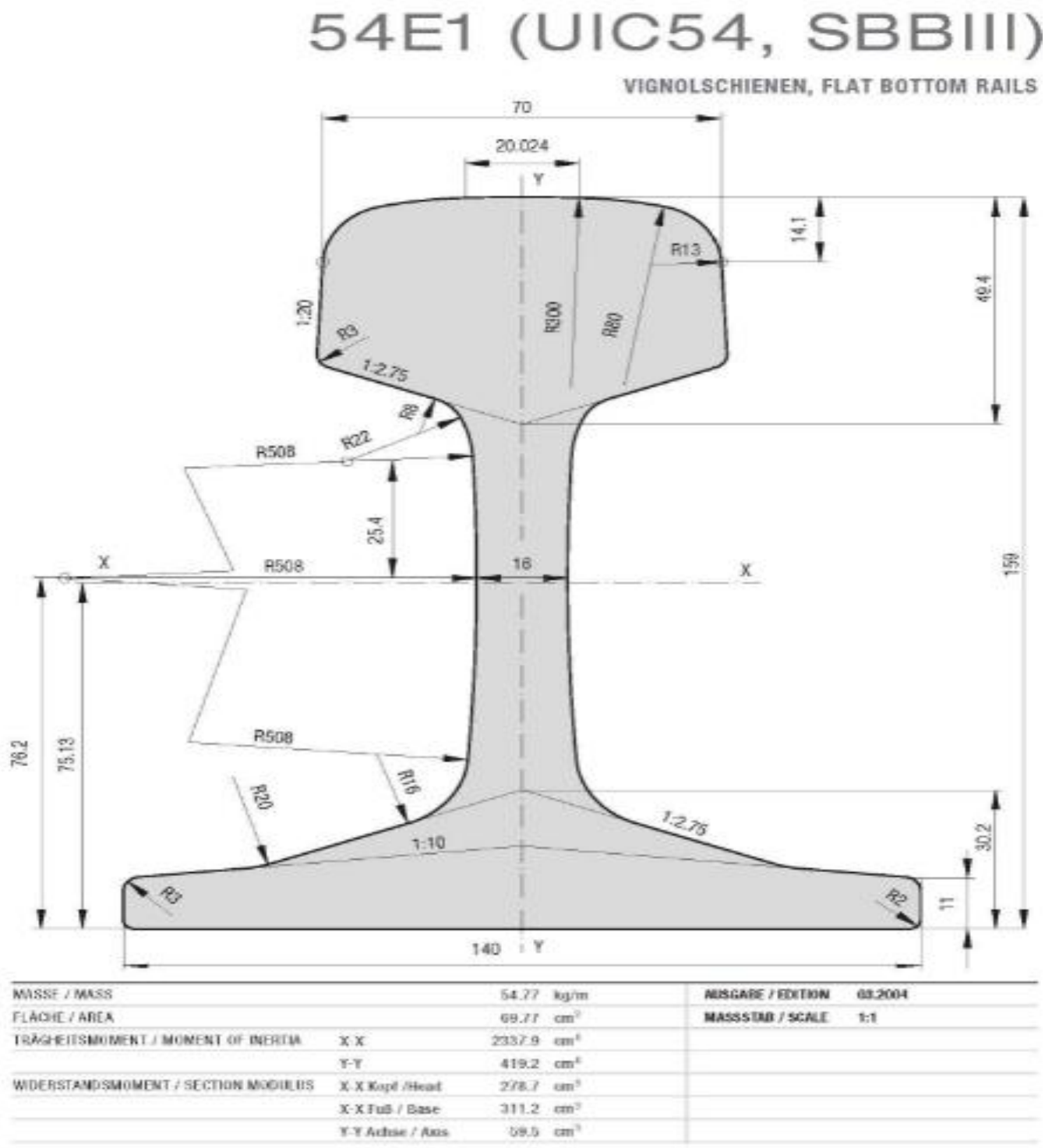

(b). contact points and RRD function of S1002 wheel on UIC54 (1:4) rail.

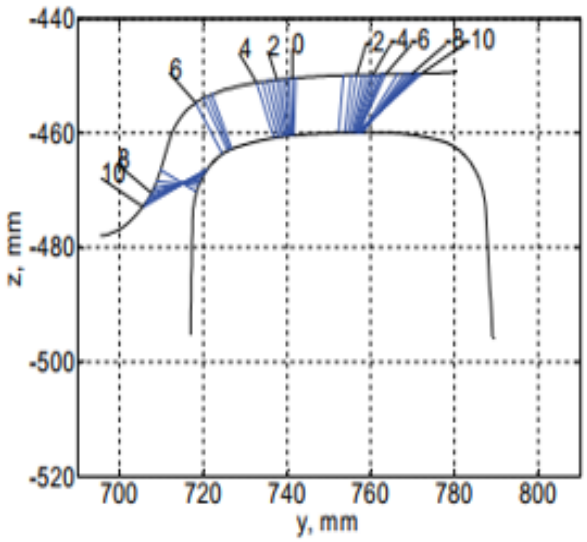

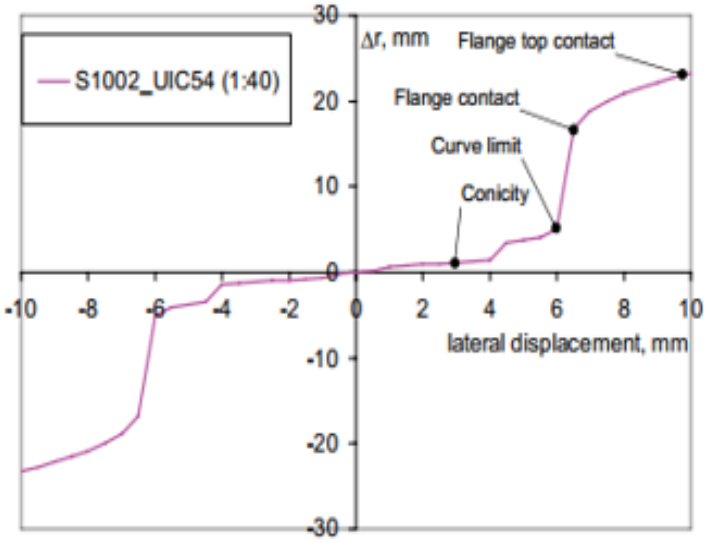

(c). Convergency curves to show convergency of the results from ANSSYS result based on the rail equivalent stress.

- ✓ For 9000A Material Property: for the three track conditions (a) straight, (b) transition and (c) circular curve respectively.

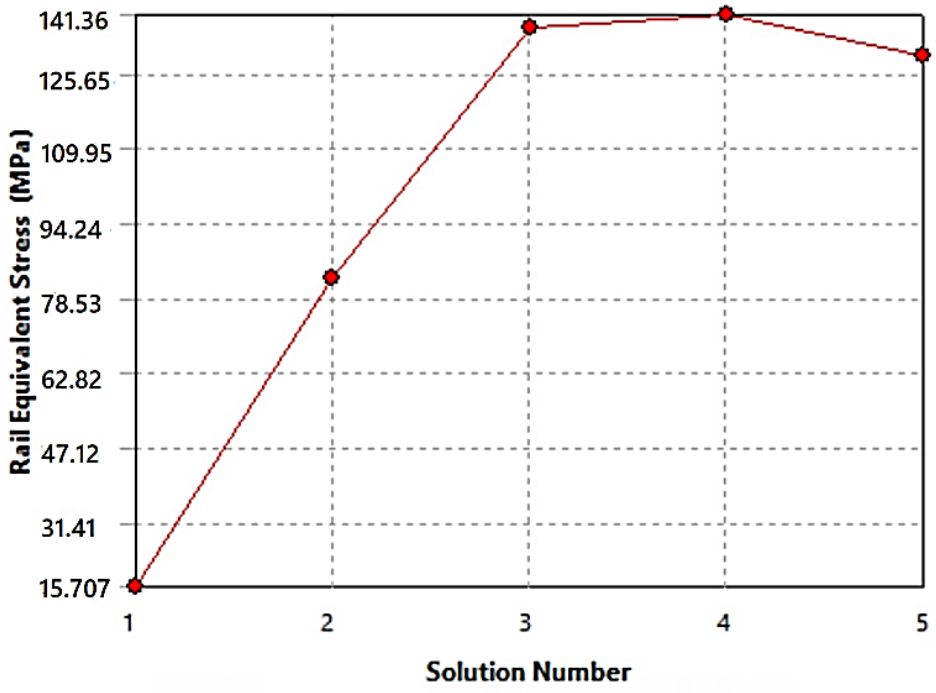

(a)

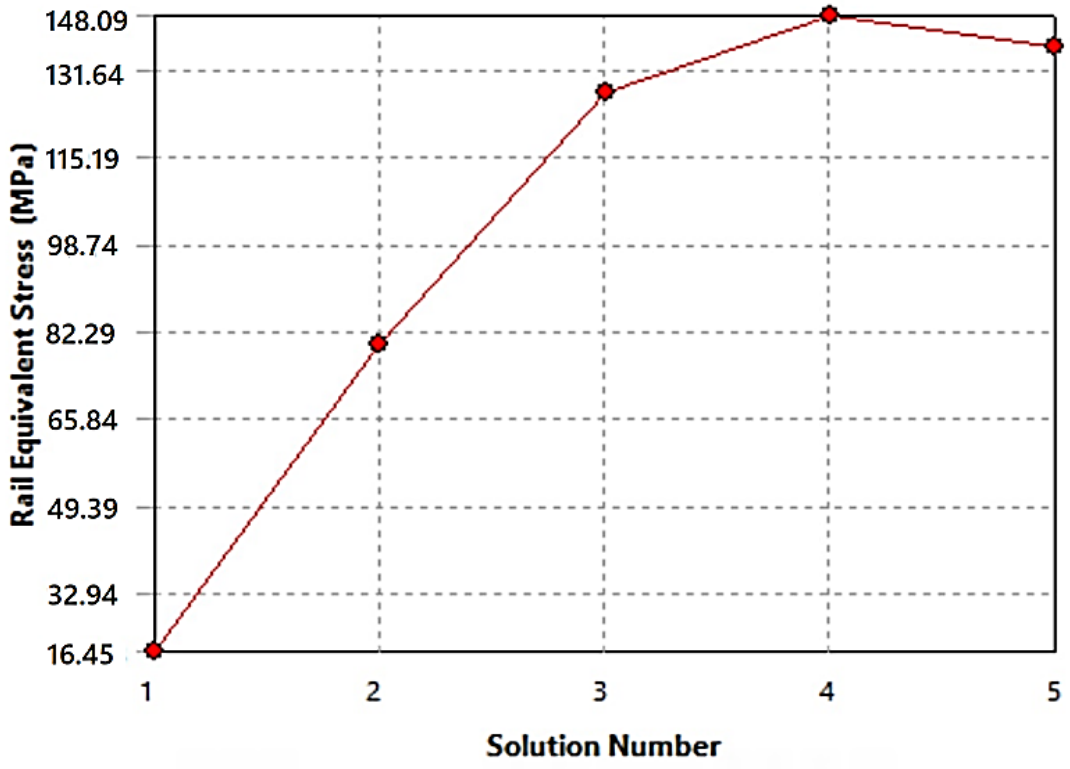
148.09
131.64
115.19
98.74
82.29
65.84
49.39
32.94
16.45
Rail Equivalent Stress (MPa)
1
2
3
4
5
Solution Number

(b)

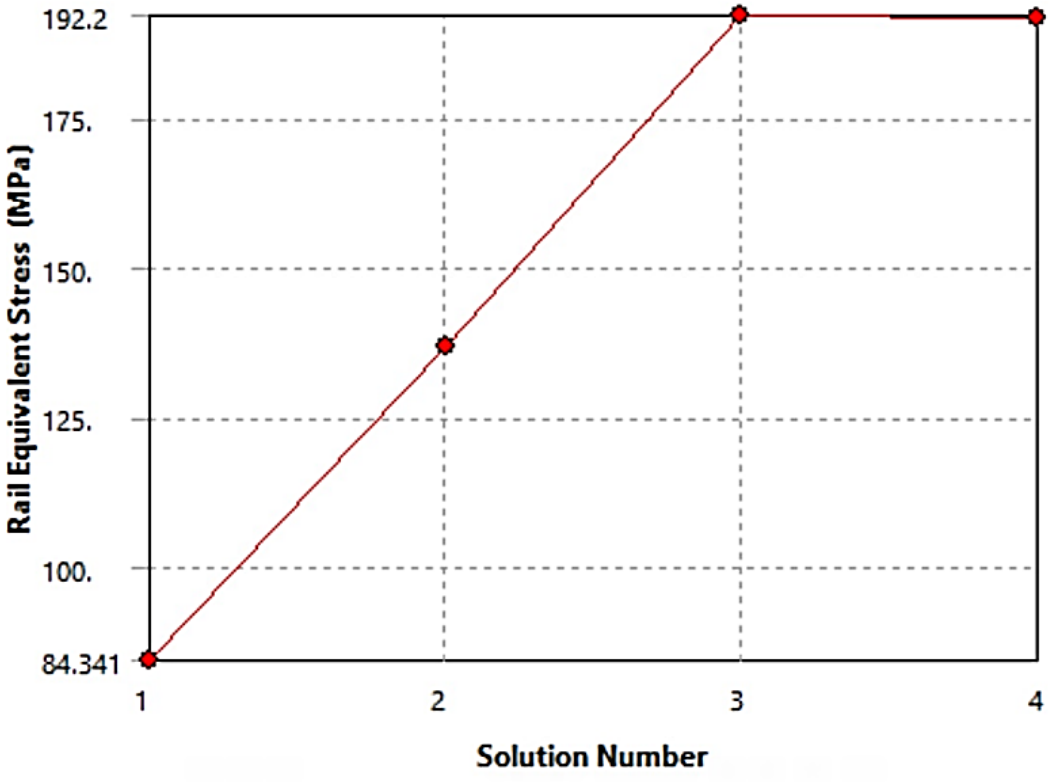
192.2
175.
150.
125.
100.
84.341
Rail Equivalent Stress (MPa)
1
2
3
4
Solution Number

(c)

- ✓ For AS60 Material Property: for the three track conditions (a) straight, (b) transition and (c) circular curve respectively).

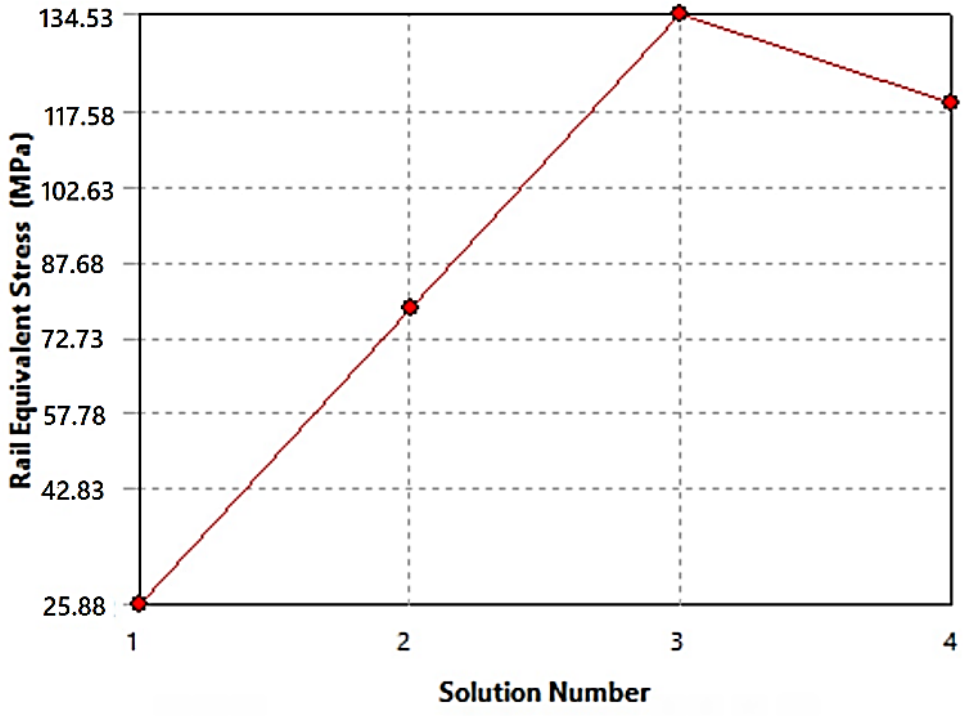

(a)

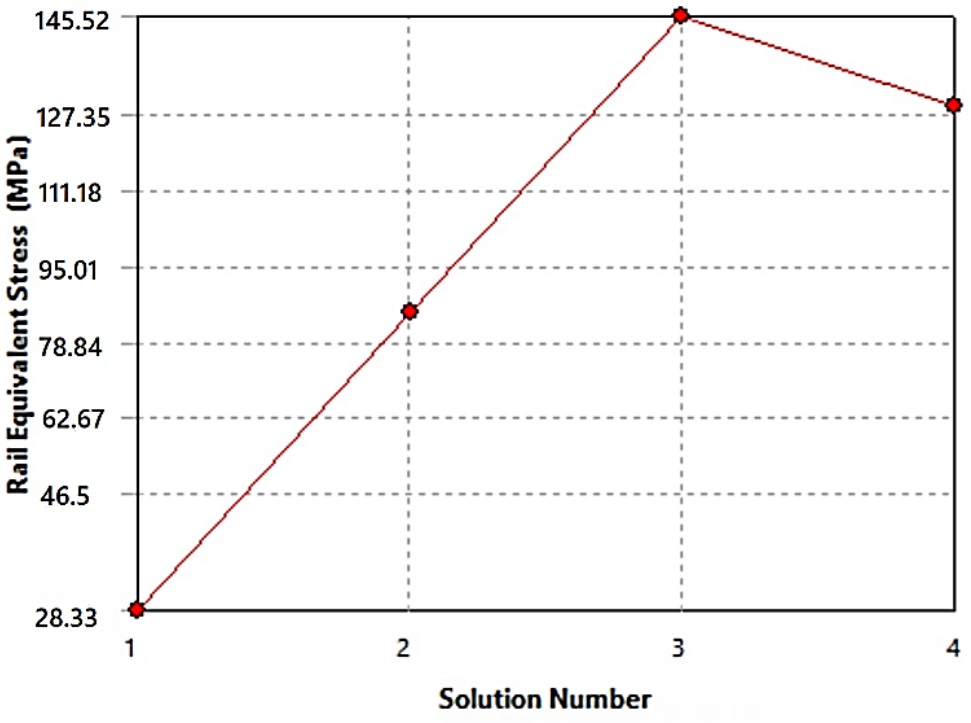

(b)

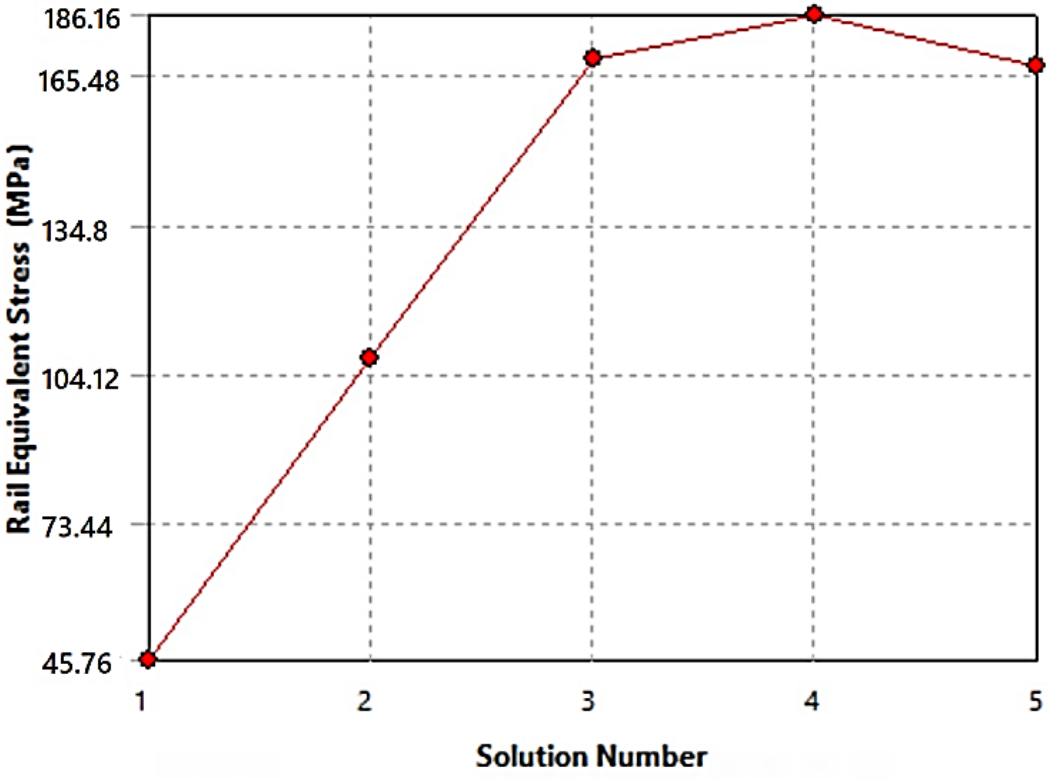
186.16
165.48
134.8
104.12
73.44
45.76
Rail Equivalent Stress (MPa)
1
2
3
4
5
Solution Number

(c)

References

[1] Ayana Gebremichael, Research conducted on Rolling Contact Fatigue damage, Straight Rail Track, (under Graduate School of Addis Ababa University Addis Ababa Institute of Technology for Railway Head Center)-2014.

[2] Anders Ekberg, Elena Kabo Fatigue of railway wheels and rails under rolling contact and thermal loading - an overview, 2004.

[3] Marine Vidaud, Willem-Jan Zwanenburg, Current situation on rolling contact fatigue – a rail wear phenomenon, Conference paper STRC, 2009.

[4] Nayan Chandaka, Mayank Yedea, Prashant Malviyaa, M.K. Pradhanb. Analysis of railway wheel to study crack initiation due to thermal loading and calculating life cycle.

[5] Bhushan B., John Wiley & Sons, Principles and Applications of Tribology, New York, 1999.

[6] Eric Magel, Peter Sroba, Kevin Sawley and Joe Kalousek, Research conducted Control of Rolling Contact Fatigue of Rails, (Centre for Surface Transportation Technology, National Research.

[7] Zerbst U, Mädler K and Hintze H. Fracture mechanics in railway applications. An overview. Engineering Fracture Mechanics.

[8] Qian Xiao, *, Jifeng Zheng, Jihua Liu1and Jun Fang. Analysis of the wheel/rail rolling contact fatigue of a high-speed train under the transient mechanism

[9] Johnson, K. L. (1985): Contact Mechanics. Cambridge University Press, Cambridge (UK).

[10] Bogdanski, S. and Brown, M.W. (2002): Modelling the three-dimensional behaviour of shallow rolling contact fatigue cracks in rails. Wear 253, 17-25.

[11] Marine Vidaud and Willem-Jan Zwanenburg (Conference paper STRC 2009): Current situation on rolling contact fatigue – a rail wear phenomenon.

[12] Jay Prakash Srivastava, Prabir Kumar Sarkar, V R Kiran Meesala and Vinayak Ranjan (2017): Rolling Contact Fatigue Life of Rail for Different Slip Conditions.

[13] Ajay Kapoor et.al. Tribology of Rail Transport, Chapter 34, By CRC Press LLC, 2001.

[14] M. Ueda, K. Uchino, A. Kobayashi, Effects of carbon content on wear property in pearlitic steels, Wear 253 (2002) 107–113.

[15] K.M. Lee, A.A. Polycarpou, Wear of conventional pearlitic and improved bainitic rail steels, Wear 259 (2005) 391–399.

[16] K.K. Wang, Z.L. Tan, G.H. Gao, X.L. Gui, R.D.K. Misra, B.Z. Bai, Ultrahigh strength toughness combination in bainitic rail steel: the determining role of austenite stability during tempering, Mater. Sci. Eng. A 662 (2016) 162–168.

[17] JFE Steel Corporation Web site: http://www.jfe-steel.co.jp/en/

[18] P. Pointner, High strength rail steels-the importance of material properties in contact mechanics problems, Wear 265 (2008) 1373–1379.

[19] Madler, K.: Suitability of AID as an alternative material for railcar wheel. http://www.ductile.org/magazine/2000_2/railcar.htm

[20] Ringsberg J.W., Franklin F., Josefsson B.L., Kapoor A., and Nielsen J. C.O., Fatigue evaluation of surface coated railway rails using shakedown theory, finite element calculations and lab and field trials, International Journal of Fatigue, 2005, 27, pp. 680–694

[21] T. Kimura, M. Takemasa, M. Honjo, Development of SP3 rail with high wear resistance and rolling contact fatigue resistance for heavy haul railways, JFE Technical Report 26 (2010) pp.11 16.

[22] Aregay Haile, Research conducted on the Effect of Rolling Contact Fatigue damage, Straight, Transition and Circular Curve Rail Track, on Addis Ababa Light Rail Transit (under Graduate School of Addis Ababa University Addis Ababa Institute of Technology for Railway Head Center), 2015.

[23] THERMAL DETERIORATION OF RAILWAY WHEEL STEELS, D. Nikas*, J. Ahlström* *Chalmers University of Technology, Department of Materials and Manufacturing Technology, SE-41296 Gothenburg, Sweden

[24] W. Zhong, J.J. Hu, Z.B. Li, Q.Y. Liu, Z.R. Zhou, A study of rolling contact fatigue crack growth in U75V and U71Mn rails, Wear 271 (2011) 388–392.

[25] A New Approach to Study the Wheel-Rail Contact Problem in Railway Dynamics João Pombo, Jorge Ambrósio IDMEC/Instituto Superior Técnico, Lisbon, Portugal 07 January 2015.

[26] A.H. Wickens. Fundamentals of Rail Vehicle Dynamics: Guidance and Stability. Swets & Zeitlinger, Lisse, Netherlands, 2003.

[27] R.V. Dukkipati. “Vehicle Dynamics”, Boca Raton: CRC Press, (2000), ISBN 0-8493-0976-X.

[28] S. Iwnicki, Handbook of Railway Vehicle Dynamics (CRC, Boca Rotan, FL, 2006).

[29] Norman E. Dowling, " Mean Stress Effects in Stress Life and Strain Life Fatigue ", 2nd SAE Brasi International Conference on Fatigue June 2004.

[30] C.M. Kuo, C.C. Hiang Lin, Rail and Rapid Transit, pp.1-6, (2015).

[31] Andersson, E., Berg, M., Stichel, S.: Rail Vehicle Dynamics, Fundamentals and Guidelines. Royal Institute of Technology (KTH), Stockholm (1998).

[32] Dukkipati, R.V., Amyot, J.R.: Computer-Aided Simulation in Railway Dynamics. Dekker, New York (1988).

[33] Draper J. Modern Metal Fatigue Analysis. United Kingdom, Emas Publishing; 2007.

[34] Kihl DP, Sarkani S. Mean stress effects in fatigue of welded steel joints. Probabilistic Engineering Mechanics 1999; 14: 97-104.

[35] Mann T. The influence of mean stress on fatigue crack propagation in aluminum alloys. International Journal of Fatigue 2007; 29: 1393–1401.